Studying the Role of Mechanical Contraction in Cardiac Muscle Development Using Genetically Engineered Non-Contractile Human Stem Cell-Derived Cardiomyocytes

Dasom Yoo

A dissertation

submitted in partial fulfillment of the

requirements for the degree of

Doctor of Philosophy

University of Washington

2021

Reading Committee:

Michael Regnier, Chair

Thomas Daniel

April Stempien-Otero

Program Authorized to Offer Degree:

Bioengineering

University of Washington

Abstract

Studying the Role of Mechanical Contraction in Cardiac Muscle Development Using Genetically Engineered Non-Contractile Human Stem Cell-Derived Cardiomyocytes

Dasom Yoo

Chair of the Supervisory Committee:

Michael Regnier

Department of Bioengineering

Mechanical contraction is an inherent function of cardiomyocytes but much of the effect of contraction on multiple cellular functions and therapeutic potential remains unknown. Due to the complete lethality of mechanical quiescence in cardiomyocytes, many researchers have used antagonists to mimic and study the effect of mechanical inactivity *in vitro*. However, this poses a great barrier as the antagonists are toxic and transient and cannot be used for long-term studies. With the emergence of human induced pluripotent stem cells (hiPSCs), we are now able to circumvent this shortcoming by creating *in vitro* models to induce stable and long-term mechanical quiescence in human cardiomyocytes. The following dissertation reports on the effects of mechanical

contraction in human cardiomyocytes on regenerative stem cell therapeutics after myocardial infarction (MI), proliferation, and early development cardiac biology. To evaluate if mechanical contraction from the cardiac grafts after MI contribute to the overall functional improvement, we transplanted non-contractile and contractile hiPSC-cardiomyocytes (hiPSC-CMs) into the infarcted rat hearts. At 3 months post transplantation, non-contractile cardiomyocytes were equipotent with contractile cardiomyocytes in preventing the decline of systolic function after MI. These results suggest that force production by cardiac grafts is not necessary to prevent decline in cardiac function post MI in rodents. However, during this study, we observed significantly larger graft sizes from non-contractile cardiomyocytes compared to contractile cardiomyocytes. To understand this difference in graft sizes, we investigated the effect of mechanical contraction on cardiomyocytes proliferation by studying the relationship between cyclin B1 and p53. We found that mechanical contraction, one of the most demanding metabolic activities, increases p53 activity that degrades cyclin B1 due to increased oxidative stress from contracting sarcomeres. This results in decreased cardiomyocyte proliferation that inhibits cardiac regeneration upon injury. Additionally, we further investigated if cardiomyocytes can form sarcomeres, the fundamental contractile units, in the absence of contraction to understand if mechanical activity is needed for structural development. By investigating the effect of contraction in areas ranging from therapeutic mechanism to developmental biology, these findings provide new understanding of how contraction affects cellular mechanisms and development.

Table of Contents

List of Figures

List of Tables

Acknowledgements

I would first like to thank my advisor, Dr. Michael Regnier, for his mentorship and guidance throughout my graduate studies. I still remember learning about muscle and Nernst equation in your Bioengineering 345 class as an undergraduate in 2011. Your lectures sparked my interest in cardiac biology and stem cells that paved my academic career for the next five years. You believed in me to pursue my curiosity and scientific interests and I am amazed by your endless enthusiasm for science and discoveries. I will forever be grateful for your support and mentorship in my growth both as a scientist and a person.

I would also like to thank my supervisory committee members, Dr. Thomas Daniel, Dr. Jennifer Davis, and Dr. April Stempien-Otero. You all played a tremendous role in my graduate experience and I have become a better scientist and a thinker with your support and guidance. I would also like to thank Dr. Charles Murry for his expertise and collaboration on the *in vivo* heart regeneration project. I have learned so much from planning and executing an *in vivo* project that I have a deeper level of appreciation for *in vivo* studies and how impactful these projects can be.

I have learned a lot in the past five years and this was possible with the help from so many people from the ISCRM village. Thank you to the past and present members of the Regnier Lab for their friendship and support during my graduate school. You all inspire me with your work ethics and kindness and I will miss our chats filled with timers going off and coffee breaks at Fresh Flours. Also, I would like to thank the past and present members of the Murry Lab for helping me learn a wide variety of techniques that enriched my academic experiences. Special thanks to my dear friends Nicole Zeinstra and Sonette

Steczina for always being there for me every step of the way. I am lucky to have met such lifelong friends and I am excited to see what amazing things you will do after graduate school.

Most importantly, I would like to say a huge thank you to my beloved family. Mom and dad, thank you for your unconditional love and support throughout my life. From immigrating to America without speaking the language to provide me and my brother more educational opportunities to being ready to pick up my calls whenever I needed you, you have always been there for me. Your love and dedication made me into the strong, independent woman I am today.

Lastly, I would like to thank my amazing husband, William Walker, for making this possible. Your emotional and scientific support helped me reach this finish line. This is not only my accomplishment, but also yours. Thank you for believing in me when my faith was wavering and being strong for the both of us. I love you and I will always be grateful to have you as my husband.

DEDICATION

To my amazing parents and husband for showing me unconditional love and support

Chapter 1. Motivation and Specific Aims

1.1 Research Motivation

Mechanical contraction in cardiomyocytes plays a number of roles in stem cell therapeutics, cellular processes, and cardiac developmental biology. For therapeutic applications, contractile human stem cell-derived cardiomyocytes have been transplanted *in vivo* to regenerate the heart after a myocardial infarction to improve cardiac function. In the field of cardiac development, mechanical contraction has been studied in cellular hypertrophy, disease progression, and cardiomyocyte maturation. The goal of this work is to study the role of mechanical contraction in cardiac regenerative cell therapy, proliferation, and myofibril development using genetically engineered non-contractile human stem cell-derived cardiomyocytes. This will be achieved through the following specific aims:

1.2 Specific Aims

1.2.1 Aim 1: Investigate the Mechanical Contributions of Transplanted Stem Cell-Derived Cardiomyocytes After Myocardial Infarction

Rationale: Transplanting human stem cell-derived cardiomyocytes after myocardial infarction (MI) has shown beneficial effects ranging from preventing further decline in systolic function in rodent MI models to improving cardiac function in non-human primate MI model. However, it is unknown whether force production from the cardiac grafts directly contributes to the improvement in cardiac function after MI or whether passive mechanisms such as secretion of paracrine factors, modulation of

inflammatory response, or reduction in wall stiffness are the primary underlying mechanisms behind functional improvement.

Hypothesis: Mechanical contraction in transplanted cardiomyocytes is necessary to improve global cardiac function after MI.

Approach: Human induced pluripotent stem cells (hiPSCs) without both slow skeletal and cardiac troponin I will be used as a model for non-contractile cardiomyocytes. Non-contractile or contractile hiPSC-CMs will be transplanted into an acute MI rat model to directly compare the functional differences. Cardiac function will be evaluated by echocardiography and cardiac MRI at three months after transplantation.

1.2.2 Aim 2: Define the Relationship Between Sarcomere Assembly and Mitosis Through Cyclin B1

Rationale: Adult human cardiomyocytes have minimal proliferation capacity but can replicate DNA resulting in progressive mononuclear polyploidization by unclear mechanism. Adult human heart is composed of predominantly polyploid cardiomyocytes and studies have shown polyploidization in cardiomyocytes leads to a decrease in cell division activity, limiting endogenous cardiac regeneration after an injury. Cyclin B1 plays an important role in cell division but the mechanism behind how cardiomyocytes regulate cyclin b1 during polyploidization remains unknown.

Hypothesis: Increased oxidative stress from mechanical contraction in cardiomyocytes leads to polyploidization and decreased cell division through the inhibition of cyclin B1 expression.

Approach: hiPSC with eGFP fused to cyclin B1 will be used to perform genome-wide CRISPR screen to identify modifier genes of the pre-mitotic checkpoint. Cardiac Troponin T knock-out and slow skeletal and cardiac troponin I knock out hiPSC-CMs will be used as models for sarcomere-deficient cardiomyocytes to investigate the dynamics between sarcomere assembly and polyploidization. Wildtype and Troponin I knock out hiPSC-CMs will be transplanted into a rat MI model to compare the proliferation and engraftment.

1.2.3 Aim 3: Determine the Role of Mechanical Contraction During Development and Myofibril Formation

Rationale: During cardiomyocyte development, mechanical contraction plays an essential role including cellular hypertrophy and force generation. However, it is unknown how mechanical contraction impacts myofibrillogenesis and the process of sarcomere protein isoform switches in developing cardiomyocytes. Studies have shown inhibition of contraction in both hiPSC-CMs and adult rat cardiomyocytes leads to complete abrogation of sarcomeres, suggesting sarcomere structures cannot be maintained in the absence of contraction. Other studies with sarcomere proteins partially or fully knocked out resulting in non-contractile cardiomyocytes have shown cardiomyocytes cannot assemble sarcomeres upon differentiation.

Hypothesis: Mechanical contraction is required for myofibril formation and sarcomere isoform changes in early-stage human cardiomyocytes.

Approach: Genetically engineered iPSCs with a point mutation – D65A – in cardiac troponin C (cTnC) to prevent calcium binding will be used as a model for non-

contractile cardiomyocytes. We will transduce contractile and non-contractile cardiomyocytes with adenoviruses encoding either wildtype cTnC or the mutant cTnC to initiate or inhibit contraction to observe the structural changes myofibrils undergo with the change in mechanical activity. To observe myofibril formation, we will perform immunocytochemistry, imaging on both confocal microscopy and structured illumination microscopy. Myosin heavy chain isoforms will be compared from wildtype and non-contractile cardiomyocytes at different time points to evaluate isoform switches.

Chapter 2. Introduction

2.1 Human Induced Pluripotent Stem Cell Derived-Cardiomyocytes to Study Development and Myofibril Formation

The discovery of reprograming factors that allow induction of pluripotent stem cells from differentiated cells has quickly expanded the fields of developmental biology and regenerative medicine.[1] With the development of robust directed differentiation protocols for cardiomyocytes, human induced pluripotent stem cells (hiPSCs) are a valuable *in vitro* model to study cardiac developmental biology such as maturation and myofibrillogenesis and loss-of-function and gain-of-function mutations in cardiac genes.[2-4] Also, they can be used to model genetic diseases by generating hiPSCs from patients with inherited cardiomyopathies to study disease progression and underlying molecular mechanism of the pathogenesis.[5-8] Despite the versatility of hiPSCs as a research tool, due to the 2D nature of *in vitro* culture, hiPSC-derived cardiomyocytes (hiPSC-CMs) are immature and do not exhibit the morphological and functional characteristics of adult cardiomyocytes.[9] Although this shortcoming may limit research that studies late-onset cardiomyopathies, the immaturity of hiPSC-CMs is an advantage when studying developmental biology in cardiomyocytes.[10] Upon differentiation, early-stage hiPSC-CMs have been used to study sarcomere assembly, electrophysiological phenotypes, changes in gene expression, and metabolic profile.[11-13] Due to the ability of studying cardiomyocytes from the moment they are differentiated and assembling contractile apparatus, hiPSC-CMs are essential in studying human cardiac development and is the main approach used in this work.

2.2 Human Induced Pluripotent Stem Cell Derived-Cardiomyocytes as a Cell Therapy for Heart Regeneration

Cardiovascular disease is the leading cause of death worldwide, responsible for more than 17.3 million every year and will increase to an astounding 23.6 million by 2030.[14] When a myocardial infarction (MI) occurs due to an occluded coronary artery, it is estimated up to a billion adult cardiomyocytes die.[15] After an MI, the heart undergoes irreversible structural remodeling to compensate for the lost myocardium through pathological fibrosis response, which ultimately results in heart failure. Since the heart is one of the least regenerative organs, it remains a challenge to remuscularize the infarcted heart and to rescue the cardiac function.[16] Currently, treatment for MI is palliative and is only used to slow down the progression of heart failure. Recently, stem cell-based regenerative therapies have emerged as a promising therapeutic approach to tackle the shortcomings of current treatments. To regenerate the heart after MI, many strategies have been explored, including intramyocardial injection of human embryonic stem cell-derived cardiomyocytes (hESC-CMs), attachment of engineered cardiac tissue onto the epicardium, gene therapy to improve cardiomyocyte contractility, direct reprogramming of the fibrosis, and modulation of the innate repair response after injury.[17-21] Of these approaches, transplantation of stem cell-derived cardiomyocytes via intramyocardial injection has been extensively investigated and shown improvements in cardiac function and remuscularization of the infarct in many acute MI models ranging from rodents to non-human primates.[17, 22-25] Other studies have also injected other cell types from cardiac lineage differentiation such as smooth muscle cells, cardiac progenitor cells, and endothelial cells after MI and reported enhanced angiogenesis and global cardiac function

followed by engraftment.[26-28] Despite this progress, the underlying mechanism of how the cardiac grafts is improving the cardiac function is unclear. Although the extent of graft's paracrine-mediated cardiac repair remains unknown, secretion of key regulatory molecules such as VEGF, HGF, TGF-β, bFGF, TNF-α and MMPs have been investigated and shown to improve graft/host survival, contractility, and angiogenesis.[29] Others have exploited the mechanical contraction of the cardiomyocytes to remuscularize the fibrotic scar tissue to contribute to the host cardiac function. However, these functional benefits were also observed when cells derived from cardiac mesoderm lineage other than cardiomyocytes were transplanted into acute MI animal models. Thus, further studies are necessary to determine the contribution of mechanical contraction in transplanted cardiomyocytes to improve cardiac function after MI.

2.3 Various Approaches to Regenerate the Heart After an MI

To regenerate the heart after an MI, many approaches have been explored ranging from cardiac tissue engineering to the use of synthetic biomaterials. Cell-based therapies for cardiac repair deliver various cell types to the infarcted region in different delivery routes. The cells that have been used for MI treatment include bone marrow-derived cells, mesenchymal stem cells (MSCs), cardiac progenitor cells (CPCs), smooth muscle cells, and stem cell-derived cardiomyocytes.[30] Different delivery routes such as intramyocardial injection, cardiac patch, and cardiac micro-tissue particles have been used to optimize cell survival and engraftment.[31] Previous study by Gerbin et al. directly compared the engraftment efficiency of different routes of delivery for human embryonic stem cell-derived cardiomyocytes by intramyocardially injecting dispersed-cells and

micro-tissue particles and implanting cardiac patch on to the epicardium of an infarcted rat heart. They reported all three delivery methods resulted in engraftment with no difference in graft sizes.[32] Different delivery routes also have different host-graft integration efficiency as direct injection in to the infarct tends to promote better integration with the patch implantation resulting in poor integration due to the fibrotic barrier between the patch and the epicardium.[32]

Acellular approaches, such as the Injection and delivery of paracrine factors to the infarcted region, also have been used to promote cardiac regeneration.[33] There are many forms of paracrine factors that can be used as a therapeutics such as growth factors, mRNAs, microRNAs, and exosomes.[34] These can be delivered via direct myocardial injection in to the infarct or systemic delivery. However, despite promising *in vivo* results, some of the paracrine factors used in clinical trials to treat heart failures, such as vascular endothelial growth factor A (VEGFA) and fibroblast growth factor 2 (FGF2), did not show therapeutic efficacy in patients.[35, 36] Many suspect this discrepancy in results is due to the low availability of the administered paracrine factors at the site of injury. To circumvent this shortcoming, efforts are being made to prolong the half-life and promote targeted and sustained delivery of the paracrine factors.[37, 38] A use of biosynthetic materials to create scaffolds that can encapsulate a cocktail of paracrine factors for sustained release at the site of infarct has been emerging as a promising new delivery route.[39]

Also, stimulating endogenous cardiac repair through viral transduction to control would healing response or promote cardiomyocyte proliferation to compensate for the loss of myocardium has been investigated for therapeutic potentials. Mohamed et al. has

reported injection of adenoviruses into the peri-infarct region to overexpress cyclin-dependent kinase 1 (CDK1), CDK4, cyclin B1, and cyclin D1 led to improved cardiac function and increased cardiomyocyte proliferation after MI in mice.[40] As cardiac fibroblasts play an essential role in would reparative process after the MI, other groups have investigated the feasibility of controlling the fibrotic response *in vivo* to attenuate pathological cardiac remodeling.[41, 42] Molkentin et al. has proposed a future clinical use of p38 inhibitors to reduce cardiac fibroblast differentiation into myofibroblasts after the injury.[41] Moon et al. reported the use of Wnt-974, an inhibitor of Wnt acyltransferase Porcupine (Porcn), after an MI led to a reduction in fibrosis formation and collagen production.[42] Although excess fibrotic response leads to pathological cardiac remodeling that results in heart failure, reparative fibrosis is essential in preventing rupture of the ventricular wall.[43] Therefore, further understanding of wound healing response is necessary to modulate the fibrotic response after MI to maintain the balance between reparative and pathological remodeling.

2.4 Cell Cycle Activity in Human Cardiomyocytes

During fetal cardiac development, the mammalian heart grows due to the rapid cell division of cardiomyocytes, leading to an increase in total number of cardiomyocytes. However, after birth, cell division dramatically decreases and cardiomyocytes undergo hypertrophy.[44, 45] In human hearts, this decrease in cell division results in cardiomyocytes' annual self-renewal rates of 0.5 to 2% and this lack of regeneration leads to irreversible damage upon cell loss in cardiac diseases.[46] In postnatal cardiomyocytes, one of three cell cycle activities occurs: (1) nuclear polyploidization, (2) multinucleation, and (3) cell

division.[47, 48] Nuclear polyploidization occurs via endocycling, a process in which a cell duplicates its DNA during S phase but does not undergo nuclear division. This results in a tetraploid (4n) nucleus. Multinucleation in cardiomyocytes often happens due to failed cytokinesis, in which a cell successfully completes nuclear division but does not spilt into two daughter cells, resulting in binucleated cells. Lastly, under normal cell division, cardiomyocytes undergo nuclear division and the 2 nuclei are separated into 2 daughter cells during cytokinesis.[49] Various methodologies have been used to study cardiomyocyte polyploidization and multinucleation such as flow cytometry, imaging of tissue sections, and fluorescent in situ hybridization (FISH).

Human ventricles are composed of 57.5% mononucleated polyploid, 25.5% multinucleated, and less than 10% diploid cardiomyocytes.[45] Increased polyploid and multinucleated cardiomyocyte populations have been suggested to limit heart regeneration by their reduced proliferation capacity compared to mononucleated diploid cardiomyocytes.[50-52] Interestingly, cardiomyocyte polyploidy varies widely among vertebrates with endotherm mammalian and bird species' hearts predominantly composed of polyploid cardiomyocytes while ectotherm species such as zebrafish and newt have hearts predominantly composed of diploid cardiomyocytes.[53] The capacity for cardiac regeneration decreases with the increase in polyploid cardiomyocyte population. In mice, cardiac regeneration depends on the proportion of mononucleated diploid cardiomyocytes, suggesting they are the primary cell reservoir for potential regeneration in human hearts.[51]

To uncover the regulatory pathway of cardiomyocyte polyploidy, studies have investigated metabolic cues, oxidative stress, and molecular regulators as potential

mechanisms for polyploidization. Fetal heart primarily uses glucose as a source of energy *in utero*. After birth, the heart switches to using fatty acid β-oxidation to generate energy.[54] This metabolic transition leads to increased levels of oxidative stress in the heart after birth and it has been reported that this increased oxidative stress leads to DNA damage and ultimately results in cell cycle arrest.[40] It has also been shown that reducing aerobic respiration after MI to decrease the production of reactive oxygen species leads to decreased myocardial fibrosis and improvement of systolic function in mice.[55]

Cyclin-dependent kinases (CDKs) are activated by cyclins and they regulate mammalian cell cycle. Overexpression of cyclin D1 to upregulate CDK4 resulted in increased multinucleation in mouse cardiomyocytes.[56] Cyclin G1 overexpression was reported to increase binucleation in neonatal rat cardiomyocytes.[57] Hippo-YAP signaling pathway regulates cellular processes such as proliferation and apoptosis and cell cycle regulation of cardiomyocytes.[58] In adult mice, activation of YAP led to an increase in the mononucleated cardiomyocyte population, suggesting YAP promotes cardiomyocyte proliferation.[59] Though studies have reported the effect of cyclin and CDK levels on polyploidization, the mechanism of how cardiomyocytes regulate cyclin expression levels remains unclear.

2.5 Formation of Myofibrils

Myofibrils in cardiomyocytes are composed of basic contractile units, sarcomeres, and are responsible for the generation of coordinated contraction. The process of myofibrilogensis contains formation of premyofibrils, nascent myofibrils, and mature myofibrils.[60] During premyofibril formation, Z-bodies containing α-actinin form

along the periphery of the cell with non-muscle myosin IIB (NMMIIB) assembling between the Z-bodies.[61] These structures are commonly known as muscle stress fibers (MSFs).[62] MSFs serve as a template for the developing myofibrils. As premyofibrils develop into nascent myofibrils, muscle-specific myosin isoform replaces non-muscle myosin and gets incorporated into the filaments.[63] Titin during this period gets inserted into the Z-discs and helps organizing the sarcomere structure and myosin incorporation.[64] As nascent myofibrils fuse together to form mature myofibrils, A-bands and Z-discs become highly organized and striations appear. As myofibrils mature, sarcomere proteins such as troponin I and myosin heavy chain (MHC) undergo isoform changes from fetal to adult isoforms. In early-stage cardiomyocytes, α-MHC is the predominant isoform and it switches to β-MHC isoform in adult cardiomyocytes.[65] Within the troponin complex, troponin I establishes myofibrillar calcium sensitivity. During embryonic development, cardiomyocytes express slow skeletal troponin I and switch to cardiac troponin I after birth.[66] Although mechanical contraction is the inherent function of myofibrils, further studies are necessary to understand the effect of contraction on myofibril formation and myofilament protein isoform changes.

Chapter 3. Investigate the Mechanical Contributions of Transplanted Stem Cell-Derived Cardiomyocytes After Myocardial Infarction

3.1 Abstract

Transplantation of human stem cell-derived cardiomyocytes after myocardial infarction (MI) has become a promising therapeutic approach to regenerate the heart after ischemic injury. However, the underlying mechanism of cardiomyocyte transplantation remains unknown as it is unclear whether mechanical contraction from the transplanted cardiomyocytes is necessary to improve cardiac function after MI. In order to address this question, we conducted a comparative *in vivo* study to evaluate cardiac function after transplanting contractile and non-contractile cardiomyocytes into the infarcted rat hearts. As a non-contractile cardiomyocyte model, we generated hiPSCs with both slow skeletal and cardiac troponin I knocked-out (denoted TNNI DKO) using CRISPR/Cas9 system. Upon cardiac differentiation, we confirmed TNNI DKO-cardiomyocytes (TNNI DKO-CMs) do not contract spontaneously or under electrical stimulation. Immunostaining of TNNI DKO-CMs showed severe sarcomere defects as punctate Z-bodies were seen instead of sarcomere striations. Also, TNNI DKO-CMs did not express troponin complex as confirmed by both immunostaining and western blot. To test if non-contractile cardiomyocytes are able to engraft in the ischemia/reperfusion injured athymic rat hearts, TNNI DKO-CM and wildtype cardiomyocytes (WTC-CMs) were injected into the infarcts three days after the injury. Both cell types showed robust engraftment after 4 weeks with TNNI DKO-CMs showing no sarcomere structures in the graft. To assess whether contractile cardiomyocytes will further improve the cardiac function after MI by

contributing to the overall systolic function of the rat myocardium, we transplanted WTC-CMs, TNNI DKO-CMs, and control (vehicle-only) to directly compare the cardiac function with echocardiography and cardiac MRI after 3 months. At 3 months, there was no difference in infarct size between the three groups but TNNI DKO-CM resulted in significantly bigger grafts compared to WTC-CM. WTC-CMs had clear sarcomere structures that were well aligned but TNNI DKO-CMs had no distinguishable sarcomere striation. Echocardiography analysis showed control continued to decline over the course of 3 months after MI while both WTC-CM and TNNI DKO-CM preserved fractional shortening and had improved systolic function compared to control at 3 months. Cardiac MRI results showed similar trend of improved left ventricular ejection fraction in both WTC-CM and TNNI DKO-CM compared to control at 3 months. From this study, we demonstrate for the first time mechanically quiescent cardiomyocytes preserve cardiac function after MI similar to the effect seen with contractile cardiomyocytes, suggesting mechanical contraction in transplanted cardiomyocytes is not needed for improvement in cardiac function after MI in rats.

3.2 Introduction

Ischemic heart disease is the leading cause of death worldwide.[67] A myocardial infarction (MI), commonly known as a heart attack, occurs due to an occluded coronary artery resulting in the death of up to a billion adult cardiomyocytes.[15] After an MI, the heart undergoes irreversible structural remodeling to compensate for the lost myocardium, which ultimately results in heart failure.[68] Since the heart is one of the least regenerative organs, it remains a challenge to remuscularize the infarcted heart to not only prevent

heart failure, but also to improve cardiac function after the initial injury.[69] Currently, treatment for MI is palliative and can only delay the progression of heart failure.[70] To tackle the shortcomings of current treatments, stem cell-based regenerative therapeutics has emerged as a promising approach.[71]

Transplantation of human stem cell-derived cardiomyocytes (hPSCs) after MI into the infarcted region has been well-investigated in various animal models for their regenerative therapeutic benefits of cardiac repair and improvement in cardiac function.[17, 72, 73] Various transplantation methods have been studied such as injection of dispersed cells in the infarcted region, attachment of tissue engineered constructs to the epicardium, and use of biomaterials for a wide range of effects such as improvement of graft survival, degradation of fibrosis, and modulation of immune response.[74-77] Many groups have reported the formation and maintenance of cardiac grafts after the delivery of stem cell-derived cardiomyocytes that resulted in reduction of scar formation and improvement in systolic function.[17, 25, 78] However, these functional benefits were also observed when cells other than cardiomyocytes that were derived from cardiac mesoderm lineage or mesenchymal stem cells were transplanted into acute MI animal models.[79-81] Studies with intramyocardial injection of smooth muscle cells (SMCs) and cardiac progenitor cells (CPCs) have shown improvement in fractional shortening post MI compared to control.[27, 28, 82] Similar therapeutics results between the transplantation of cardiomyocytes and other cell types after MI have led to a long standing question in the field regarding the underlying mechanism behind reparative and regenerative benefits of the transplanted cells.

It remains unknown whether transplanted cardiomyocytes directly contribute to the overall force production, or whether other mechanisms such as secretion of paracrine

factors, modulation of immune response, and improvement in myocardium compliance are the predominant mechanism.[83-85] There has been an increase in evidence suggesting the paracrine factors are mostly responsible for the cardiac regenerative effect. Numerous studies have demonstrated that transplanted cells contribute to tissue repair and regeneration by releasing essential paracrine factors such as VEGF, HGF, FGF, PDGF, IFG-1, SDF1α, TGF-β, and TSG-6 that promote cell survival, angiogenesis, and inflammatory response.[29, 86-89] Gnecchi et al. has reported intramyocardial injection of paracrine factors secreted by mesenchymal stem cells expressing Akt1 gene led to myocardial protection – reduction in infarct size and apoptotic cells – after MI.[90] Secreted paracrine factors can affect multiple different pathways such as survival, immunomodulation, proliferation, structural remodeling, metabolism, contraction, angiogenesis, and endogenous CPC activation post-MI, which have been summarized in **Table 1**.[91]

Paracrine factors	Survival	Proliferation	Immune response	Remodeling	Angiogenesis	Contraction	CPC activation
Angiopoietin	✓				✓		
FGF		✓			✓		
HGF-1			✓		✓		
IGF-1	✓	✓				✓	
NRG1		✓			✓		
PDGF	✓	✓					✓
Periostin		✓					
PGE2		✓	✓				✓
SDF1					✓		✓
TGFβ			✓	✓			
VEGF				✓	✓	✓	

Table 1 The effects of paracrine factors after MI. Table adapted from Hodgkinson et al.[91]

Also, recent study has suggested the underlying biologic mechanism of action is the acute inflammatory response that triggers the cardiac wound healing process by macrophages from the injection of cells post MI. Vagnozzi et al. has shown that the injection of zymosan, a non-cellular activator of immune response, resulted in improved systolic function after MI that was sustained for 2 months in mice, similar to the results seen with the injection of bone marrow mononuclear cells.[21] Together, these demonstrate various pathways stem cell regenerative therapy can improve cardiac function and that it is unclear if mechanical contraction from the transplanted cardiomyocytes adds an additional benefit to remuscularize the infarct and improve cardiac function after MI.

In this study, we addressed this question by directly comparing the cardiac function after MI from transplanting contractile human induced pluripotent stem cell-derived cardiomyocytes (hiPSC-CMs) and non-contractile hiPSC-CMs. We developed a human cardiomyocyte that were unable to contract by knocking out essential components of troponin complex – slow skeletal troponin I (ssTnI) and cardiac troponin I (cTnI) (denoted TNNI DKO). Upon differentiation, TNNI DKO-derived cardiomyocytes (TNNI DKO-CMs) did not spontaneously contract yet displayed calcium transients, confirming the successful inhibition of excitation-contraction coupling. We then transplanted wildtype cardiomyocytes (WTC-CMs) and TNNI DK-CMs into the infarcted hearts of athymic rats and compared their cardiac function with echocardiography and cardiac MRI at 1 month and 3 month post injury. We hypothesized transplantation of contractile cardiomyocytes would lead to a greater improvement in systolic function from the graft electromechanically coupling with the host myocardium to contribute to the overall force production. However, after MI, the non-contractile cardiomyocytes were equipotent with

contractile cardiomyocytes in preventing the decline of systolic function in rats. This suggests contraction from the transplanted cardiomyocytes does not contribute to the overall force production after MI and the therapeutic benefits of transplanted cardiomyocytes are primarily through paracrine and other non-force production mechanisms in rats.

3.3 Materials and Methods

3.3.1 *CRISPR/Cas9 Targeting of TNNI1 and TNNI3 in WTC-11 hiPSCs (TNNI DKO)*

Single guide RNAs (sgRNAs) targeting *TNNI1 and TNNI3* were designed using the online CRISPR design tool (crispr.mit.edu). The gRNA sequence for TNNI1 is CTTACACTTCCGGCA, and gRNA sequence for TNNI3 is TGAGTCTCAGCATGGCGGAT; sgRNAs were ligated into vector PX459v2 (Cas9-2A-Puro). First, 300,000 WTC-11 hiPSCs (Gladstone Institute of Cardiovascular Disease, UCSF) were transfected with 1µg plasmid using GeneJuice (EMD Millipore) during replating with PX459v2 having the TNNI1 gRNA, and selected with 0.5µg/mL puromycin (ThermoFisher) for 2 days beginning the day after transfection. After selection, cells were replated to grow as single-cell colonies. Genomic DNA was isolated from the cell colonies. Colonies were screened by amplifying the region around the targeted sgRNA site from 100-300ng genomic DNA using GoTaq Flexi DNA polymerase (Promega) following manufacturer's guidelines. Following visualization by electrophoresis on a 0.8% agarose gel stained with ethidium bromide, PCR products were sequenced (Eurofins genetics). After genotyping, the second run of similar procedure was performed to knock out TNNI3.

For the cell line generated, colonies with homozygous mutations causing premature stop codons were also screened for mutations in the exon regions of the top 10 genes predicted to be most susceptible to off-target effects. Mutant cell lines were cryopreserved and karyotyped (Diagnostic Cytogenetics Inc, Seattle, WA, **Figure S19**).

3.3.2 HiPSC-Derived Cardiomyocyte Culture and Differentiation

The WTC-11 and TNNI DKO hiPSC lines were maintained in mTeSR1 (STEMCELL Technologies) on Matrigel-coated tissue culture plates (Corning).[92] Media was changed daily and cells were passaged as single cells with Versene (ThermoFisher). Directed cardiomyocyte differentiation was induced via Wnt/β-catenin signaling with modifications from a published method.[3, 4, 93] In summary, 1.5 x 10^5 cells were seeded per well of a Matrigel-coated 12-well plate in mTeSR and 10 µM ROCK inhibitor Y-27632 (Tocris) for 24 hours, denoted day -2. Media was changed to 1 µM CHIR-99021 (Cayman) in mTeSR on day -1. On day 0, differentiation was induced after a PBS (Gibco) wash with 5 µM CHIR-99021 in RPMI (Gibco) supplemented with 500 µg mL^{-1} bovine serum albumin (BSA; Sigma) and 213 µg mL^{-1} ascorbic acid (Sigma), denoted RBA media. On day 2, cells were washed with PBS and treated with 2 µM Wnt-C59 (Selleck) in RBA media. On day 4, media was changed to RBA only without small molecules. On day 6, media was changed to RPMI with 1X B27 supplement (Thermo Fisher), with further media changes every other day until cells were collected (**Figure 1**).

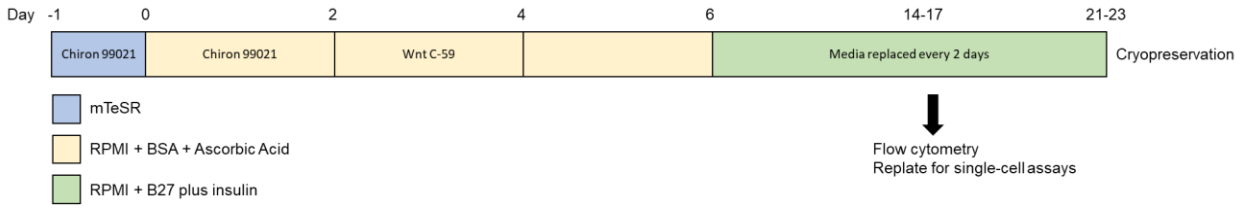

Figure 1 Outline of cardiac differentiation protocol and the timeline for hiPSC-CMs used in experiments.

3.3.3 Flow Cytometry to Quantify Cardiac Purity

Flow cytometry analysis was performed using a BD FACSCanto and data were acquired with the BD FACSDIVA software. Cells were washed with PBS, treated with 0.05% Trypsin-EDTA (Gibco) for 5 minutes at 37°C, and collected in RPMI. Cells were spun down and fixed in 4% paraformaldehyde for 15 minutes at room temperature. Cells were spun down and resuspended in 5% FBS in PBS. To determine the cardiac purity, fixed cells were incubated for 1 hour in room temperature with mouse cardiac Troponin T (cTnT) antibody (ThermoFisher MA5-12960, 1:100) or mouse α-actinin antibody (Abcam 9465, 1:100) or mouse immunoglobulin G1 isotype control (eBioscience 14-4714, 1:100) in PBS + 5% FBS + 0.75% saponin (Sigma). After primary antibody incubation, cells were spun down and washed with PBS + 5% FBS + 0.75% saponin. Cells were then incubated for 45 minutes in room temperature with goat anti-mouse PE secondary (Jackson 115-116-072, 1:200) or goat anti-mouse 488 secondary (Invitrogen A11001, 1:200) resuspended in PBS + 5% FBS + 0.75% saponin. Analysis was performed using FloJo version 10 software.

3.3.4 Multielectrode Array (MEA) to Assess Electrophysiological Function of Cardiomyocytes

48-well MEA plates (Axion Biosystems; 16 electrodes per well) were coated with 20 µg mL^{-1} laminin (BioLamina) in 37°C for 2 hours, as previously described.[94] Day 14-16 post differentiation cardiomyocytes were plated onto the electrodes at the density of 25,000 cells/well and 50,000 cells/well in total of 6 µL volume. Cells were incubated in 37°C for 2 hours. To prevent cells from drying out, 300 µL media was added to each well and further media changes occurred every other day until data were collected. On the day of the data acquisition, 1.8 mM Ca^{2+} Tyrdoe's buffer was added to each well 5 minutes before the recording. Data were acquired using the Maestro MEA system (Axion Biosystems) and the standard recording settings for spontaneous cardiac field potentials were used (Axis software, version 2.1).

3.3.5 Cryopreservation and Cell Preparation for Transplantation

Cardiomyocytes used in the *in vivo* study were cryopreserved on day 20-22 of differentiation and thawed immediately prior to cell injection, following our previously described protocol[17, 32]. One day prior to cryopreservation, cells were heat-shocked for 30 minutes at 42°C. Cells were treated with 10 µM ROCK inhibitor Y-27632 for 1 hour and were dispersed by incubation with 0.25% trypsin in EDTA. Cells were spun down, resuspended in CryoStor (Sigma) at 10 x 10^6 cells/mL, and frozen in cryovials. To thaw cryopreserved cells, cryovials were thawed briefly at 37°C followed by addition of RPMI + B27 + 200 U/mL DNAse. Cells were washed and resuspended in an RPMI-based pro-survival cocktail containing 50% (vol/vol) growth factor-reduced Matrigel, 100 µM ZVAD

(benzyloxycarbonyl-Val-Ala-Asp(O-methyl)-fluoro-methyl ketone, Millipore), 50 nM Bcl-XL BH4 (cell-permeant TAT peptide, Millipore), 200 nM cyclosporine A (Novartis), 100 ng/mL IGF-1 (Peprotech), and 50 µM pinacidil (Sigma).

3.3.6 Ischemia/Reperfusion Injury and Cell Transplantation

All animal procedures were conducted in accordance with the US NIH Policy on Humane Care and Use of Laboratory Animals and the UW Institutional Animal Care and Use Committee (IACUC). There were two experimental groups (WTC-11 and TNNI DKO) and one control group (sham) for this study. Fourteen rats were enrolled per experimental group and twelve rats were enrolled in the sham group. The protocol for ischemia/reperfusion surgery has been previously published[17, 32, 78]. Briefly, male athymic Sprague-Dawley rats (Harlan/Envigo) were anesthetized with intraperitoneal injection of 68.2 mg kg^{-1} ketamine and 4.4 mg kg^{-1} xylazine, and were intubated and mechanically ventilated. To maintain body temperature of 37°C, the animals were placed on a heating pad with a rectal probe. A thoracotomy was performed and the left anterior descending coronary artery (LAD) was ligated for 60 minutes, reperfused, and the chest was aseptically closed. Animals received subcutaneous injections of 5 mg kg^{-1} Cyclosporine A for seven consecutive days starting the day before cell transplantation. Animals underwent second thoracotomy 4 days after ischemia/reperfusion injury under 5% isoflurane supplemented with oxygen. Animals were randomly assigned to one of the three groups. Each animal in the treatment group received 10 x 10^6 cells resuspended in 100 µL pro-survival cocktail. Cell suspension was injected into three different areas within the infarct – one into the center of the infarct and two in the lateral infarct border zone.

Sham control animals received intramyocardial injection of 100 μL pro-survival cocktail only. To assess proliferation in the grafts, all animals received intraperitoneal injection of 50 mg kg^{-1} BrdU (Sigma) on days 1, 7, 30, 60, and 90 post cell transplantation.

3.3.7 Echocardiography

The cardiac function of all animals was evaluated with echocardiography at one day before cell transplantation (denoted Baseline), 28 days after cell transplantation, and 84 days after cell transplantation. Briefly, animals were lightly anesthetized with 1-2.5% isoflurane (Novaplus) and scanned by transthoracic echocardiography (GE Vivid 7) using 10 S pediatric probe. The parameters acquired included fractional shortening (%), left ventricular end diastolic dimension (LVEDd), and left ventricular end systolic dimension (LVESd).

3.3.8 Magnetic Resonance Imaging (MRI)

Three months after cell transplantation, the cardiac function of rats was also evaluated by high-resolution MRI as described previously.[17] In summary, rats were lightly anesthetized with 1.2.5% isoflurane delivered through a nose cone and placed in a ^{1}H transmit-receive volume coil. ECG was recorded with needle electrodes attached to the animals' limbs. MRI acquisitions were triggered with ECG. Multislice short-axis images were collected to analyze left ventricle volumes at end systole and end diastole.

3.3.9 Histology and Immunohistochemistry

Histological stains and subsequent analysis were conducted as described previously[17, 23, 32]. Briefly, hearts were perfused with PBS and 150 mM KCl solution after harvesting, fixed overnight in 4% paraformaldehyde, sliced into 1-2 mm thick sections, processed, sectioned, and stained with appropriate primary and secondary antibodies. To visualize grafts, sections were deparaffinized, incubated overnight with mouse MYH7 antibody (Developmental Studies Hybridoma Bank A4.951, supernatant) followed by a one-hour incubation with biotin-SP goat anti-mouse antibody (Jackson ImmunoResearch 115-065-003, 1:500) and developed with diaminobenzadene (DAB, Vector Labs) for brightfield images. To visualize sarcomere structures within cardiac grafts, sections were deparaffinized, boiled in Tris-EDTA buffer pH 9.0 for antigen retrieval, incubated overnight with mouse MYH7 and rabbit α-actinin antibody (Abcam ab68167; 1:100 dilution). The next day, sections were incubated at one hour at room temperature with Alexa Fluor 488 goat anti-mouse (Invitrogen A11011; 1:100 dilution) and Alexa Fluor 594 goat anti rabbit (Invitrogen A11037; 1:100 dilution) and imaged with Nikon A1R Confocal.

3.3.10 Statistical Measurements

All histological measurements were performed using ImageJ and statistical analysis were done in either Excel or Prism Grahpad. Stained slides were scanned using a Hamamatsu Nanozoomer whole slide scanner and the images were exported from NDP software. Infarct size was quantified using picrosirius red staining and normalized to left ventricular area. Graft size was quantified using MYH7 DAB stained slides and normalized to both infarct area and left ventricular area. Data were presented as mean ±

standard error of the mean (SEM). Statistical analysis was conducted with Student's t test and ANOVA.

3.4 Results

3.4.1 Cardiomyocytes Without Slow Skeletal Troponin I and Cardiac Troponin I (TNNI DKO-CM) Do Not Contract and Have Disrupted Sarcomeres

Upon cardiac differentiation, we confirmed TNNI DKO-CMs do not contract spontaneously or under electrical pacing, demonstrating the absence of slow skeletal and cardiac Troponin I successfully inhibit excitation-contraction coupling. To determine if cardiomyocytes without slow skeletal and cardiac troponin I can form sarcomeres, we stained for α-actinin, β-myosin heavy chain (βMHC), and cardiac troponin T. In TNNI DKO-CMs, we found no clear sarcomeres and instead saw punctate α-actinin expression with no discernible structure (**Figure 2A**). Also, we did not see distinct thin filament striations from cTnT staining and the overall cTnT expression profile was punctate and sparse (**Figure 2B**). This punctate cTnT expression became a problem when we performed flow cytometry on TNNI DKO-CMs to determine the cardiac purity upon differentiation. When stained with cTnT, TNNI DKO-CMs did not distinguish between isotype control and $cTnT^+$ populations. However, when we stained TNNI DKO-CMs with α-actinin, we were able to get distinct isotype control and $\alpha\text{-actinin}^+$ populations (**Figure 2C**). α-actinin staining to quantify cardiac purity was confirmed with wildtype cardiomyocytes, WTC-CM, as both α-actinin and cTnT staining produced similar cardiac purities (**Figure 2D**). We hypothesized from the punctate cTnT expression that TNNI DKO-CMs may not have troponin complexes due to the absence of troponin I.

To investigate this hypothesis, we isolated myofibrils from TNNI DKO-CMs and performed western blots to specifically look at the myofibrillar troponins. The results showed TNNI DKO-CMs do not have myofibrillar cardiac troponin C (cTnC), indicating the knock-out of troponin I is disrupting the formation of troponin complex (**Figure 2E**).

To understand how the absence of myofibrillar cTnC impacts the calcium handling and electrophysiological properties of TNNI DKO-CMs, we performed Fura-2 calcium transient measurements on IonOptix and multielectrode array (MEA), respectively. Both wildtype and TNNI DKO-CMs were paced in Tyrode buffer with three different Ca^{2+} concentrations (0.6, 1.8, and 2.5 mM Ca^{2+}) to evaluate the effect of various extracellular calcium concentration on these hiPSC-CMs as immature cardiomyocytes depend more heavily on extracellular calcium handling. Interestingly, TNNI DKO-CMs displayed higher peak amplitude compared to wildtype, while times to 50% and 90% decay were shortened (**Figure S20**). We suspect higher peak amplitude is due to the absence of myofibrillar cTnC, a major cardiomyocyte cytosolic calcium buffer. These results demonstrate TNNI DKO-CMs have calcium transients despite the mechanical quiescence but have altered calcium transients.

Analysis of MEA showed TNNI DKO-CMs have faster beat period (**Figure 2F**). Also, we found that the field potential duration (FPD), which is the *in vitro* analog of the QT interval, is longer in TNNI DKO-CMs (**Figure 1G**). FPD is measured from the initial Na^{+} spike to the maxima of the K^{+} repolarization wave and has been shown to correlate with action potential duration measurements in *in vitro* patch-clamp studies.[95] Conduction velocity was slower in TNNI DKO-CMs compared to WTC-CMs (**Figure 2H**). Conduction velocity is measured by calculating the time it takes for the depolarizing wave to reach

neighboring electrodes in a given distance away. Previous study has shown hiPSC-CMs have conduction velocity of 10-20 cm s^{-1} compared to 50 cm s^{-1} in human left ventricles.[96]

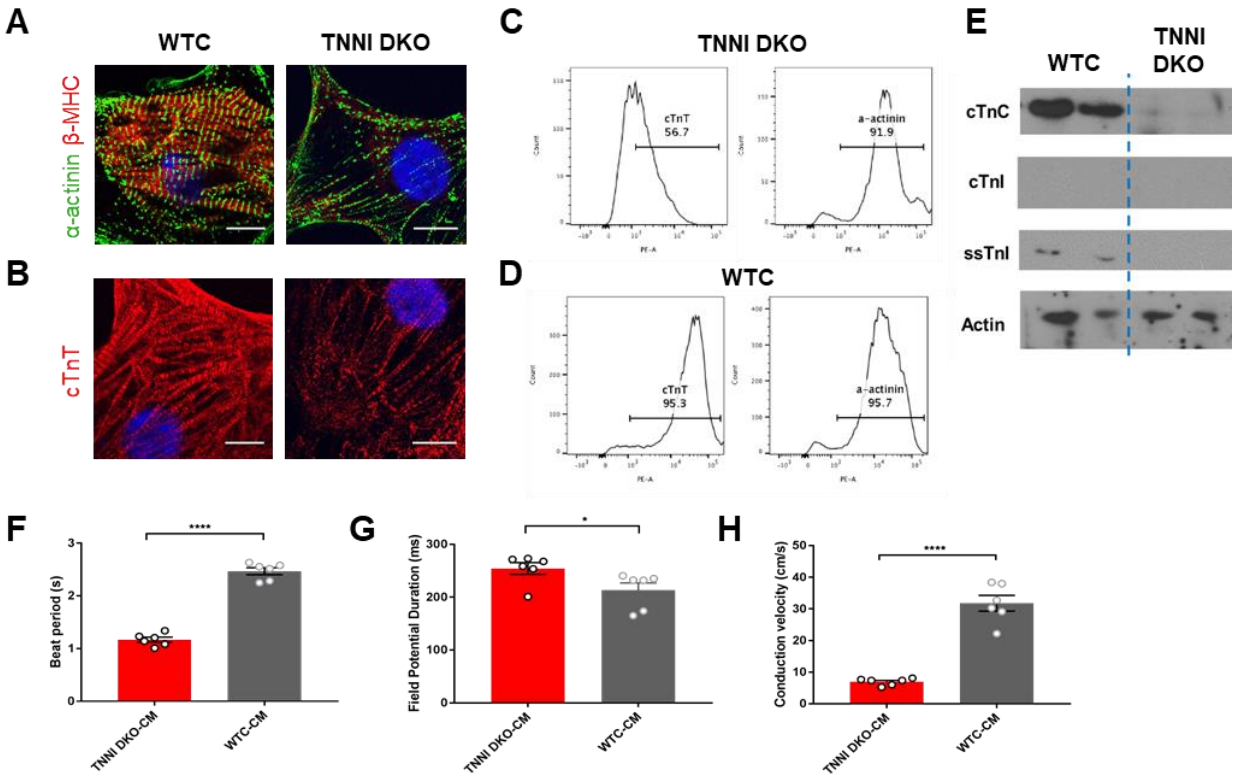

Figure 2 Characterization of TNNI DKO-CM

Representative confocal images of 30-day-old WTC-CM and TNNI DKO-CM stained for **(A)** α-actinin (green), β-myosin heavy chain (βMHC; red), and DAPI (blue). TNNI DKO-CMs are unable to form striated sarcomere structures. Scale bar = 10 μm. **(B)** cardiac troponin T (cTnT; red) and DAPI (blue). cTnT expression in TNNI DKO-CMs is disrupted and punctate. Scale bar = 10 μm. Representative cTnT and α-actinin flow cytometry results of 14-day-old **(C)** TNNI DKO-CMs show cTnT cannot be used to quantify cardiac purity upon differentiation but α-actinin can and **(D)** both cTnT and α-actinin staining yield similar cardiac purities in 14-day-old WTC-CMs. **(E)** Representative myofibrillar immunoblots probed with antibodies to cardiac troponin C (cTnC), cardiac troponin I (cTnI), and slow skeletal troponin I (ssTnI). TNNI DKO-CMs do not have myofibrillar cTnC, ssTnI, and cTnI. Figure courtesy of Dr. Yuanhua Cheng. Electrophysiological assessment of 35-day-old TNNI DKO-CMs was measured with multielectrode array and the results showed **(F)** TNNI DKO-CMs have faster beat period, **(G)** longer field potential duration, and **(H)** slower conduction velocity in comparison to control. Data are n = 6 wells per condition and mean±SEM; significance assessed by Student's t-test.$p \leq 0.05$ (*) and $p \leq 0.0001$ (****).

3.4.2 Contractile and Non-Contractile hiPSC-CMs are Differentiated to Generate High Purity Cardiomyocytes

Differentiation protocols described above produced high purity cardiomyocytes for both WTC hiPSCs and TNNI DKO hiPSCs. Robust and spontaneous beating was observed around day 8-10 post differentiation for WTC hiPSCs. Flow cytometry analysis for cardiac troponin T (cTnT) expression was used to quantify cardiomyocyte purity for WTC-CMs. The average purities of WTC-CMs used for the pilot *in vivo* study was 92.3% $cTnT^+$ and 90.4% $cTnT^+$ for the 3 month study. The average purities of TNNI DKO-CMs used for the pilot *in vivo* study was 42.2% $\alpha\text{-actinin}^+$ and 95.4% $\alpha\text{-actinin}^+$ for the 3 month study. (The big difference in purities was due to optimization of differentiation protocol with concentration of CHIR99021 and plating density)

3.4.3 Both Contractile and Non-Contractile hiPSC-CMs Engraft in Infarcted Rat Myocardium by 1 Month Post MI

To assess the ability of non-contractile cardiomyocytes (TNNI DKO-CMs) to engraft in the injured rat heart, we conducted a pilot *in vivo* study and performed histological staining at 4 week after cell transplantation (**Figure 3A**). Three athymic nude rats were enrolled into each treatment group. Histological analysis for βMHC was used to detect cardiac engraftment of human cardiomyocytes and it showed both WTC-CM and TNNI DKO-CM engrafted in the rat myocardium (**Figure 3B**). WTC-CM graft showed striated sarcomeres with circumferential expression of connexin-43 (Cx43). TNNI DKO-CM graft showed similar Cx43 expression pattern but showed no sarcomere striations (**Figure 3C**). Circumferential expression of Cx43 in both grafts was expected as Cx43 is

circumferentially expressed in immature hiPSC-CMs while it is polarized and localized at the intercalated disks in mature cardiomyocytes.[97, 98] However, we expected to see more organization in sarcomere proteins in transplanted TNNI DKO-CMs than filamentous organizations observed *in vitro*, as previous studies have shown *in vivo* transplantation accelerates cardiomyocyte maturation, resulting in better striation in sarcomeres.[99] We hypothesize there is even more lack of sarcomere structure present in the TNNI DKO-CM graft compared to *in vitro* due to the mechanical activity in the surrounding rat myocardium that causes disruption in the internal filamentous structures. There was no difference in graft size and apoptotic cells between WTC-CM and TNNI DKO-CM grafts (**Figure 3 D-E**), suggesting there is little to no difference in the engraftment capability between the contractile and non-contractile cardiomyocytes.

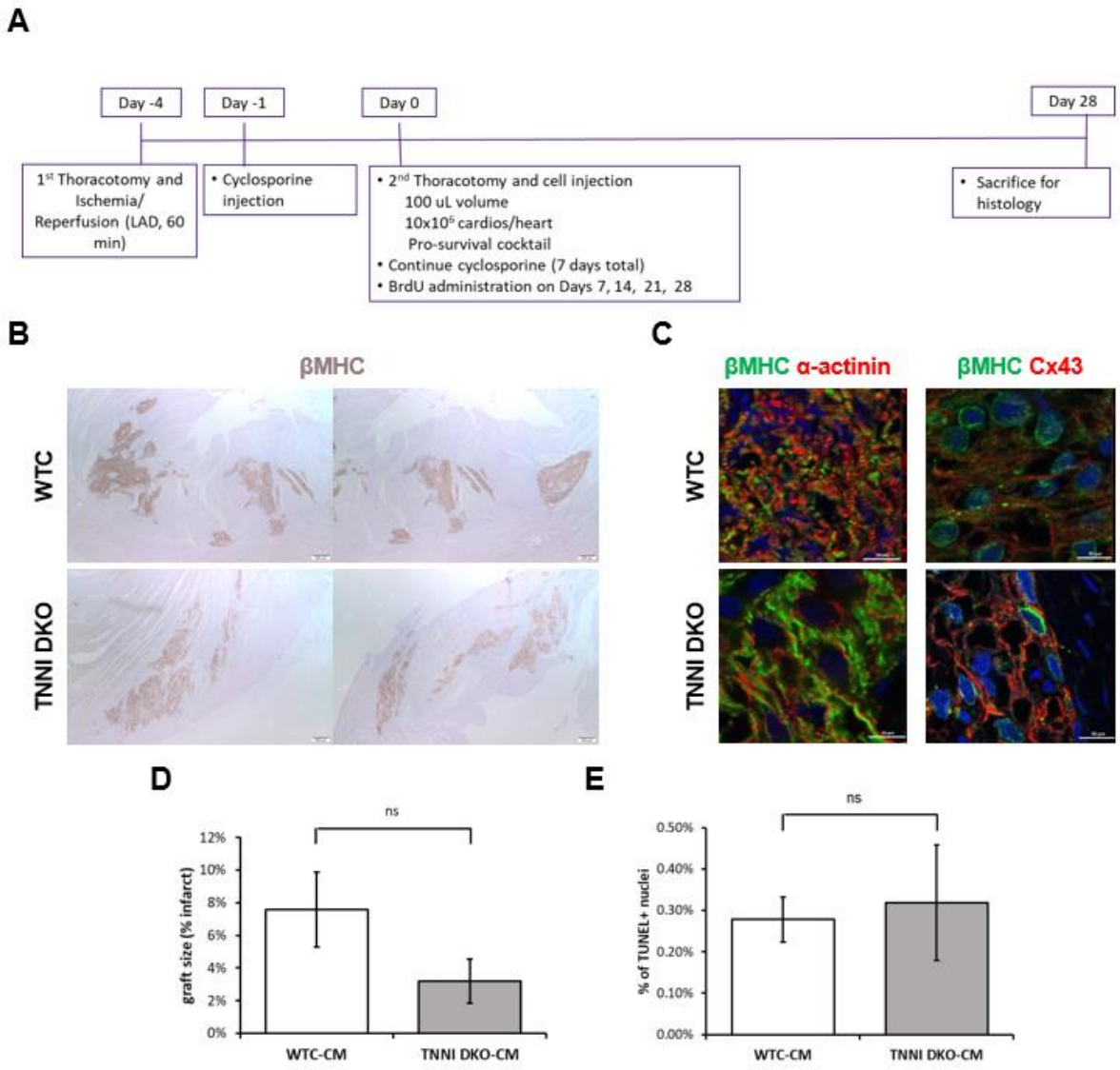

Figure 3 Non-contractile cardiomyocytes engraft in infarcted rat myocardium.

(A) Overview of experimental timeline for the pilot *in vivo* study to assess the engraftment of TNNI DKO-CMs in I/R injured rat hearts. **(B)** Representative immunohistochemistry images of human cardiac engraftment indicated by β-MHC (brown) in rat myocardium. **(C)** Representative immunofluorescence images of the engraftment stained for (left) α-actinin (red) and βMHC (green) show sarcomere striations in WTC-CM but no defined sarcomere structures in TNNI DKO and (right) connexin-43 (Cx43; red) and βMHC (green) show circular expressions of the gap junctions. Quantification shows there is no difference in **(D)** graft sizes and **(E)** apoptotic cell identified with TUNEL^{+} nuclei between WTC and TNNI DKO at 1 month post MI.

3.4.4 Graft Size is Bigger in Non-Contractile Cardiomyocytes than Contractile Cardiomyocytes at a Longer Transplantation Time Point

To investigate if mechanical contraction is needed to improve cardiac function after MI, athymic nude rats underwent ischemia/reperfusion injury to induce MI and received contractile cardiomyocytes (WTC-CM) or non-contractile cardiomyocytes (TNNI DKO-CM) or vehicle only (no cells) four days later. To compare the functional outcome from the three groups, we performed echocardiography one day before cell injection to establish the baseline and one month and three months after cell transplantation as well as cardiac magnetic resonance imaging (MRI) at three months post cell transplantation (**Figure 4A**). As observed previously, sarcomere structures were strikingly different between WTC-CM and TNNI DKO-CM at 3 months. WTC-CM showed sarcomere striations with better structural organization at 3 months than 4 weeks. However, TNNI DKO-CM still had no sarcomere structures at 3 months, consistent with the observations at 4 weeks (**Figure 4B**). Infarct size identified by picrosirius red staining was similar between the three groups at 3 months after either cell or vehicle injection with 26.1% infarct size for sham and 22.8% and 23.31% infarct sizes for WTC-CM and TNNI DKO-CM, respectively. (**Figure 4C**). However, graft sizes were significantly bigger in rats that received TNNI DKO-CM compared to those that received WTC-CM when compared against the size of both left ventricle and infarct (**Figure 4D-E**). This was an interesting finding, which the molecular mechanism underlying this difference will be explained further in Chapter 4.

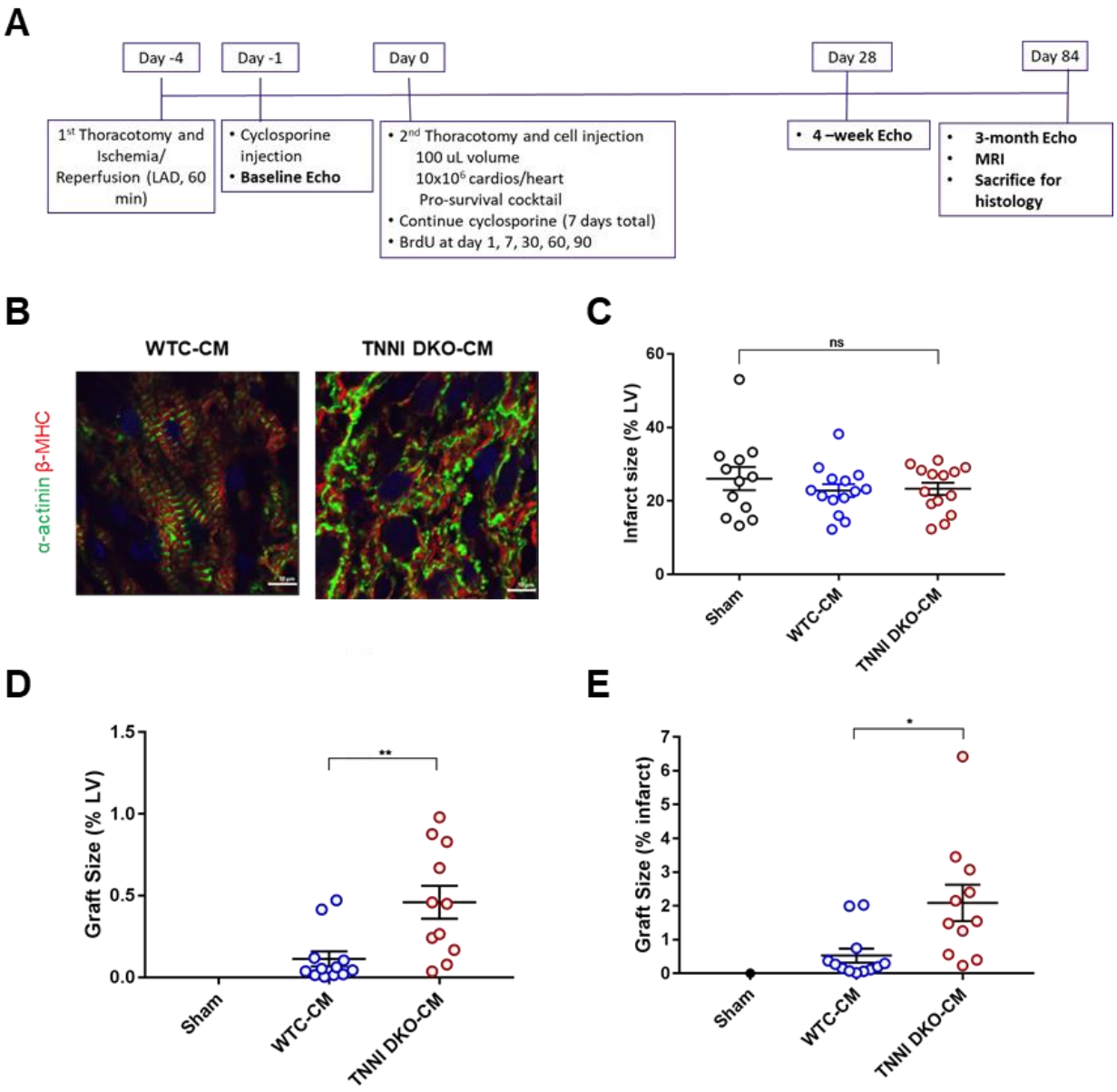

Figure 4 Non-contractile cardiomyocytes result in bigger engraftment at 3 months.

(A) Experimental timeline to evaluate cardiac function between rats that received contractile (WTC-CM) and non-contractile (TNNI DKO-CM) cardiomyocytes. **(B)** Representative immunofluorescence images of the engraftment stained for α-actinin (green) and βMHC (red) show WTC-CM forms striated sarcomeres but TNNI DKO-CMs do not form sarcomeres. **(C)** Infarct size shows no difference at 3 months between groups, normalized to LV area. Graft sizes normalized to **(D)** LV area and **(E)** infarct area both show bigger grafts in rats that received non-contractile cardiomyocytes. Data are mean±SEM. Significance assessed by one-way ANOVA for the infarct size and Student's t-test.for graft sizes. $p \leq 0.05$ (*), $p \leq 0.01$ (**), and $p \leq 0.001$ (***).

3.4.5 Force Production from the Engrafted Cardiomyocytes is Not Necessary to Improve Cardiac Function After MI in Rodent Model

To assess the functional effects of contractile and non-contractile cardiac grafts on global heart function after MI, echocardiography was performed at 4 weeks and 3 months post transplantation as well as cardiac magnetic resonance imaging at 3 months. Three months after vehicle injection, left ventricular systolic function, measured by fractional shortening, was significantly declined in control hearts, decreasing from 33.8±2.0% to 26.7±2.0%. However, there was no statistical difference in fractional shortening between baseline and 3 months for both cell-treatment groups (33.5±1.8% to 33.2±2.0% for WTC-CM and 32.3±1.7% to 34.6±2.3% for TNNI DKO-CM) (**Figure 5A**). Although there was no improvement in cardiac function compared to baseline within each cell treatment group at 3 months post transplantation, rats that received cell injection had greater fractional shortening at 3 months when compared to control ($p=0.040$ for sham versus WTC-CM and $p=0.009$ for sham versus TNNI DKO-CM at 3 months). Therefore, both contractile and non-contractile cardiomyocyte grafts were able to prevent further decline in systolic function after MI over the course of 3 months (**Figure 5B**). Assessment of the left ventricular ejection fraction (LVEF) by cardiac MRI at 3 months also showed a similar positive trend in LVEF in both contractile and non-contractile cardiomyocyte treatment groups compared to control (**Figure 5C**). Ejection fraction was 41.9±3.3% for sham and 50.3±3.0% and 50.1±%3.3 for WTC-CM and TNNI DKO-CM, respectively (**Figure 5D**). Taken together, these data suggest mechanical contraction in transplanted cardiomyocytes is not needed to improve global cardiac function after MI in rats.

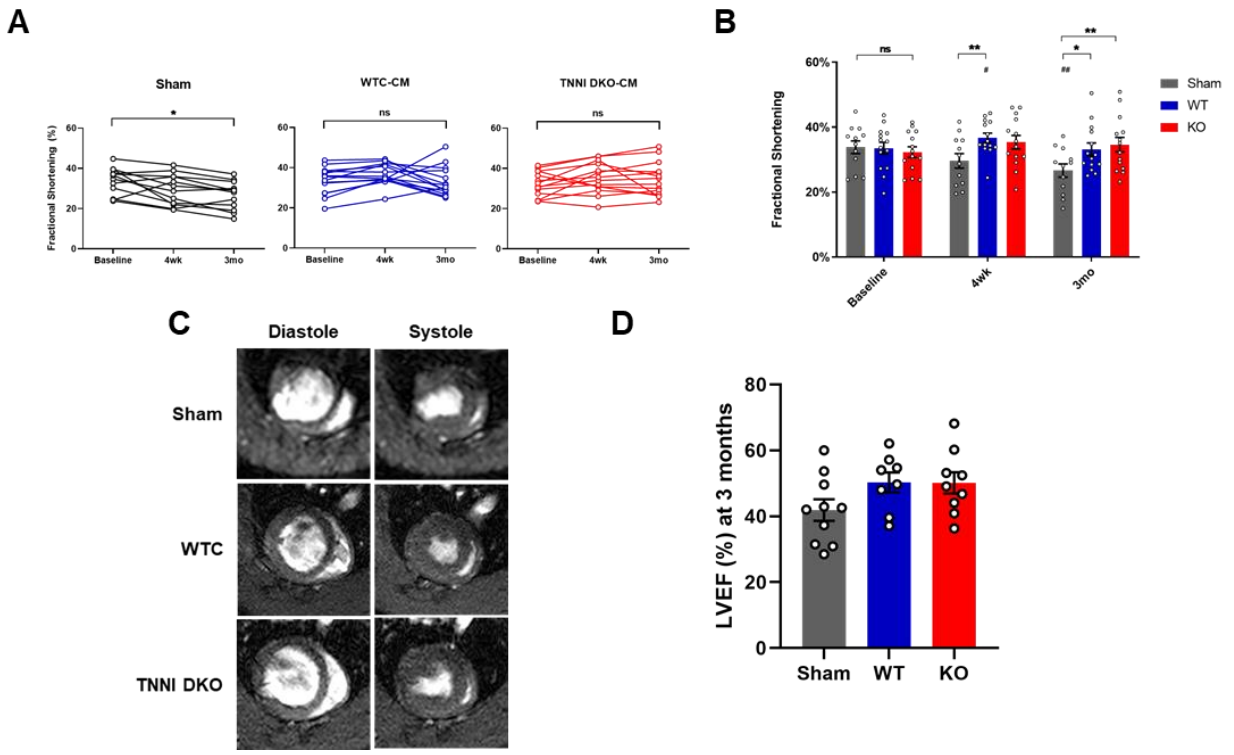

Figure 5 Both non-contractile and contractile cardiomyocytes grafts prevent further decline in global cardiac function after MI.

(A,B) Echocardiographic results (n = 12 infarcted rats receiving pro-survival cocktail only (sham), n = 14 infarcted rats receiving contractile cardiomyocytes (WTC-CM), and n=14 infarcted rats receiving non-contractile cardiomyocytes (TNNI DKO-CM)) of fractional shortening. Fractional shortening is reported at 72 hours post infarct (Baseline) and 4 weeks and 3 months post cell transplantation. Over the course of 3 months, sham group exhibited a worsened fractional shortening compared with their paired, baseline value at 72 hour post infarct (##, $p \leq 0.01$). At 3 months, fractional shortening was significantly greater in the hearts that received contractile or non-contractile cardiomyocytes compared with those that received vehicle only. **(C)** Representative short-axis MR images show hearts that received vehicle only (sham), contractile cardiomyocytes (WTC), or non-contractile cardiomyocytes (TNNI DKO). **(D)** Quantitative MRI evaluation of left-ventricular ejection fraction for infarcted rats receiving pro-survival cocktail only (n = 10), WTC-CM (n = 8), and TNNI DKO-CM (n = 9). Transplantation of both non-contractile and contractile hiPSC-CMs showed a trend of higher ejection fraction at 3 months, although it does not show statistical significance. Data are mean±SEM. Significance assessed by ANOVA and Student's t-test. $p \leq 0.05$ (*), $p \leq 0.01$ (**), $p \leq 0.001$ (***), $p \leq 0.05$ (#) when compared with Baseline, and $p \leq 0.01$ (##) when compared with Baseline.

3.5 Discussion

This study was designed to investigate the mechanical contribution from the transplanted cardiomyocytes in the overall cardiac function improvement after MI in rats. Previous studies have demonstrated the cardiac regenerative potentials of transplanting human stem cell-derived cardiomyocytes in MI animal models. It has been shown that transplanted cardiomyocytes remuscularize the infarcted regions by engrafting in the host myocardium.[17, 32] Formation of human myocardium has led to improvements in cardiac function in multiple acute MI models from rats to non-human primates.[17, 23, 24] However, it remains unclear if force production from the engrafted cardiomyocytes contributes to the overall systolic function and ultimate rescue of cardiac function. To address this gap in knowledge, we conducted a comparative *in vivo* study to evaluate the cardiac function after transplantation of contractile cardiomyocytes and non-contractile cardiomyocytes in acute MI rat model. If the transplantation of contractile cardiomyocytes leads to improved cardiac function while cardiac function continues to decline in non-contractile cardiomyocytes treatment group, this suggests mechanical contraction in cardiac grafts is a crucial component in the improvement of host cardiac function. However, if we observe no difference in cardiac function between the two cell treatment groups, this suggests mechanical contraction in the cardiac graft is not necessary to improve cardiac function.

To model non-contractile cardiomyocytes, we generated a hiPSC line without slow skeletal and cardiac troponin I (TNNI DKO). Upon differentiation, we confirmed mechanical quiescence in TNNI DKO-CMs and immunostaining showed TNNI DKO-CMs do not form sarcomeres with no troponin complex. Despite the absence of mechanical

activity and sarcomere formation, TNNI DKO-CMs had calcium transients with higher peak amplitudes and faster calcium reuptake mostly due to the absence of myofibrillar cTnC.

Initial *in vivo* engraftment study demonstrated that mechanical contraction in transplanted cardiomyocytes does not affect engraftment as both contractile and non-contractile cardiomyocytes resulted in robust cardiac grafts at 1 month post MI. Mature sarcomere structures were seen in wildtype grafts, indicating enhanced maturation process upon *in vivo* transplantation.[99] However, TNNI DKO grafts did not have defined sarcomere structures, consistent with *in vitro* findings. For the functional study, contractile and non-contractile cardiomyocytes were injected into I/R injured rat hearts and cardiac function was assessed at 1 month and 3 months post transplantation with echocardiography and cardiac MRI. Both contractile and non-contractile hiPSC-CMs groups preserved cardiac function after MI as control continued to decline in function. Furthermore, both cell treatment groups showed improved systolic function compared to control at 3 months after cell injection. From these results, we conclude that mechanical contraction in the cardiac graft does contribute to the improvement of the host cardiac function after MI in rats.

However, it is important to note that the species mismatch between the grafted cells and the host seems to have an impact on the magnitude of the improvement seen in cardiac function after cell injection. In rat MI models, injection of human cardiomyocytes leads to prevention of further decline in cardiac function and, at best, slight functional improvement.[17, 100] However, when human cardiomyocytes are injected after MI in to the closest available animal model to humans, non-human primates, significant improvement

in cardiac function is reported, restoring function to similar levels pre-MI.[24] This may be suggesting the differences in electrical properties between rodent and human could prevent electromechanical coupling from contributing to the additional improvement in cardiac function.[101, 102] Also, the mismatch of endogenous beating frequencies between rodent and human could add another barrier to a successful long term graft-host integration.[103] It is possible that the secreted paracrine factors, subsequent tissue remodeling, modulation of innate immunity, and increase in myocardium mass from cardiomyocyte transplantation are needed to prevent further decline in cardiac function while the addition of mechanical contraction is necessary to restore cardiac function to healthy levels. To investigate this, future studies should address this limitation of species mismatch by conducting a comparative *in vivo* study by injecting contractile and non-contractile rat iPSC-CMs into rat MI models or human iPSC-CMs into non-human primate.

For the first time, we have directly compared functional benefits of transplanting contractile and non-contractile hiPSC-CMs in rats after MI to uncover underlying mechanism for the improvement in cardiac function. In order to optimize the best therapeutic approach to repair the heart after MI, it will be important to directly compare cardiac function after transplantation of non-contractile cardiomyocytes, non-cardiomyocytes from cardiac lineage, and an immune response activator to understand which method leads to the best regenerative outcome.

Chapter 4. Define the Relationship Between Sarcomere Assembly and Mitosis Through Cyclin B1

This chapter has been published in *Cell Reports*:

Anthony M. Pettinato*, **Dasom Yoo***, et al. “Sarcomere Function Activates a p53-dependent DNA damage response that promotes polyploidization and limits *in vivo* cell engraftment” Cell Reports, 2021, * equal contribution.[104]

This work is a collaboration between Dasom Yoo, Dr. Xiulan Yang, Dr. Michael Regnier, and Dr. Charles Murry at the University of Washington and Dr. Travis Hinson’s group at The Jackson Laboratory and UConn Health. Of the following described experiments, iPSC-CM preparation, flow cytometry analysis for ploidy and CCNB1+ CMs, protein lysate preparation for western blot, *in vivo* engraftment study, histology, and quantification of histological analysis were completed by Dasom Yoo. The methods for *in vivo* study reported herein were described previously in Chapter 3. All other experiments were performed by the Hinson group.

4.1 Abstract

The adult cardiomyocyte has minimal regenerative capacity but can replicate DNA resulting in progressive mononuclear polyploidization by unclear mechanisms. We collaborated with Dr. Travis Hinson at The Jackson Laboratory and UConn Health to discover an unexpected signaling role contracting sarcomeres has in the regulation of cyclin B1 levels through p53 activation. A human cardiomyocyte model was developed to study polyploidization by fusing GFP to endogenous cyclin B1 (CCNB1) in pluripotent

stem cells with CRISPR technology. Then using an iPSC-based CRISPR genome-wide screen, we discovered p53 as an activator for cardiomyocyte polyploidization. Through single cell transcriptomics and epigenetic analyses, we discovered the contracting sarcomeres are the activator of p53 signaling, which results in cardiomyocyte polyploidization. To confirm the relationship between the sarcomeres and cardiomyocyte polyploidization experimentally, we used two independent iPSC models that cannot assemble sarcomeres – TNNT2 knock-out (cTnT-KO) and slow skeletal and cardiac troponin I knock-out (TnI DKO). Due to the absence of troponin T and Troponin I, cTnT KO-CMs and TnI DKO-CMs did not contract. Upon differentiation into cardiomyocytes, both cTnT KO-CMs and TnI DKO-CMs exhibited decreased polyploidization and expressed lower p21 levels, a direct p53-target, compared to WT-CMs.[105] Also, TnI DKO-CMs showed higher expression of CCNB1 at both Days 14 and 30 relative to WT-CMs. To test if disruption in sarcomere assembly in WT-CMs would lead to a decrease in p21, we treated WT-CMs with verapamil and saw decreased p21 and increased CCNB1 expressions. Also, WT-CMs transduced with lentivirus to overexpress CCNB1 showed decreased polyploid population, confirming polyploidy can be reduced with either sarcomere disruption or overexpression of CCNB1. We then tested whether oxidative phosphorylation could be a causal link between sarcomere assembly and p53 activation. Flow cytometry analysis and seahorse assay of cTnT KO-CMs showed reduction in superoxide production and oxygen consumption rates, respectively. Next, we wanted to assess if these phenotypes of sarcomere-deficient cardiomyocytes could be exploited to improve cardiac engraftment upon *in vivo* transplantation after MI. To test this, rats underwent ischemia/reperfusion surgery to induce MI, followed by cell injection (WT or

TnI DKO-CMs) and periodic bromodeoxyuridine (BrdU) injections to evaluate graft proliferation rate. At three months post transplantation, TnI DKO-CMs showed significantly larger engraftment compared to WT-CMs. BrdU quantification revealed TnI DKO-CMs are more proliferative than WT-CMs even at 3 months post transplantation, which may explain the enhanced graft size. Thus, we demonstrate an unexpected signaling role for the sarcomere assembly in the regulation of CCNB1 levels through p53 activation.

4.2 Introduction

The adult human heart is characterized by insufficient regenerative capacities due to low rates of existing cardiomyocyte renewal and the lack of cardiomyocyte progenitor pool.[46, 106] The cardiac regeneration is known to be inversely correlated with cardiomyocyte polyploidization rates. In zebrafish, it has been shown that cardiac regeneration is completely suppressed by induction of polyploidization, identifying cardiomyocyte polyploidization as a barrier to heart regeneration.[107] Polyploidization has also been demonstrated to regulate mammalian cardiac regeneration in mouse model.[51] However, it is still not fully understood how mammalian cardiomyocyte polyploidization is regulated, and discovering the mechanism could provide new insights into cardiac regeneration. Before the second decade of human life, the majority of cardiomyocytes become mononuclear polyploid. Although both the total number of cardiomyocytes and number of nuclei per cardiomyocyte do not significantly change during this process, the average DNA content per cardiomyocyte increases 1.7 fold.[45] This transition of mononuclear polyploidy suggests that the human cardiomyocyte primarily lacks the

capacity to undergo mitosis. Due to the lack of model for human cardiomyocyte polyploidization and scarcity of human heart samples, there is a gap in our understanding about the molecular mechanisms underlying human cardiomyocyte polyploidization. To address this issue, we engineered a cellular model to study human cardiomyocyte polyploidization using induced pluripotent stem cell (iPSC) and CCNB1 as a reporter on Gap 2/mitosis (G2/M) cell cycle status. Using a CRISPR screen, we demonstrate that p53 is a regulator of polyploidy through CCNB1 inhibition. We then identified a list of polyploidy-associated enhancers and enrichment motifs. Cardiomyocytes activate p53 through a DNA damage response regulated by sarcomere assembly that ultimately results in cardiomyocyte endocycling. Finally, we demonstrate that polyploidization can be suppressed by sarcomere disassembly or CCNB1 overexpression.

4.3 Materials and Methods

4.3.1 IPSC-Cardiomyocyte Preparation

Following the directed differentiation described previously, cells underwent metabolic selection on day 13 with glucose-free DMEM (Gibco) supplemented with 4 mM lactate (Sigma) for 48 hours. Following lactate treatment, cells were trypsinized and replated onto fibronectin-coated tissue culture plates (Fisher) in RPMI + B27 supplement + 10 μM ROCK inhibitor Y-27632 + 5% FBS (BioWest).

4.3.2 Flow Cytometry Analysis

Flow cytometry analysis was performed using a BD FACSCanto and data were acquired with the BD FACSDIVA software. Cells were fixed and prepared following the protocol described previously. For ploidy and CCNB1 expression analysis, fixed cells were incubated for 1 hour in room temperature with mouse cyclin B1 antibody (ThermoFisher MA5-14319, 1:100) or mouse immunoglobulin G1 isotype control in PBS + 5% FBS + 0.75% saponin. After a spin down and wash, cells were incubated for 45 minutes in room temperature with goat anti-mouse 488 secondary and 10 µM Hoechst 33342 (ThermoFisher) in PBS + 5% FBS + 0.75% saponin. Analysis was performed using FloJo version 10 software.

4.3.3 Western Blotting

To obtain protein lysates, cells were washed once with PBS and then lysed in RIPA buffer (Cell Signaling) containing protease inhibitor cocktail (Roche), 1 mM PMSF, and phosphatase inhibitor (Pierce). Lysates were centrifuged to remove cell debris, quantified, and normalized via Pierce BCA (Thermo) and then reduced and denatured in sample buffer (Thermo). Protein lysates were separated on 4-20% Mini-PROTEAN TGX precast gels (Bio-Rad), transferred onto PVDF membranes (Bio-Rad), washed once in TBS-T (50 mM Tris-Cl, 150 mM NaCl, 0.1% TWEEN-20), blocked for 1 hour in TBS-T with 5% BSA (Fisher), and then probed overnight with primary antibody in TBS-T with BSA. The following day, blots were washed three times in TBS-T for 15 minutes, probed for 1 hour at room temperature with HRP-linked secondary antibody (Cell Signaling), and then washed three times in TBS-T for 15 minutes. Signal detection was performed using

ECL substrate (Thermo) and a Bio-Rad ChemiDoc MP imaging system. Blot images were digitally processed and analyzed in ImageJ. The primary antibodies used were: 1:500 mouse anti-cardiac troponin T (Invitrogen), 1:1000 rabbit anti-p53 (Cell Signaling), 1:1000 rabbit anti-p21 (Cell Signaling), 1:1000 rabbit anti-phospho-Histone H2A.X (Cell Signaling), 1:1000 rabbit anti-phospho-cyclin B1 (Cell Signaling), and 1:1000 rabbit anti-GAPDH (Cell Signaling).

4.3.4 *In vitro* Cardiomyocyte Proliferation Experiments

HiPSC-CMs were replated onto fibronectin-coated glass cover slides as described above. The following day, hiPSC-CMs were treated with 10 μM EdU (Click-iT Plus EdU 488 imaging kit; Thermo C10637) in RPMI + B27 supplement for 4 hours. After EdU treatment, cells were washed with PBS and fixed in 4% paraformaldehyde. Fixed cells were incubated with mouse α-actinin (1:100) in PBS + 5% FBS + 0.75% saponin for 1 hour in room temperature. Then the cells were incubated with goat anti-mouse 594 (ThermoFisher A11005, 1:200) and Alexa Fluor 488 (provided in the Click-iT Plus EdU kit).

4.3.5 Immunohistochemical Analysis

To quantify cell proliferation in the grafts, sections were incubated overnight with MYH7 antibody followed by a one hour incubation with rabbit anti-mouse 488 (ThermoFisher, 1:100). Subsequently, sections were incubated overnight with either peroxidase-conjugated anti-BrdU primary antibody (Roche, 1:40) followed by AF647

tyramide (ThermoFisher) to amplify BrdU and 10 μM Hoechst 33342 or Alexa Fluor 647 Mouse anti-Ki67 antibody (BD Biosciences 558615, 1:20) overnight in the dark. Cardiomyocyte proliferation was quantified by counting $BrdU^+$ and βMHC^+ double-stained cells or $Ki67^+$ and βMHC^+ from images captured on a Nikon A1R confocal microscope.

Apoptotic cells were identified with Click-iT Plus Terminal deoxynucleotidyl transferase dUTP nick end labeling (TUNEL) Assay with Alexa Fluor 594 dye (ThermoFisher C10618) using the manufacturer's protocol. Briefly, paraffin-embedded tissues sections were deparaffinized initially in xylene followed rehydration in serial dilutions of EtOH. Slides were then fixed in 4% paraformaldehyde for 15 minutes at 37°C, washed twice in PBS, and permeabilized with Proteinase K at room temperature for 15 minutes. After permeabilization, slides were fixed in 4% paraformaldehyde for 5 minutes at 37°C. Positive control slides were treated with DNAse I and incubated at room temperature for 30 minutes. Terminal deoxynucleotidyl transferase reaction and Click-iT Plus reaction were performed using the components in the kit. Slides were then incubated with 10 μM of 1X Hoechst 33342 for 30 minutes in the dark. To identify grafts, serial sections were deparaffinized and incubated with mouse MYH7 antibody (Developmental Studies Hybridoma Bank A4.951, supernatant) and rabbit α-actinin (Abcam ab68167, 1:100) overnight, followed by a one hour incubation with goat anti-rabbit 568 (Invitrogen A11011, 1:100) and goat anti-mouse 488 (Invitroge A11001, 1:100) and 30 minutes incubation with 10 μM of 1X Hoechst 33342 in the dark. Apoptotic cells were quantified by counting $TUNEL^+$ nuclei in the βMHC^+ positive graft regions from images captured on a high-resolution widefield microscope.

4.3.6 Statistical Analysis

All histological measurements were performed using ImageJ and statistical analysis were done in either Excel or Prism GraphPad. Data were presented as mean ± standard error of the mean (SEM). Statistical comparisons were conducted via Student's t-test or one-way ANOVA.

4.4 Results

4.4.1 Sarcomere Function Inhibits CCNB1 Through p53 Activation

We used an iPSC line with the endogenous CCNB1 fused to GFP to study polyploidization in human cardiomyocytes (Appendix B. **Figure S21**). Upon iPSC-based CRISPR genome-wide screening of polyploid (4n CCNB1+ for G2/M and 4n CCNB1- for arrested cell cycle) and diploid (2n) CMs, we discovered p53 as an activator for cardiomyocyte polyploidization by inhibiting CCNB1 expression (Appendix B. **Figure S22**). Through single cell transcriptomics and epigenetic analyses performed by the Hinson group, we discovered sarcomere assembly to be the p53 activator by identifying sarcomere transcripts like TNNT2 and MYH6 preceded the expression of p53 downstream targets such as CDKN1A and GADD45A. To study the role of sarcomere function in CM replication and polyploidization, we engineered sarcomere assembly-deficient CM models based on knowledge that the troponin (Tn) complex is necessary for sarcomere assembly and contractile function.[108, 109] We used CRISPR/Cas9 to generate iPSC lines containing either a homozygous frameshift in TNNT2 (denoted cTnT-KO) and one harboring frameshift mutations in both *TNNI1* and *TNNI3* (encoding skeletal and

cardiac troponin I, respectively; denoted TnI-DKO). The engineered CMs showed the expected absence of their respective troponin isoforms (**Figure 6E-G**), and neither KO line visibly contracted, in contrast to wildtype (WT) CMs that spontaneously contract. Correspondingly, α-actinin immunofluorescence revealed that both KO lines had impaired sarcomere formation, lacking the well-formed Z-disks that result from myofibril bundling (**Figure 6A**). In support of our hypothesis, we observed decreased polyploidization in sarcomere-deficient CMs compared to controls (**Figure 6B-C**), increased CCNB1+ CMs at two different post differentiation time points (**Figure 6D**), and increased positivity of EdU, Ki67, Aurora, and p-H3, indicating higher proliferation in sarcomere-deficient CMs (**Figure S23**). We next tested whether CCNB1 overexpression could prevent the high polyploidization and low CCNB1 observed in sarcomere-containing CMs. We transduced lentivirus encoding CCNB1 fused to a nuclear localization signal (NLS-CCNB1), as we found that nuclear CCNB1 promoted mitosis, to provide overexpression co-incident with sarcomere assembly in WT CMs, which reduced CM polyploidization and increased the proportion of CCNB1+ CMs. Taken together, these results demonstrate that myofibrils promote polyploidization, and this can be antagonized by enhancing CCNB1 levels.

With multiple datasets implicating a link between the sarcomere and p53 activation in promoting polyploidization and CCNB1 inhibition, we analyzed WT, cTnT-KO, and TnI-DKO lysates for relevant protein marks. We confirmed increased p-CCNB1 and decreased p21 in both Tn-KO models (**Figure 6E-H**), similar to our p53 genetic KD studies. Unlike p53 KD, however, total p53 levels were not consistently different in Tn-KO CMs relative to WT. Additionally, treatment with verapamil, an L-type calcium channel blocker that inhibits sarcomere function, also demonstrated a similar molecular phenotype

including increased p-CCNB1, decreased p21, and no change in total p53 protein levels (**Figure 6I-J**).[110, 111] As total p53 levels may not reflect p53 activity and p21 can be activated by other factors, we additionally studied WT and cTnT-KO CMs by p53 ChIP-qPCR targeting known p53-enriched response elements on *CDKN1A*.[112-114] Relative to WT, we found decreased enrichment of p53 at polyploidy-associated *CDKN1A* response elements in cTnT-KO CMs (**Figure 6K**), suggesting that inhibiting sarcomere assembly decreases p53 activity through a post-translational mechanism.

Direct molecular connections between sarcomere function and p53 activation have not been well established in human cardiomyocytes. We hypothesized that sarcomere function could regulate p53 through a DNA damage response, as sarcomere gene expression was related to activation of oxidative stress pathways by pseudotime, and polyploid CMs exhibited increased oxidative signaling pathway activation. To test this, we measured levels of both phospho-H2AX, an epigenetic marker of DNA damage, and 8-oxo-2'-deoxyguanosine (8-OHdG), a DNA-level marker highly-specific for oxidative damage.[115, 116] Both markers exhibited decreased levels in the absence of sarcomere assembly (**Figure 6L-N**). To assess potential sources of sarcomere-dependent oxidative damage, we quantified mitochondrial mass and superoxide production by flow cytometry analysis of MitoTracker- and MitoSOX-stained CMs, respectively (**Figure 6O**). We observed reductions in both parameters in the absence of sarcomere assembly, as well as reductions in oxygen consumption rates (**Figure 6P-Q**). To test whether inhibition of oxidative stress could rescue the reduced proportion of CCNB1+ CMs observed in sarcomere-containing CMs, we treated WT CMs with the antioxidant N-acetylcysteine

(NAC). NAC increased the proportion of CCNB1+ CMs and reduced polyploidization (**Figure S24A**).

To identify potential molecular linkages between sarcomere function and oxidative metabolism, we hypothesized that sarcomere function-dependent changes in ATP hydrolysis could be sensed by AMP-activated protein kinase (AMPK), which is an activator of oxidative metabolism.[117] To test this, we measured the levels of AMPK phosphorylation (p-AMPK) in cTnT-KO relative to WT CMs. We observed that cTnT-KO relative to WT CMs exhibited reduced p-AMPK levels (**Figure 6R-S**), which was similarly observed after acute inhibition of sarcomere function using verapamil (**Figure 6T-U**). While AMPK can also be activated by calcium, we found no differences in calcium transients between cTnT-KO relative to WT CMs (Figure S6D), and verapamil treatment had no effect on p-AMPK levels in cTnT-KO cells despite inhibition of calcium transients (**Figure S24B-D**).[117] Taken together, these functional studies illuminate how the sarcomere promotes polyploidization through metabolic reprogramming in association with AMPK activation, oxidative stress, and ultimately p53 activation.

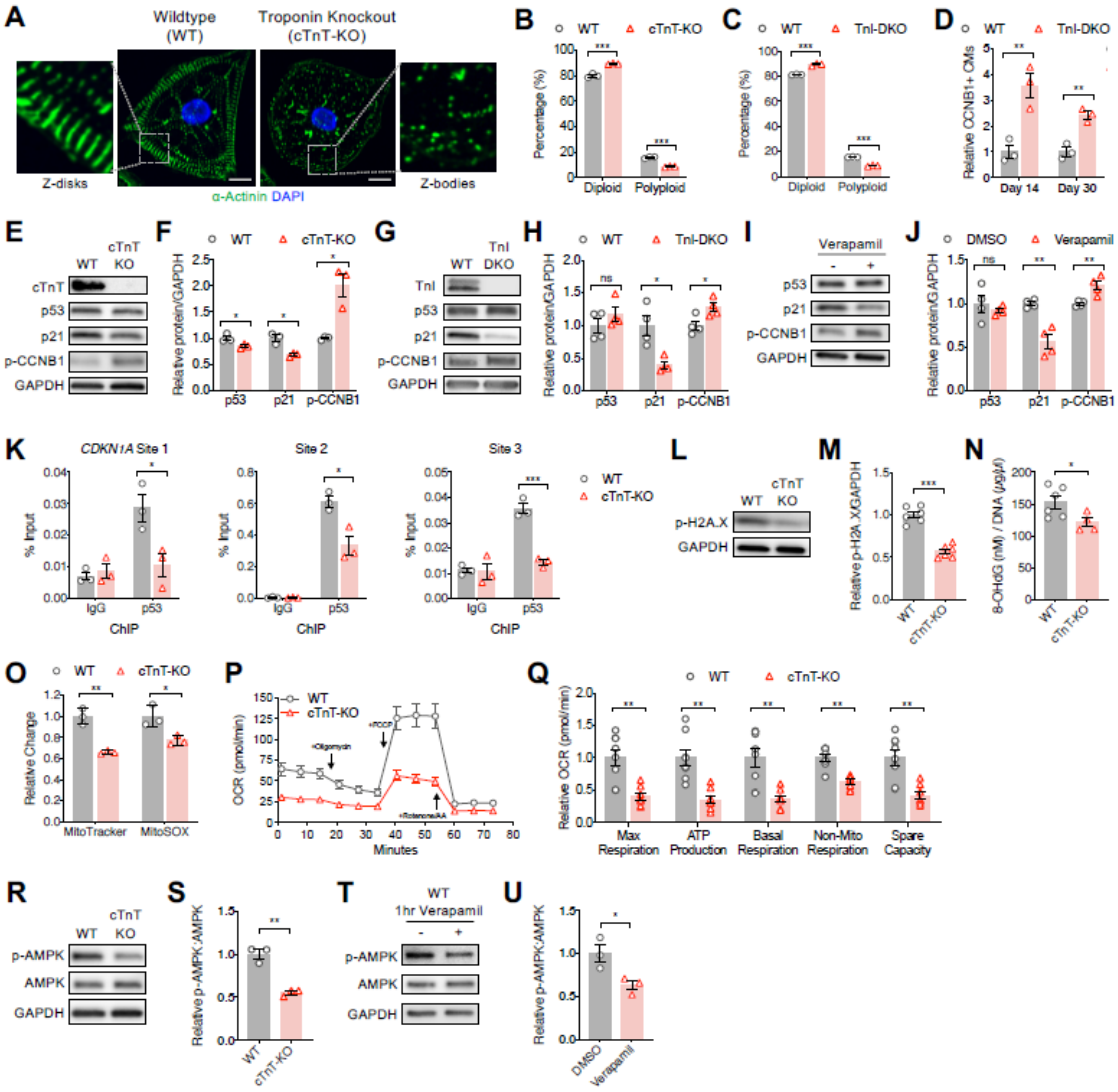

Figure 6 Cellular and molecular consequences of sarcomere assembly.

(A) Representative confocal images of wildtype (WT) control and cardiac troponin T knockout (cTnT-KO) CMs stained for α-actinin (green; sarcomere Z-disk) and DAPI (blue; nuclei). KO of troponin, either cTnT-KO or double KO of skeletal and cardiac troponin I (TnI-DKO), leads to lack of striated sarcomere Z-disks. Scale bar = 10 μm. **(B)** Flow cytometry of Hoechst-stained CMs demonstrates decreased polyploidy in cTnT-KO and **(C)** TnI-DKO CMs relative to WT. **(D)** Flow cytometry of CCNB1-stained WT and TnI-DKO CMs demonstrates increased relative CCNB1 expression in TnI-DKO CMs, which reduces with age. **(E)** Representative immunoblots with **(F)** quantification of protein lysates from WT and cTnT-KO CMs probed for cTnT, p53, p21, phospho-CCNB1, and GAPDH. **(G)** Representative immunoblots with **(H)** quantification of protein lysates from WT and TnI-DKO CMs probed for TnI (cardiac and skeletal), p53, p21, p-CCNB1, and GAPDH. **(I)** Representative immunoblots with **(J)** quantification of protein lysates from Day 20 WT CMs treated with verapamil from Day 9 and probed for p53, p21, p-CCNB1, and GAPDH. **(K)** Anti-p53 ChIP-

qPCR of WT and cTnT-KO CMs targeting previously-reported p53-bound ChIP-seq peaks directly upstream of *CDKN1A* [114], which demonstrates decreased p53 binding of *CDKN1A* in cTnT-KO CMs at three separate genomic sites (see Figure 3D). **(L)** Representative immunoblots probed for phospho-H2AX and GAPDH with **(M)** quantification demonstrates sarcomere assembly activates a DNA damage response in WT CMs. **(N)** Quantification of genomic DNA lysates from WT and cTnT-KO CMs probed via ELISA for 8-OHdG, a marker of oxidative DNA damage. **(O)** Flow cytometry quantification of MitoTracker and MitoSOX dyes in WT and cTnT-KO CMs demonstrates reduced mitochondrial content and ROS in cTnT-KO CMs. **(P)** Seahorse Mito Stress oxygen consumption rates (OCR) with **(Q)** quantification shows a decrease in respiration across all parameters in cTnT-KO CMs compared to WT, demonstrating that sarcomere assembly promotes oxidative metabolism. **(R)** Representative immunoblots with **(S)** quantification of protein lysates from WT and cTnT-KO CMs probed for p-AMPK, AMPK, and GAPDH. **(T)** Representative immunoblots with **(U)** quantification of protein lysates from WT CMs treated with verapamil for 1 hr and probed for p-AMPK, AMPK, and GAPDH. Data are n≥3 and mean±SEM; significance assessed by t-test and defined by $P > 0.05$ (ns), $P \leq 0.05$ (*), $P \leq 0.01$ (**), and $P \leq 0.001$ (***).

4.4.2 Inhibiting Sarcomere Function Enhances CM Engraftment and Proliferation in a MI Model

As sarcomere function decreased CM replication and increased polyploidization, we hypothesized that inhibiting sarcomere formation could improve CM engraftment in a myocardial infarction (MI) rat model, since improving engraftment rates has been a long-standing obstacle for cell therapy strategies.[118, 119] To test this, rats underwent ischemia/reperfusion (I/R) surgery to induce acute MI, followed by injection of $1x10^7$ human CMs (WT or TnI-DKO) four days later (**Figure 7A**), as we have previously described.[120, 121] Bromodeoxyuridine (BrdU) was injected periodically to measure DNA synthesis, and rats were sacrificed 3 months post-transplantation for histological analysis. Sections of the left ventricle (LV) were immunohistochemically stained for β-myosin heavy chain (β-MHC), the predominant isoform expressed in human CMs, which was used to visualize the human-derived graft (**Figure 7**). WT CMs produced a mean graft size of 0.11

± 0.05% of the LV, while TnI-DKO CMs produced a size of 0.46 ± 0.10%, more than four-fold larger (**Figure 7C**; P=0.0041), demonstrating improved *in vivo* cardiac engraftment when transplanting TnI-DKO CMs. Additionally, immunofluorescence was performed on LV sections to assess proliferation of human CMs following *in vivo* engraftment using cumulative BrdU incorporation and active Ki67 expression as markers. Sections were labeled for β-MHC (human CMs), Hoechst (nuclei), and either BrdU (**Figure 7D**) or Ki67 (**Figure 7F**). BrdU staining demonstrated that WT CMs were 0.40 ± 0.22% BrdU+, while TnI-DKO CMs were 1.52 ± 0.30% BrdU+ (**Figure 7E**; P=0.012), and Ki67 staining demonstrated that WT CMs were 0.14 ± 0.08% Ki67+, whereas TnI-DKO CMs were 0.50 ± 0.10% Ki67+ (**Figure 7G**; P=0.021). To also assess the contribution of cellular apoptosis to the engraftment phenotypes, we performed terminal deoxynucleotidyl transferase dUTP nick end labeling (TUNEL) assays at 3 months post-engraftment, in which we observed no difference in apoptosis between WT and TnI-DKO CMs (**Figure 8**). We conclude that mechanical contraction from sarcomeres impairs CM engraftment and remuscularization after cell therapy, in part, through reduced replicative capacity.

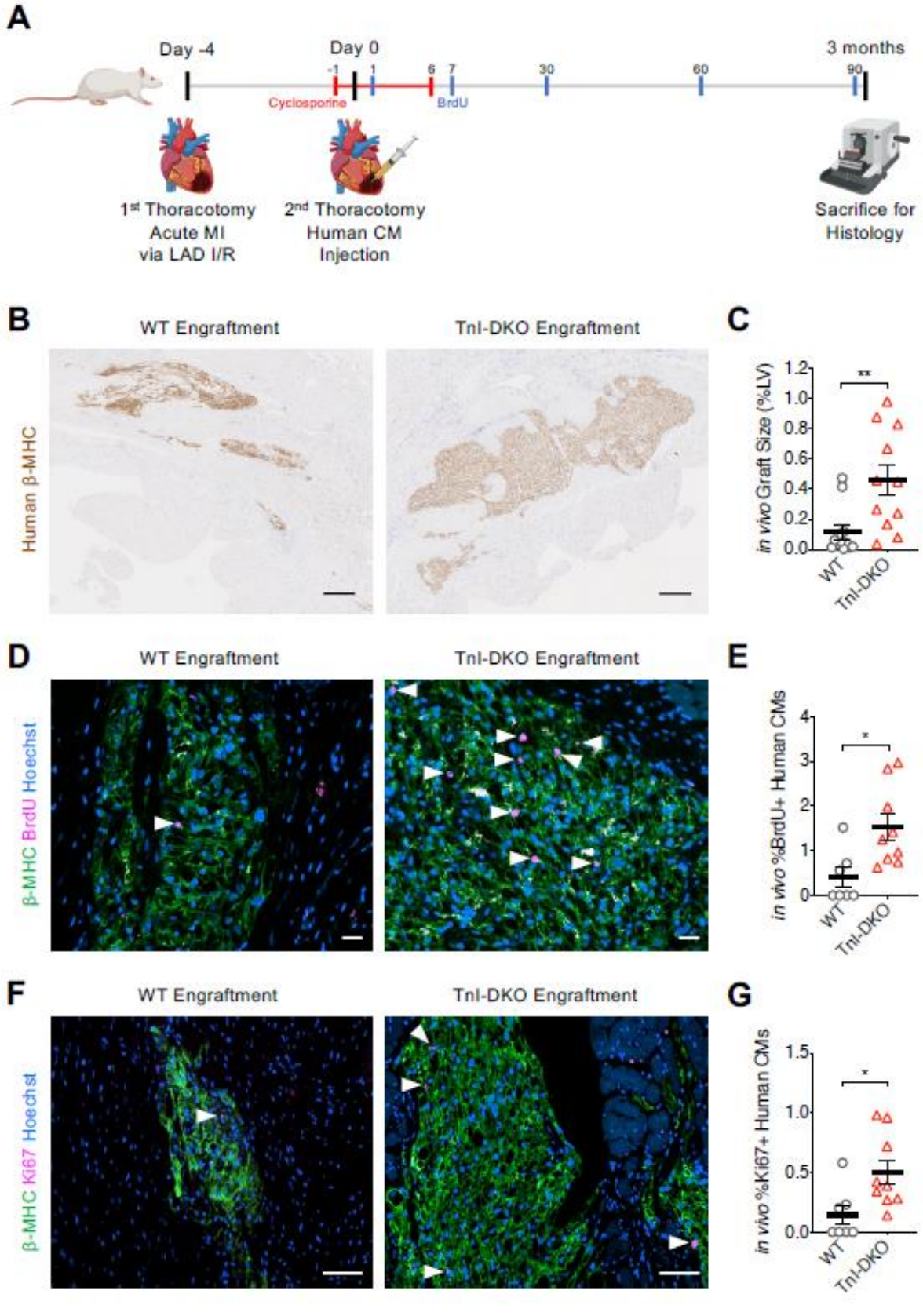
A
Day -4
Day 0
3 months
-1
1
6
7
30
60
90
Cyclosporine
BrdU
1st Thoracotomy
Acute MI
via LAD I/R
2nd Thoracotomy
Human CM
Injection
Sacrifice for
Histology
B
WT Engraftment
TnI-DKO Engraftment
Human β-MHC
C
in vivo Graft Size (%LV)
1.2
1.0
0.8
0.6
0.4
0.2
0.0
**
WT
TnI-DKO
D
WT Engraftment
TnI-DKO Engraftment
β-MHC BrdU Hoechst
E
in vivo %BrdU+ Human CMs
4
3
2
1
0
*
WT
TnI-DKO
F
WT Engraftment
TnI-DKO Engraftment
β-MHC Ki67 Hoechst
G
in vivo %Ki67+ Human CMs
1.5
1.0
0.5
0.0
*
WT
TnI-DKO

Figure 7 Sarcomere-deficient CMs enhance *in vivo* cardiac engraftment.

(A) Overview of experimental workflow used to study *in vivo* cardiac engraftment of human CMs using a rat model of myocardial infarction (MI). Four days prior to cell injection (Day -4), the 1st thoracotomy was performed to induce acute MI through ischemia/reperfusion (I/R) ligation of the left anterior descending (LAD) artery. One day prior to cell injection (Day -1), cyclosporine was injected and continued for seven consecutive days. The following day (Day 0), a 2nd thoracotomy was performed and WT or TnI-DKO CMs were injected. At Days 1, 7, 30, 60, and 90, BrdU was injected, and rats were sacrificed 3 months post-cell transplantation. **(B)** Representative immunohistochemistry images (scale bar = 250 um) and **(C)** quantification of 3,3'-diaminobenzidine (DAB) stained human β-myosin heavy chain (β-MHC) to asses human CM graft size in rat left ventricle (LV) sections, which demonstrated improved graft size when using TnI-DKO CMs relative to WT. **(D)** Representative immunofluorescence images (scale bar = 25 um) and **(E)** quantification of rat LV sections probed for β-MHC (green; stains human CMs), Hoechst (blue; stains nuclei), and BrdU (magenta; cumulative proliferation), which demonstrates increased %BrdU+ human CMs when using TnI-DKO CMs for engraftment relative to WT, suggesting enhanced proliferation capacity of these cells. **(F)** Representative immunofluorescence images (scale bar = 50 um) and **(G)** quantification of Ki67 (magenta; active proliferation) nuclei. Data are n≥3 and mean±SEM; significance assessed by Student's t-test and defined by $p \leq 0.05$ (*) and $p \leq 0.01$ (**).

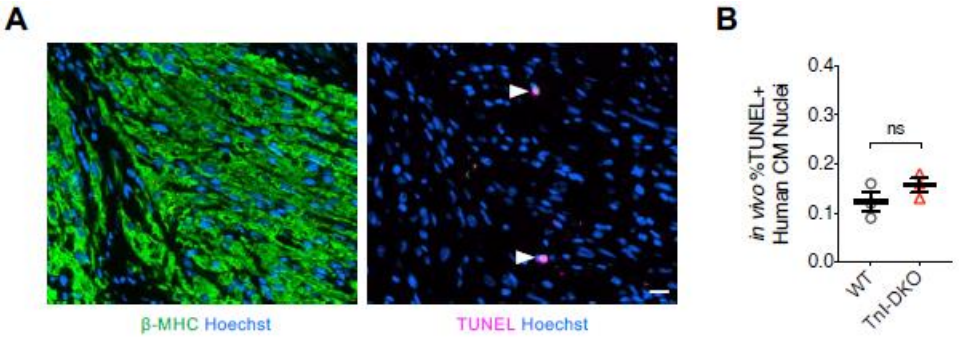

Figure 8 Apoptotic staining of human CMs following *in vivo* engraftment.

(A) Representative immunofluorescence images of 3 month post transplantation human CM grafts and **(B)** quantification of rat LV sections probed for terminal deoxynucleotidyl transferase dUTP nick end labeling (TUNEL; magenta) to quantify the apoptotic status of human WT and TnI-DKO CMs 3 months post-engraftment. β-MHC (green; human CMs) and Hoechst (blue; nuclei) were used to stain the adjacent section to identify the human CM graft region. Scale bar = 25 μm. Data are n≥3 and mean±SEM; significance assessed by t-test and defined by $P > 0.05$ (ns).

4.5 Discussion

The principal finding of this study is that human cardiomyocyte polyploidy and cell cycle arrest are driven by downregulation of cyclin B1 by the tumor suppressor p53. We provide evidence that p53 is activated through a DNA damage response that is promoted by reactive oxygen species, which appear to result from mitochondrial metabolism that is enhanced by sarcomere contraction, the principal ATP-consuming process of the cardiomyocyte. We show that this pathway can be exploited to enhance cardiac engraftment following cell transplantation in a rat model of myocardial infarction.

MIs are common events secondary to acute coronary artery blockages that result in large-scale cardiomyocyte death and progressive heart failure due to inadequate mechanical function.[122] Low adult cardiomyocyte replication rates exacerbate this condition as yearly turnover rates have been estimated to be <1%.[45] Human cardiomyocytes remain diploid during the first year of life, but age-dependent polyploidization and replicative arrest occur over the first two decades of life by incompletely understood mechanisms.[45] New knowledge of how to control endogenous human cardiomyocyte replication or to implant exogenous human cardiomyocytes as cell therapy could be transformative for these patients. To date, the majority of cardiomyocyte replication studies have focused on non-human model systems, but have revealed that low ambient oxygen, low-pressure circulation, glycolytic metabolism, and absence of polyploidy enhance cardiac regenerative capacity.[123] The knowledge of the conservation of these replicative levers to human cardiomyocytes has lagged in part due to the lack of human model systems and the relative inaccessibility of viable human heart samples.

In this study, we utilized iPSC-derived cardiomyocytes modified to track CCNB1 as a model system to study mechanisms of human cardiomyocyte replication and polyploidization. Resembling *in vivo* cardiomyocytes, we observe that iPSC-derived cardiomyocytes undergo a time-dependent, progressive replicative arrest and polyploidization. The ~25% polyploidy that we observe at differentiation day 40 in this study is similar to what has been documented in ~8-year-old human hearts.[45] Using time-lapse imaging of cardiomyocytes labeled with cTnT-mCherry and CCNB1-eGFP, we found that ~75% of CCNB1+ cardiomyocytes endocycle and become mononuclear polyploid in association with CCNB1 levels that are likely insufficient to reach the threshold required for nuclear entry and execution of mitosis, as recently described for other cell types in mouse embryos.[124] This pattern of polyploidization is distinct from rodent cardiomyocytes, which are mostly multinuclear polyploid, and further illustrates the unique replicative characteristics of human cardiomyocytes and the rationale for the establishment of a human cardiomyocyte model system.

We also uncovered molecular signatures and pathways associated with polyploidization using chromatin state analysis and scRNA-seq. We found that while ~96% of regulatory sequences were similarly activated between diploid and polyploid cardiomyocytes, polyploid samples exhibited increased activation of elements overlapping specific transcription factors including those involved in myofibrillogenesis such as MEF2 family members and oxidative stress such as NRF2 and TP53; polyploid cells also showed reduced levels of early developmental factors like brachyury. In addition to providing transcriptional signatures and pathways associated with replication and polyploidization, scRNA-seq analyzed by pseudotime analysis uncovered potentially

causal relationships between the function of the sarcomere in cell cycle regulation. While previous studies have implicated the sarcomere's role in promoting oxidative metabolism and cell cycle arrest, our study utilized sarcomere-poor cardiomyocytes to directly link the sarcomere to metabolic reprogramming and polyploidization in human cardiomyocytes.[125, 126]

During time-lapse imaging studies, while we confirmed that sarcomere disassembly is a universal feature of cardiomyocytes undergoing mitosis, as has been observed in other studies, we observe that human sarcomere-containing cardiomyocytes fail to initiate the earliest stages of mitosis, as CCNB1 is degraded prior to nuclear entry and chromatin condensation does not occur.[127] Moreover, we find that CCNB1 overexpression is sufficient to both reduce polyploidization and increase the proportion of G2/M cardiomyocytes, in accord with replication studies using non-human cardiomyocytes, though ploidy was not specifically addressed.[40, 128] The reduction in polyploidization that we observed indicates that the presence of sarcomere-containing myofibrils is not a total block to cytokinesis in our model, in contrast to what has been proposed in rodent models that have high rates of multinuclear polyploidy. [129] Our study demonstrates that sarcomere-dependent CCNB1 inhibition appears to occur through transcriptional repression by p53 signaling, which, in turn, is activated by a DNA damage response as a consequence of increased oxidative metabolism. This is consistent with the previous finding that activation of p53 indirectly attenuates the *CCNB1* promoter and induces G2/M arrest in other cell types through a p21-dependent mechanism, as well as other studies that have implicated p53 activity in regulating mouse cardiomyocyte cell cycling and polyploidy in mouse hepatocytes.[130-133] While we could find no changes in

histone methylation or acetylation at the *CCNB1* promoter in polyploid cardiomyocytes relative to diploid cardiomyocytes, our data support a model whereby p53 activation results in progressive, and ultimately irreversible inhibition of human cardiomyocyte mitosis through CCNB1 inhibition.

To understand the functional relevance of sarcomere-dependent polyploidization and replicative arrest, we studied cardiomyocytes that were rendered non-contractile and sarcomere-poor by KO of both isoforms of troponin I in an *in vivo* cell therapy model of acute MI. We found that impaired sarcomere function enhanced cardiomyocyte engraftment in the heart by 4-fold and enhanced proliferation by >3-fold three months post transplantation. While we observed no change in apoptosis between WT and TnI-DKO engrafted CMs, we cannot exclude that differential survival may occur at earlier timepoints nor that other factors additionally contribute to the enhanced engraftment rate of TnI-DKO CMs. As delivery of *in vitro* differentiated cardiomyocytes to the injured heart is an alternative to coaxing endogenous cardiomyocyte regeneration, our study demonstrates that improved replicative capacity and reduced polyploidization can enhance engraftment, though future studies will need to assess the functional outcomes of the enhanced graft size produced by TnI-DKO cardiomyocytes.[23] Additionally, inhibition of sarcomere assembly did not completely abolish polyploidization nor the age-dependent reduction in CCNB1, indicating that other mechanisms contributing to cardiomyocyte polyploidization need to be investigated, potentially such that polyploidization can be minimized whilst maintaining sarcomere function through the discovery of additional levers that coax cardiomyocyte replication. In summary, our study provides a comprehensive assessment of human cardiomyocyte replication, refines new sarcomere

crosstalk with cell cycle regulation through engagement with p53 signaling, and provides a list of therapeutic targets that could be exploited to coax endogenous cardiomyocyte replication or enhance cardiac cell therapy for cardiac regenerative medicine applications.

Chapter 5. Determine the Role of Mechanical Contraction During Development and Myofibril Formation

5.1 Abstract

To understand the role of mechanical contraction during myofibril development and organization in human cardiomyocytes, we generated a non-contractile hiPSC-CM model with a D65A point mutation in cardiac troponin C – cTnC D65A. The D65A mutation prevents calcium from binding to cTnC, therefore, preventing cardiomyocytes from contracting. Based on complete sarcomere disassembly seen upon inhibition of contraction, we hypothesized that mechanical contraction is required to form myofibrils and for sarcomere proteins to undergo isoform switches. Once differentiated, cTnC D65A-CMs were transduced with adenoviral vectors expressing wildtype cTnC to initiate contraction to observe the effects of mechanical activity on quiescent myofibrils. To observe the opposite effects of mechanical inactivity on active myofibril structure, wild type CMs (WTC-CMs) were transduced with adenoviral vectors expressing cTnC D65A. Immunofluorescent staining showed cTnC D65A-CMs are able to form and maintain myofibrils with all sarcomere proteins present, including troponin subunits. However, upon closer view of myofibril structures with high resolution structured illumination microscopy, we found cTnC D65A-CM myofibrils were not as well aligned compared to WTC-CM myofibrils. Also, cTnC D65A-CMs were able to undergo myosin isoform switch from fetal to adult, although the switch was delayed compared to WTC-CM, suggesting isoform switch can happen regardless of mechanical activity. Despite the mechanical quiescence, we found cTnC D65A-CMs still had calcium transients with delayed calcium release and uptake. Inhibition of contraction resulted in complete myofibrillar disarray with the

emergence of muscle stress fibers in the cellular periphery. Replacement of nonfunctional cTnC with functional cTnC led to noticeable myofibrillar structural organization and assembly even before spontaneous contraction was observed. Upon spontaneous contraction, virally transduced cTnC D65A-CM had improved myofibrillar alignment, directionality, and bundling and elongated cellular morphology. To elucidate the potential mechanism for myofibril formation in the absence of mechanical contraction, cTnC D65A-CMs were cultured on nanopatterns to see whether improved cell-matrix adhesion could lead to better myofibril formation. cTnC D65A-CMs were able to follow the topographical cues and elongate in the direction of the pattern and form comparable myofibrils to wildtype. Future studies will investigate the potential mechanisms of how cardiomyocytes are able to form myofibrils in the absence of mechanical activity by comparing global protein expressions between contractile and non-contractile cardiomyocytes with mass spectrometry.

5.2 Introduction

Mechanical contraction is indispensable for both cardiac development and function. During human fetal cardiac development, the first heart beat is initiated around gestation day 22 from the primitive heart tube, the primitive structure of the embryonic heart.[134] After the initiation of contraction, the fetal heart undergoes complicated mechanical and molecular transitions *in utero*.[135] Previous studies from our group with developing human fetal cardiac muscle from gestational age 59-134 days showed increase in force production, kinetics of activation and relaxation, and relative proportion of adult to fetal protein isoforms (troponin I and myosin heavy chain) relative to the age

of the fetal cardiac myofibrils. Also, electron microscopy of the left ventricle sections from fetal hearts at 52, 108, and 127 days of gestation showed poor z-disc alignment and low myofibrillar density at 52 days that significantly improved at a more mature state at 127 days.[136] However, due to the difficulty of separating mechanical activity from cardiomyocytes, it still remains unknown whether early developing cardiomyocytes before gestation day 22 have myofibrils and can undergo protein isoform switch from fetal to adult in the absence of contraction.

To understand the impact of mechanical quiescence in cardiomyocytes, studies were performed both *in vitro* and *in vivo* to observe myofibril structures after inhibiting contraction. Transgenic mouse with homozygous knockout of cardiac troponin T was generated but it resulted in a complete embryonic lethality.[108] $cTnT^{-/-}$-CMs never contracted and showed severe sarcomere disassembly, with punctate α-actinin expression, similar to the expression seen in TNNI DKO-CMs.[104] Similar findings were reported in zebrafish with silent heart (sih) mutations that has a loss of cTnT and where sih mutant cardiomyocytes showed no contraction and defective sarcomere assembly.[137] In cell culture studies, inhibition of contraction in both hiPSC-CMs and adult rat cardiomyocytes with blebbistatin (myosin inhibitor) and verapamil (antagonists of L-type Ca^{2+} channels) led to complete abrogation of sarcomeres.[104, 110, 138-140] Although *in vitro* studies show myofibril disarray upon mechanical quiescence, we cannot conclude sarcomeres are unable to form without contraction since these studies were performed by inhibiting mechanical activity after a period of mechanical contraction. Therefore, it is still unknown if early stage cardiomyocytes can form myofibrils in the absence of mechanical contraction.

This also raises the question of whether sarcomere protein isoform switches from fetal to adult can occur without the mechanical stimulus. During mammalian cardiac development, slow skeletal troponin I (ssTnI) is the predominant isoform of troponin I in the embryonic heart and it switches over to cardiac troponin I (cTnI) upon birth.[109, 141-143] Also, α-myosin heavy chain (αMHC) is expressed in the ventricles, with the ventricular expression decreasing and β-myosin heavy chain (βMHC) expression increasing as development progresses.[144-146] Studies with human embryonic stem cell-derived cardiomyocytes (hESC-CMs) under external cyclical stretch showed more mature phenotype with increased β-myosin heavy chain expression compared to control.[147, 148] However, it is unclear whether this isoform switch can occur during mechanical quiescence, or whether mechanical contraction is needed to initiate the protein turnover.

In this work, we used a new hiPSC line to investigate the effect of mechanical contraction on myofibril structures and cardiac protein isoform switch. We furthermore used an adenoviral transduction to initiate and inhibit contraction in hiPSC-CMs to observe the changes in myofibrils and calcium transients. Although the previous cell line we have used – slow skeletal and cardiac troponin I knock-out (TNNI DKO) – does not contract, due to its inability to assemble sarcomeres and form troponin complexes, we needed a different non-contractile cardiomyocyte model for this study as the absence of troponin complex would impact myofibril formation and development. Previous work from our group has shown a point mutation of D65A in calcium binding Site II of cardiac troponin C (cTnC D65A) eliminates calcium binding and contractions in adult cardiac muscle.[149] By creating a genetically engineered hiPSC line with cTnC D65A mutation as a new model for non-contractile cardiomyocytes, we are able to use a cell line with

minimal genetic perturbation to minimize the effects of the mutation on the expression of sarcomere proteins. Our study is an important step towards understanding how the mechanical quiescence in cardiomyocytes affects myofibril assembly and cardiac maturation.

5.3 Materials and Methods

5.3.1 CRISPR/Cas9 Targeting of TNNC1 in hiPSCs

Homozygous TNNC1 D65A (denoted cTnC D65A) was generated by the Tom & Sue Ellison Stem Cell Core at the Institute for Stem Cell & Regenerative Medicine. Briefly, the gRNA sequence used to target TNNIC1 is GATGATCGATGAGGTGGACG and single stranded DNA donor sequence is TGAGGATGCTGGGCCAGAACCCCACCCCTGAGGAGCTGCAGGAGATGATCGATG AGGTGGCCGAAGACGGTGAGCCCCCTCCTCCCCAGGCTCCAGAAGAACCCCAGC TGGCTGGGGGCTG. Forward PCR primer sequence is GCAGCCTTCGACATCTTCGT and reverse PCR primer sequence is CTTGTGTAGCCCTTATGCCCA . One million WTC-11 iPSCs were electroporated with 0.3 µM Cas9 (Sigma) and 1.5 µM gRNA (Synthego) as RNP complex along with 2µM single stranded DNA donor (IDT) using Amaxa nucleofector (Human Stem Cell Kit 2) in presence of ROCK inhibitor. Individual colonies were picked and plates into 96 well plates. DNA was extracted using Quick Extract DNA extraction solution (Epicentre) and PCR was performed to confirm the mutation.

Figure 9 CRISPR/Cas9 Targeting of TNNC1 in hiPSCs

Schematic indicating the genome editing strategy used to introduce the D56A mutation in the TNNC1 locus of WTC hiPSCs. The gRNA is shown in red and the PAM sequence is shown in blue. The cutting site of Cas9 in the exon 6 of human TNNC1 is indicated by a red arrow. The base A (green square) was replaced with C, resulting in Asp65Ala (GAC>GCC). A silent mutation was introduced in the PAM region to avoid re-cutting by Cas9 (G>A: Glu). The single stranded DNA donor has the desired mutations and homologous arms. Figure courtesy of Dr. Julie Mathieu.

5.3.2 Viral Transduction

HEK293 cells were used to generate adenoviral vectors expressing either cTnC D65A or cTnC under the CMV promoter using the AdEasy system. Both vectors contained a green fluorescent protein (GFP) reporter under a separate CMV promoter and FLAG epitope was added to the C terminal of both cTnC genes. Cardiomyocytes were differentiated as previously described. On day 14 post differentiation, cardiomyocytes were trypsinized and replated at 200,000 cells/cm^2 onto fibronectin-coated tissue culture plates. 24 hours later, cells underwent lactate purification with glucose-free RPMI supplemented with 4 mM lactate for 4 days with feeding every other day. After the selection, cardiomyocytes were replated at 200,000 cells/cm^2 onto fibronectin-coated

glass coverslips for imaging. Cardiomyocytes were transduced for 4 hours at 37°C with 50 particles per cell in cardiomyocyte media (RPMI + 1X B27 plus insulin + 1X Pen/strep) and washed twice with PBS before being placed back in cardiomyocyte media. For imaging, cells were treated with 10 µM Blebbistatin (Toronto Research Chemicals) in cardiomyocytes media for 30 minutes in 37°C and then fixed for 15 minutes at room temperature in 4% paraformaldehyde.

5.3.3 Calcium Transient Measurements

Day 14 post differentiation cardiomyocytes were replated onto 25 mm diameter fibronectin-coated glass coverslips in cardiomyocyte replating media (RPMI + 5% FBS + 10 uM Rock inhibitor + 1X B27 plus insulin + 1X Pen/Strep) at a density of 20,000 cells/cm^2. Media was changed every other day until Day 30 or 60 when calcium transient measurements were collected as previously described.[150] Briefly, cells were incubated with 0.2 µM Fura-2-AM (Thermo Scientific) in 1.8 mM Ca^{2+} Tyrode's buffer at 37°C for 15 minutes, washed by incubating in RPMI (Gibco) for 15 minutes at 37°C, and then imaged during perfusion with 37°C heated 1.8 mM Ca^{2+} Tyrode's buffer while paced at 1 Hz, 2Hz, or 3 Hz. Data were analyzed with IonWizard software.

5.3.4 Western Blotting

Whole cell protein lysates were collected by washing the cardiomyocytes once with PBS and then lysing them with NP-40 with protease inhibitor (Sigma). Lysates were centrifuged to collect cell debris. Supernatant was collected and the protein concentration

was measured using Bradford assay (Bio-Rad). Protein lysates were separated on 4-20% PROTEAN TGX precast gels (Bio-Rad), transferred onto PVDF membranes (Bio-Rad), and blocked for 1 hour in blocking buffer (Rockland MB-070-003; 1:1 dilution with TBS-T; TBS-T composed of 50 mM Tris-Cl, 150 mM NaCl, 0.1% TWEEN-20). Blocked membranes were then probed overnight in 4°C with primary antibody in blocking buffer. The next day, membranes were washed three times in TBS-T 5 for 5 minutes each, probed for 1 hour at room temperature with secondary antibodies in blocking buffer, and washed three times in TBS-T for 5 minutes each. The primary antibodies used were as follows: 1:400 mouse anti-MYH6 (R&D #940344), 1:500 mouse anti-MYH7 (Developmental Studies Hybridoma Bank A4.951, supernatant), 1:400 rabbit anti-α actinin (Abcam 68167), 1:300 mouse anti-α actinin (Abcam 9465), 1:1000 rabbit anti-phosphorylated ERK (Cell Signaling 4370S), 1:1000 rabbit anti-ERK (Cell Signaling 4695S), and 1:2000 mouse GAPDH (Thermo Fisher AM4300). The secondary antibodies used were as follows: 1:2000 goat anti-mouse 488 (Invitrogen A11001), 1:2000 goat anti-rabbit 488 (Invitrogen A27034), 1:2000 goat anti-mouse 647 (Invitrogen A28181), 1:2000 goat anti-rabbit 647 (Invitrogen A27040).

5.3.5 Cell Culture on Nanopattern Substrates

Nanopatterned coverslips were generated as previously described (generously provided by the laboratory of Dr. Deok-Ho Kim at Johns Hopkins University) and coated with FBS in 37°C for 2 hours.[151] Day 19 post differentiation cardiomyocytes after lactate selection were replated at a density of 20,000 cells/cm^2 and cultured for 2 weeks. Before

fixation, cells were treated with 10 μM Blebbistatin for 30 minutes in 37°C and then fixed for 15 minutes at room temperature in 4% paraformaldehyde.

5.3.6 Immunocytochemistry

Following fixation in 4% paraformaldehyde, samples were washed three times with PBS and blocked in 3% bovine serum albumin (denoted blocking buffer) for 1 hour at room temperature. Samples were stained with the following in blocking buffer overnight in 4°C: α-actinin (mouse monoclonal antibody, Abcam 9465, 1:100 or rabbit polyclonal antibody, Abcam 137346, 1:100), cardiac troponin T (mouse monoclonal antibody, Thermo, 1:100), Phalloidin 488 (Thermo, 4.4 μM), FLAG (rabbit polyclonal, Sigma, 1:100), MYH7 (Developmental Studies Hybridoma Bank A4.951, supernatant), and α-Tubulin (mouse monoclonal antibody, Millipore, 1:100). The following day, samples were incubated in AlexaFluor-conjugated goat anti-mouse and goat anti-rabbit antibodies (Life Technologies, 1:100) for 1 hour at room temperature and then stained with 10 μM Hoechst 33342 (Thermo) for 30 minutes at room temperature. Samples were coverslipped using Vectashield without DAPI (Vector Laboratories) and imaged on Nikon A1R Confocal or Structured Illumination Microscopy.

5.3.7 Myofibril Organization Scoring Based on α-Actinin Staining

In order to ensure blind, unbiased analysis of myofibril organization and structures, fluorescent images of cardiomyocytes with α-actinin staining were randomly assigned encrypted names using ImageJ Blind Analysis Tools. Based on the previously published method of myofibril organization scoring system, each cardiomyocyte image was given a score of 1 to 5 (**Figure 10**).[152] Once the scoring was completed, the encrypted name was matched to the original name to visualize the histograms.

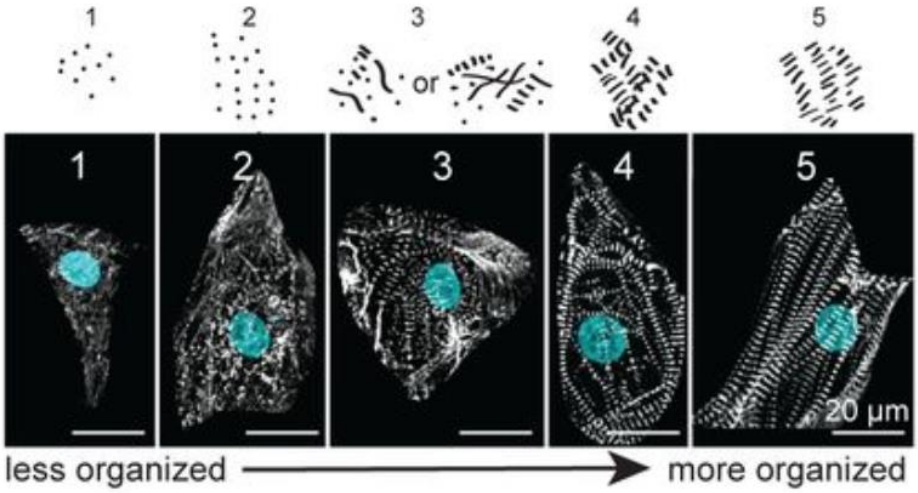

Figure 10 Representative fluorescent images of cardiomyocytes with α-actinin expression for myofibril organization scoring system.

Score of 1 represents the least organized myofibrils and score of 5 represents the most organized myofibrils. Figure adapted from Gerbin et al.[152]

5.4 Results

5.4.1 Cardiomyocytes can Form and Maintain Myofibrils in the Absence of Contraction

To determine if non-contractile cardiomyocytes can form myofibrils, we differentiated cTnC D65A into cardiomyocytes (denoted cTnC D65A-CM) and performed western blot to confirm they express all sarcomere proteins and immunocytochemistry to observe their myofibrils (**Figure 11**). Day 14 cTnC D65A-CM showed all sarcomere proteins are expressed, including cTnC (**Figure 11A**). Staining for α-actinin, β-myosin heavy chain, and cardiac troponin T revealed clear striations in Day 60 cTnC D65A-CM, similar to those seen in wildtype cardiomyocytes (WTC-CM), indicating cardiomyocytes can not only form organized thick and thin filaments, but also maintain the sarcomeres without contraction (**Figure 11B**). Phalloidin staining under structured illumination microscopy (SIM) showed clear myofibrils in cTnC D65A-CM. However, it also showed differences in myofibril bundling and defined z-lines. cTnC D65A-CM myofibrils are not bundling as compact as wildtype and the z-lines are less defined (**Figure 11C**).

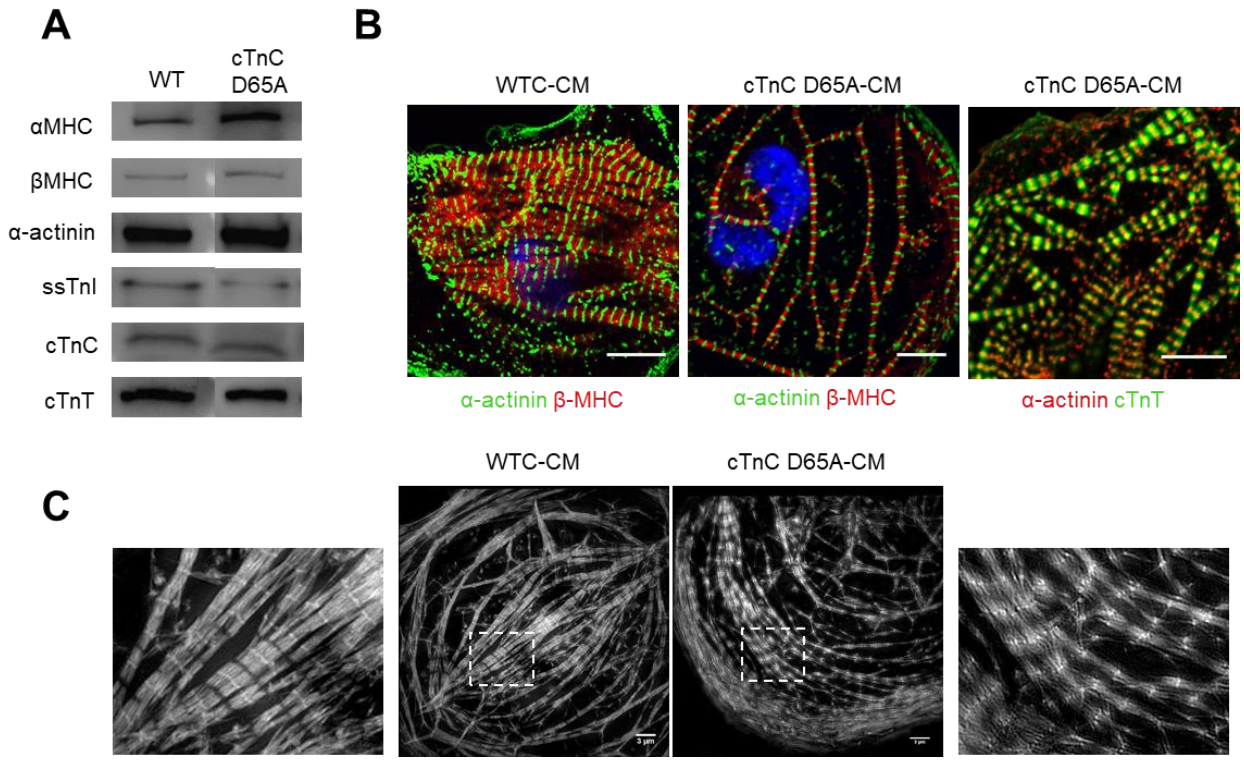

Figure 11 Cardiomyocytes can form and maintain myofibrils without mechanical contraction. **(A)** Western blot of Day 14 WTC-CM and cTnC D65A-CM to confirm expression of sarcomere proteins. **(B)** Representative confocal images of Day 60 WTC-CM and cTnC D65A-CM stained for α-actinin and β-MHC/cTnT. Even without mechanical contraction, cTnC D65A-CMs form and maintain myofibrils. Scale bar = 10 µm. **(C)** Representative structured illumination microscopy images of Day 30 post differentiation WTC-CM and cTnC D65A-CM stained for F-actin. cTnC D65A-CM myofibrils are thinner and less organized with less defined Z-lines. Scale bar = 3 µm.

5.4.2 Cardiac Maturation is Delayed Without Contraction

To understand the effect of mechanical quiescence on cardiac maturation, we looked at the expression levels of αMHC (fetal isoform) and βMHC (adult isoform) in contractile and non-contractile cardiomyocytes at three different post differentiation time points. As cardiomyocytes mature, αMHC expression level goes down as βMHC goes up.[65] Although we saw similar patterns of down regulation of αMHC and upregulation of

βMHC in both cardiomyocytes, cTnC D65A-CMs had delayed myosin heavy chain isoform switches compared to wildtype, demonstrating the importance of contraction in promoting cardiac maturation (**Figure 12A-B**). However, this finding signifies cardiomyocytes do not need mechanical activity to initiate sarcomere protein isoform switch to undergo maturation.

We next investigated whether there is a decrease in myofibril production due to the mechanical inactivity in cTnC D65A-CMs. We have observed from our myofibrillar images that although Day 14 cTnC D65A-CMs have similar myofibrillar density as wildtype, Day 60 cTnC D65A-CMs have visibly lower myofibrillar density than wildtype. Other groups have previously reported a decline in myofibrillar volume density and a degradation of myofibrils once contractile cardiomyocytes became mechanically quiescent.[138, 153] However, it is unknown whether the same phenomenon is seen when the cardiomyocytes are inherently mechanically quiescent. We looked at ERK activation, a hypertrophic growth signaling pathway, at different maturation time points to see whether ERK activation levels change throughout the long-term culture.[154, 155] As wildtype cardiomyocytes maintained consistent levels of activated ERK throughout the culture, cTnC D65A-CMs showed a decrease in activated ERK as the cells matures (**Figure 12C**). This decrease in activated ERK supports the observation of decreased myofibrillar density as cTnC D65A-CMs mature.

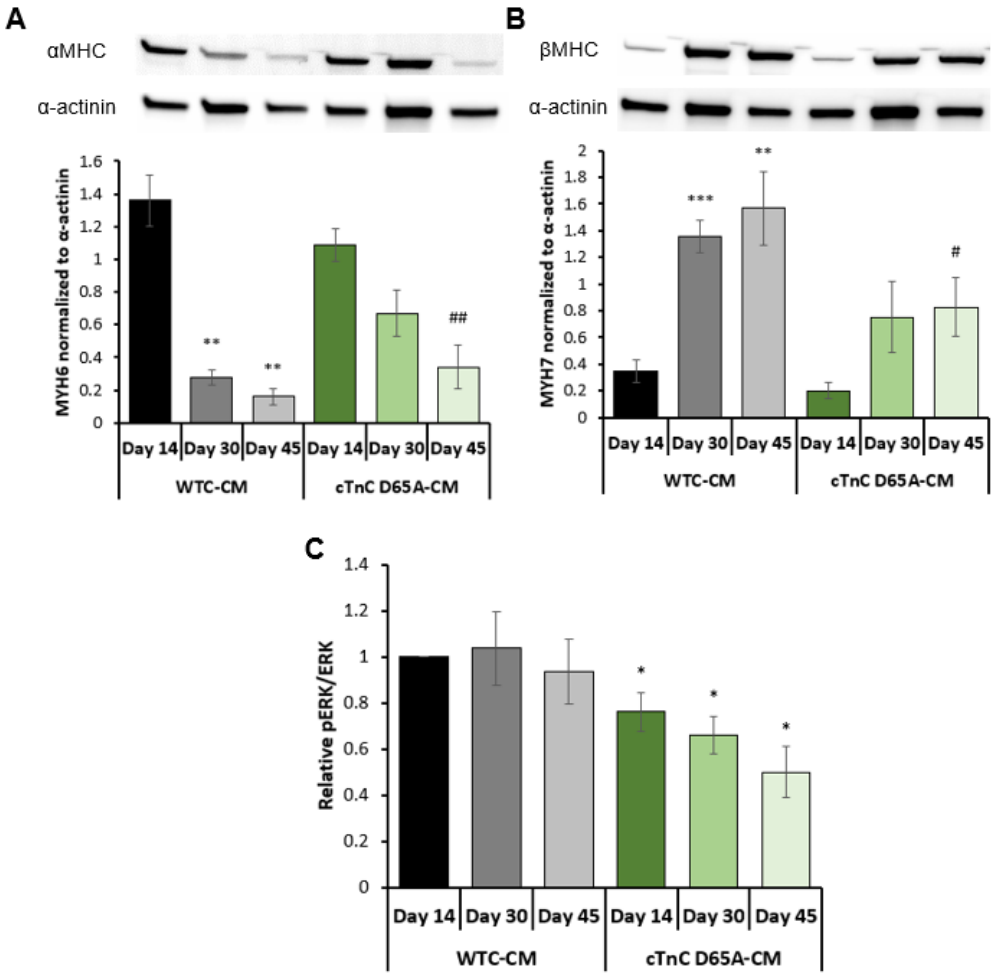

Figure 12 Cardiac maturation is delayed without contraction.

Western blot analysis of Day 14, 30, and 45 WTC-CM and cTnC D65A for **(A)** MYH6 shows a decrease in MYH6 expression over time, **(B)** MYH7 shows an increase in MYH7 expression as cardiomyocytes mature, and **(C)** phosphorylation of the hypertrophic signaling pathway proteins ERK shows steady expression of pERK/ERK in WTC-CM and a continuous decrease in cTnC D65A-CM over time. Data are n≥3 and mean±SEM; significance assessed by Student's t-test and defined by $p \leq 0.05$ (*), $p \leq 0.01$ (**) and $p \leq 0.001$ (***) when compared with Day 14 WTC-CM. $p \leq 0.05$ (#) and $p \leq 0.01$ (##) when compared with Day 14 cTnC D65A-CM.

5.4.3 cTnC D65A-CMs have Calcium Transients

In order to study the differences in calcium handling that are caused by inhibiting contraction by mutating cTnC, we measured Ca^{2+} transients of single cells under three different pacing frequencies in 1.8 mM Ca^{2+} Tyrode's buffer (**Figure 13**). We hypothesized cTnC D65A-CMs would have higher calcium transient peak amplitude since the cardiac troponin C, major buffer of cytosolic calcium in cardiomyocytes, is unable to bind to calcium. Despite the cTnC D65A-CM average overall calcium transient trace showing higher peak amplitude when paced at 1 Hz (**Figure 13A**), we found that the magnitudes of calcium transients were not statistically different from wild type controls at all three frequencies (**Figure 13B**), and in fact the calcium release was significantly slower than in the control group as indicated by slower peak time, time to 50% peak, and time to 90% peak (**Figure 13C-E**). Additionally, cTnC D65A-CMs produced significantly slower calcium reuptake at 1Hz and 3Hz as shown by time to 50% decay (**Figure 13F**). However, there was no difference in time to 90% decay (**Figure 13G**). An interesting observation to note is although there was no contraction, the endogenous frequency of cTnC D65A-CMs was higher than 1Hz, therefore, some cells could not be paced at 1Hz. Based on this data, we conclude that even in the absence of functional cardiac troponin C, there are no differences in peak amplitudes but the calcium release is slower than the control.

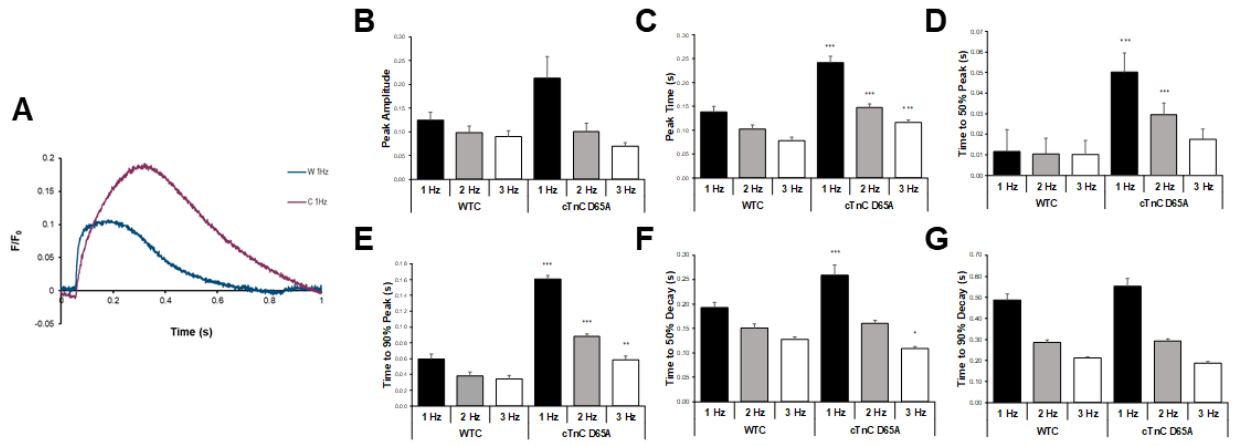

Figure 13 Cardiomyocytes with non-functioning cTnC show slower calcium release.

(A) Representative traces of calcium transient measurement for Day 60 WTC-CM and cTnC D65A-CM paced at 1 Hz. Calcium transient measurements indicate **(B)** peak amplitudes are not significantly different between WTC-CM and cTnC D65A-CM at all three frequencies, **(C)** peak times are significantly longer in cTnC D65A-CMs, both **(D)** times to 50% peak and **(E)** times to 90% peak are significantly longer in cTnC D65A-CMs, **(F)** times to 50% decay are significantly longer in cTnC D65A-CMs paced at 1Hz and 3Hz, and **(G)** times to 90% decay are not significantly different. WTC-CM: n=14 for 1Hz, n=14 for 2Hz, n=14 for 3Hz; cTnC D65A-CM: n=19 for 1Hz, n=22 for 2Hz, n=10 for 3Hz; Data are mean±SEM; significance assessed by Student's t-test and defined by *p<0.05, **p<0.01, ***p<0.001.

5.4.4 Inhibition of Contraction Leads to Complete Myofibrillar Disarray

To investigate the impact of inhibiting contraction on myofibril architecture in contractile cardiomyocytes, we transduced wild type cardiomyocytes with cTnC D65A adenoviruses (denoted AV-cTnC D65A). Three days after transduction, all spontaneous contraction was stopped. WT cardiomyocytes without virus treatment showed striated myofibrils with clear Z-lines and bare zone around the M-band. Although all cardiomyocytes were treated with 50 viral particles per cell, due to the heterogeneities in viral transduction and cTnC D65A expression, we saw varying degrees of myofibrillar disarray (**Figure 14A**). In minimally disarrayed myofibrils, Z-lines were still distinct but not

as well-aligned as the control and most of the FLAG expression was seen in the nucleus. For moderately disarrayed myofibrils, striation is hardly observed with the emergence of punctate Z-bodies with more disrupted Z-line structures. However, more FLAG expression can be seen in the filaments compared to the minimally disarrayed myofibrils. In severely disarrayed myofibrils, striated myofibril structures were completely abrogated and thin actin filaments emerged in the periphery of the cell. We next sought to test if these actin filaments are muscle stress fibers (MSFs), which would indicate the regression of myofibril assembly, as MSFs are precursors to sarcomere-containing myofibrils based on the Template Model and Pre-Myofibril Model.[61, 62, 156] MSFs are primarily composed of non-muscle II (NMMII) motors with NMMIIA and NMMIIB as predominant isoforms.[157] Upon probing for NMMIIB, we found the thin actin filaments in the periphery of the cell heavily express NMMIIB, indicating that inhibition of contraction gives rise to MSFs (**Figure 14B**). On the other hand, when non-contractile cTnC D65A-CMs were transduced with AV-cTnC WT to replace the nonfunctional cTnC in hopes of inducing spontaneous contraction, we didn't observe much MSF formation.

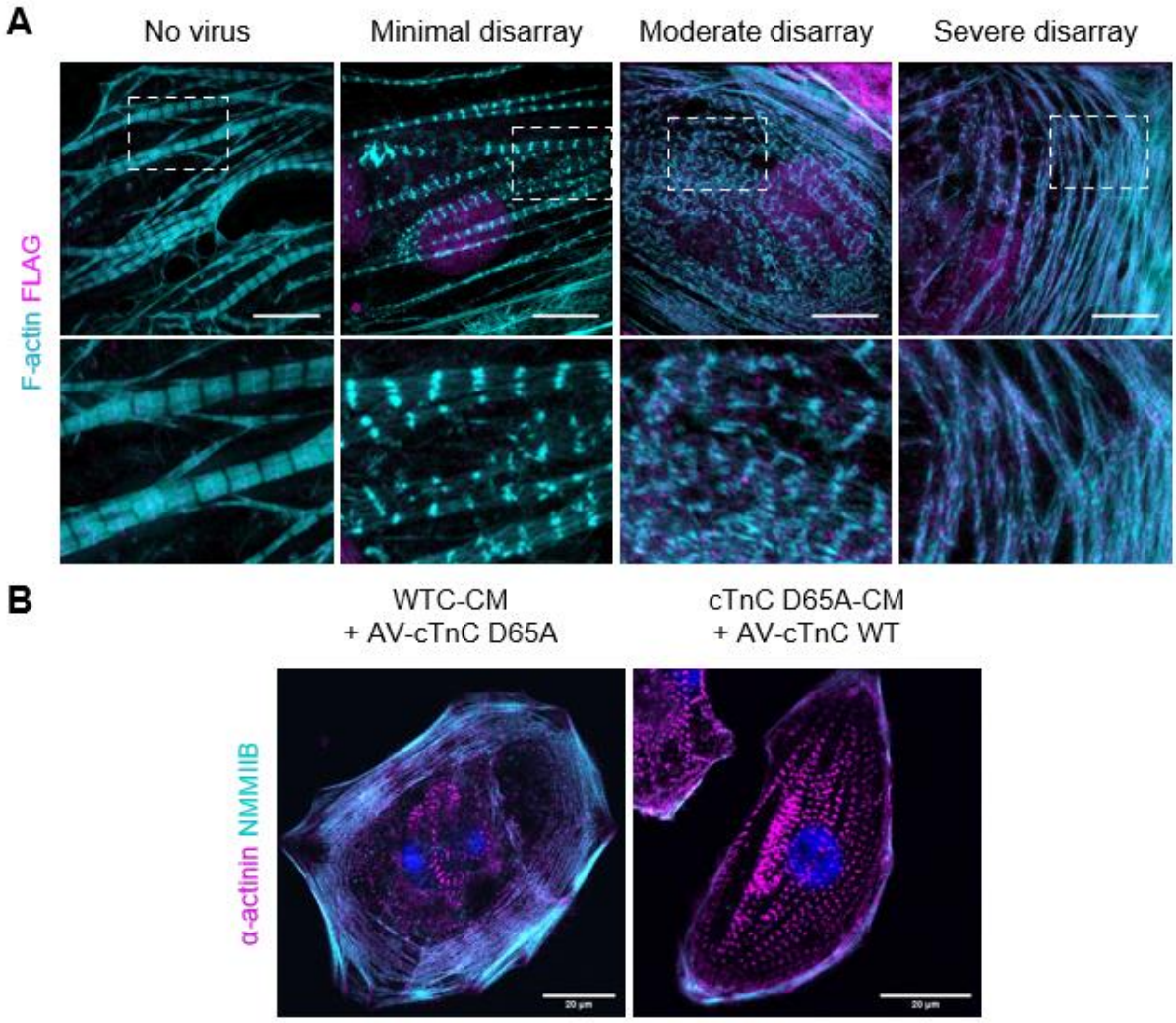

Figure 14 Inhibition of contraction leads to myofibrillar disarray.

(A) Immunostaining for F-actin (cyan) and FLAG-tag (magenta) in AV-cTnC D65A transduced WTC-CM shows varying degrees of myofibrillar disarray. No virus treatment shows no expression of FLAG and F-actin shows nicely formed myofibrils. As the myofibrillar disarray becomes more severe, FLAG expression is found along the filaments rather than in diffusive pattern and Z-lines become more disrupted and indistinguishable from muscle stress fibers. Scale bar = 10 µm. **(B)** Immunostaining for NMMIIB (cyan) and α-actinin (magenta) in AV-cTnC D65A transduced WTC-CM and AV-cTnC WT transduced cTnC D65A-CM. Inhibition of contraction leads to emergence of muscle stress fibers (MSFs) in the periphery of the cell, as shown by NMMIIB expression. However, when nonfunctional cTnC is replaced with functional cTnC, due to assembly of myofibrils, little NMMIIB expression is seen.

5.4.5 Replacement of Nonfunctional cTnC With Functional cTnC Initiates Myofibrillar Alignment and Bundling Before Spontaneous Contraction

Next, we further investigated the developmental role of mechanical contraction in myofibril assembly by replacing nonfunctional cTnC with functional cTnC via adenoviral transduction. This transition would mimic the structural changes fetal cardiomyocytes undergo when they start spontaneously contracting at gestation day 22. Although there was no visible spontaneous contraction by three day post transduction, transduced cTnC D65A-CMs showed varying degrees of myofibril assembly and bundling (**Figure 15**). In control cells without any virus treatment, poorly aligned myofibrils with crooked Z-lines were seen. It is interesting to note the difference in myofibril structures between the controls of WTC-CM and cTnC D65A-CM as they were imaged at the same time under same conditions. WTC-CM control show better sarcomere striations with defined Z lines and well-aligned thin filaments. On the other hand, cTnC D65A-CMs show under-developed myofibrils that are not as striated and organized as the wildtype. This might indicate the myofibril development is delayed and slower in non-contractile cardiomyocytes. In minimally assembled myofibrils, transduced cTnC is mostly expressed in the periphery of the cell within premyofibrils. Although there are no clear sarcomere striations, Z-bodies can be seen with punctate expression of F-actin. For moderately assembled myofibrils, expression of transduced cTnC is incorporated into the thin filament with clear Z-lines. However, myofibrils are still not well-assembled. In myofibrils with maximal assembly, myofibrils are indistinguishable from the wildtype myofibrils with myofibril bundling. As myofibrils underwent structural reorganization, spontaneous contraction was observed between days 4 and 7 post transduction.

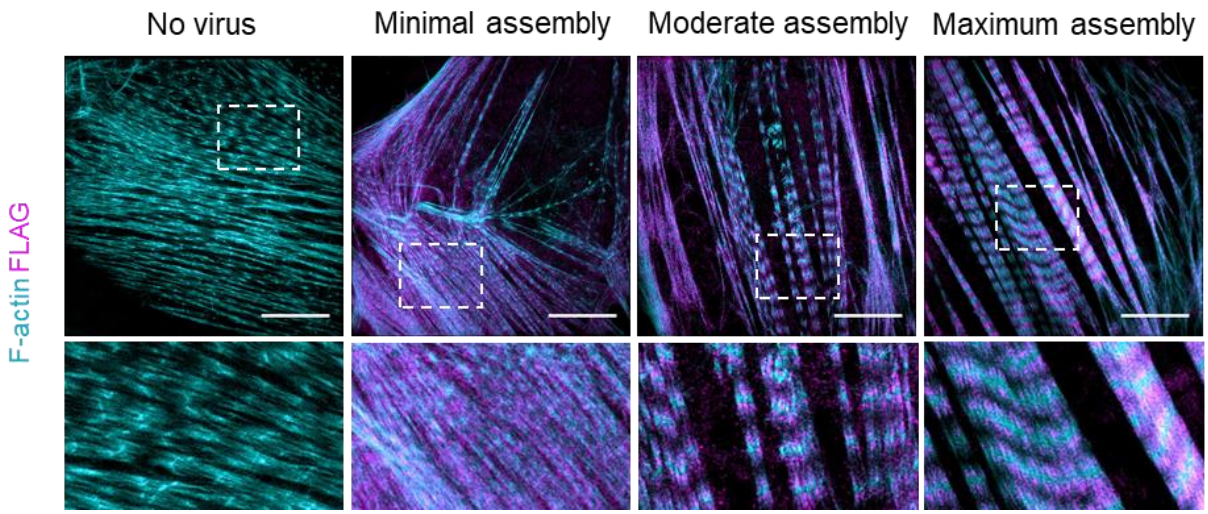

Figure 15 Myofibril assembly is initiated when nonfunctional cTnC is replaced with functional cTnC.

Immunostaining for F-actin (cyan) and FLAG-tag (magenta) in AV-cTnC transduced cTnC D65A-CM shows varying degrees of myofibrillar assembly. No virus treatment shows no expression of FLAG and poorly aligned myofibrils with crooked Z-lines. As the myofibrillar assembly increases, FLAG expression is found in the thin filaments of the sarcomeres and striated myofibrils form with well-aligned Z-lines. Scale bar = 10 µm.

5.4.6 Overall Myofibrillar Structural Changes upon Adenoviral Transduction to Exchange cTnC

Additionally, with the initiation of spontaneous contraction, the overall myofibril alignment and cellular morphology changed. Before the contraction, cTnC D65A-CMs had myofibrils that were curved and angled, almost circular at some parts. Also, we observed that fragments of myofibril went in and out of z-focal plane, indicating myofibrils lack directionality in not only x and y directions, but also, in z (**Figure 16A**). In terms of cell morphology, non-contractile cardiomyocytes had circular phenotype (**Figure 16B**). After 10 days of viral transduction to replace nonfunctional cTnC with functional cTnC, cTnC D65A-CMs were visibly beating. Upon staining for sarcomeres, we found that

myofibrils were better aligned and bundled unidirectionally (**Figure 16A**). Also, with spontaneous contraction, cardiomyocytes became elongated (**Figure 16B**).

In order to assess the overall trend in myofibrillar structural changes upon exchanging cTnC in contractile and non-contractile cardiomyocytes, we scored myofibril organization in individual cells and categorized them into 5 classes ranging from the least organized (score of 1) to most organized (score of 5) as previously reported (**Figure 16C**).[152] WTC control had a median score of 4 and upon myofibrillar disarray due to expression of cTnC D65A from adenoviral transduction, the median score dropped to 2. This left-shift in median score represents overall trend of myofibrillar disarray and poor structural organization upon expression of cTnC D65A. On the other hand, cTnC D65A control had median score of 3, slightly lower than WTC control, and upon replacing cTnC D65A with WT cTnC, the median score increased to 4. This right-shift in median score represents the process of myofibrillar assembly and bundling even before spontaneous beating when we replace the nonfunctional cTnC. This demonstrates we can control not only the contraction, but also the myofibril architecture and organization with adenoviral transduction *in vitro*.

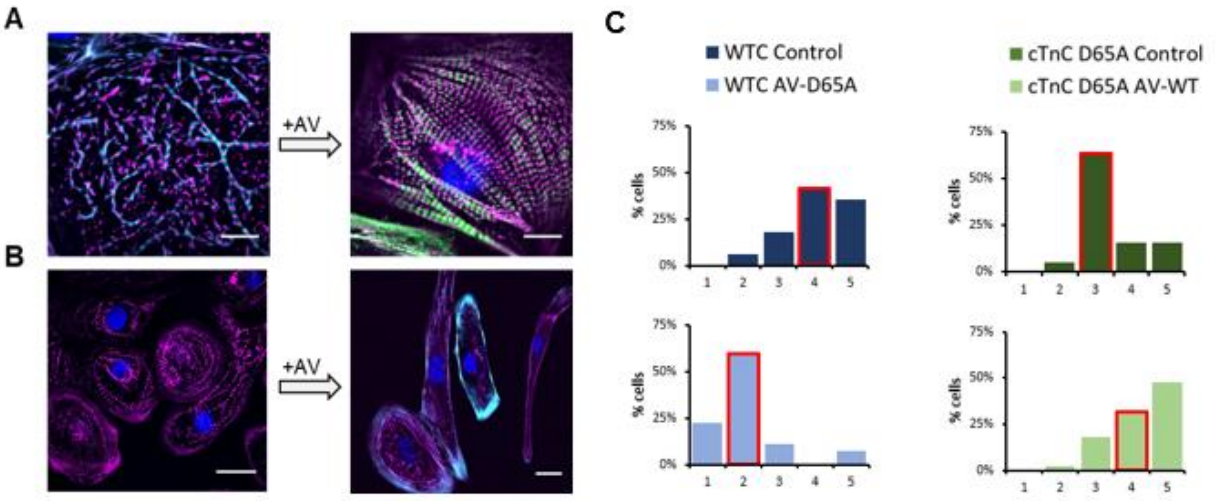

Figure 16 Contraction improves myofibril directionality and alignment and leads to cardiomyocyte elongation.

Immunostaining for α-actinin (magenta) and cardiac troponin T (cyan) before and after the transduction. **(A)** In non-contractile cardiomyocytes, myofibrils are curved and angled instead of straight. Also, fragments of myofibrils come in and out of focal plane, indicating they lack directionality. However, with spontaneous contraction 10 days post transduction, myofibrils have better directionality and alignment. **(B)** Before contraction, cardiomyocytes have circular morphology. After contraction, cardiomyocytes elongate. Scale bar = 25 µm. **(C)** Histogram showing distribution of scored cells into 5 organization classes. Red border indicates median value for each histogram. n for WTC control = 17, n for WTC AV-D65A = 27, n for cTnC D65A control = 19, n for cTnC D65A AV-WT = 44.

5.4.7 Exchange of Nonfunctional cTnC with Functional cTnC Corrects Calcium Transients

To test if replacing nonfunctional cTnC with functional cTnC will correct the calcium transients to be more like wildtype (shorter peak amplitude, faster peak time, and faster calcium release), we measured Ca^{2+} transients of single cells after transducing cTnC D65A-CMs with AV-cTnC WT under two different pacing frequencies in 1.8 mM Ca^{2+} Tyrode's buffer (**Figure 17**). We hypothesized transduced cTnC D65A-CMs that express functional cTnC would be able to handle calcium better and have more similar

characteristics to wildtype cardiomyocytes. With functional cTnC that is able to buffer cytosolic calcium in cardiomyocytes, we expected transduced cTnC D65A-CMs to have shorter peak amplitude, faster peak time, and faster calcium release. For the analysis of calcium transients, we categorized the transduced cTnC D65A-CMs into two groups based on whether they were visibly contracting to see if there is any difference in calcium transients dependent on the extent of myofibril assembly and remodeling. To our surprise, there was no difference in calcium transient parameters between the transduced cTnC D65A-CMs that were beating and not beating. This indicates although the myofibrils of transduced cardiomyocytes that were not spontaneously beating have not completed myofibril reorganization, replacing the nonfunctional cTnC with functional cTnC is enough to provide cytosolic calcium buffer. We found that magnitudes of calcium transients were significantly lower in transduced cTnC D65A-CMs compared to control at both frequencies (**Figure 17B**). Additionally, calcium release was significantly faster in transduced cTnC D65A-CMs as shown with shorter peak time (**Figure 17C**). Both times to 50% peak and 90% peak were faster in transduced cTnC D65A-CMs at 1 Hz, however, this difference was not observed when paced at 2 Hz (**Figure 17D-E**). Of note, previously, we observed it was difficult to pace cTnC D65A-CMs at 1 Hz as their endogenous frequency was faster than 1 Hz. However, after the transduction, all transduced cells were able to be paced at 1 Hz to obtain calcium transient measurements and in fact, it was rather difficult to pace them at 2 Hz.

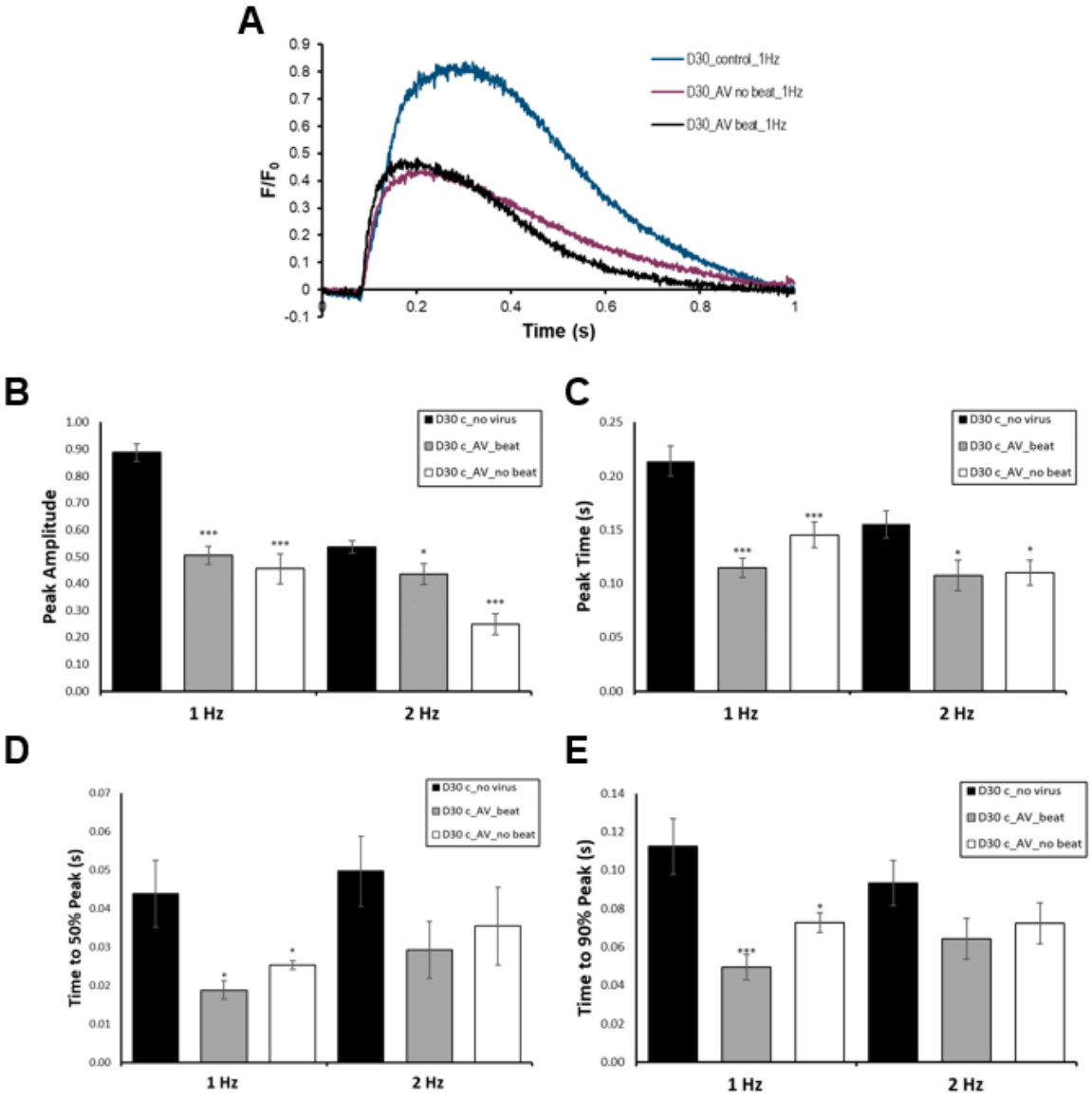

Figure 17 Replacing cTnC D65A with WT cTnC corrects calcium transients.

(A) Representative traces of calcium transient measurements of single cells stained with Fura2-AM for Day 30 cTnC D65A-CM for control and post-transduction with AV- WT cTnC paced at 1 and 2 Hz. Transduced cells were analyzed separately depending on whether they were visibly contracting upon pacing (denoted D30 c_AV_beat vs D30 c_AV_no beat). Calcium transient measurements indicate **(B)** peak amplitudes significantly decrease and **(C)** peak time significantly decrease after transduction to express WT cTnC at both frequencies regardless of their contraction state. Both times to 50% peak **(D)** and 90% peak **(E)** were significantly shorter for transduced cells paced at 1 Hz, however, there was no difference when paced at 2 Hz. D30 c_no virus: n = 19 for 1 Hz and n = 25 for 2 Hz, D30 c_AV_beat: n = 12 for 1 Hz, n = 8 for 2 Hz,

D30 c_AV_no beat: n=16 for 1 Hz and n=9 for 2 Hz; mean±SEM; significance assessed by Student's t-test and defined by $p \leq 0.05$ (*) and $p \leq 0.001$ (***) when compared with control at each frequency.

5.4.8 When Given Topographical Cues, Non-Contractile Cardiomyocytes can Form and Align Myofibrils Comparable to Contractile Cardiomyocytes

To elucidate the potential mechanism for myofibril formation without mechanical contraction, we investigated if non-contractile cardiomyocytes can follow topographical cues and elongate by culturing cTnC D65A-CMs on nanopatterns. cTnC D65A-CMs and WTC-CMs were fixed and stained after culture on nanopatterned substrates for 14 days (**Figure 18**). Both WTC-CMS AND cTnC D65A-CMs were able to follow the topographical cues and elongate to the direction of the pattern. Myofibrils in cTnC D65A-CMs were noticeably organized, aligned, and bundled, similar to those in wildtype. This indicates when non-contractile cardiomyocytes are given directional and topographical guidance, they are able to form and bundle myofibrils and elongate cellular morphology like wildtype.

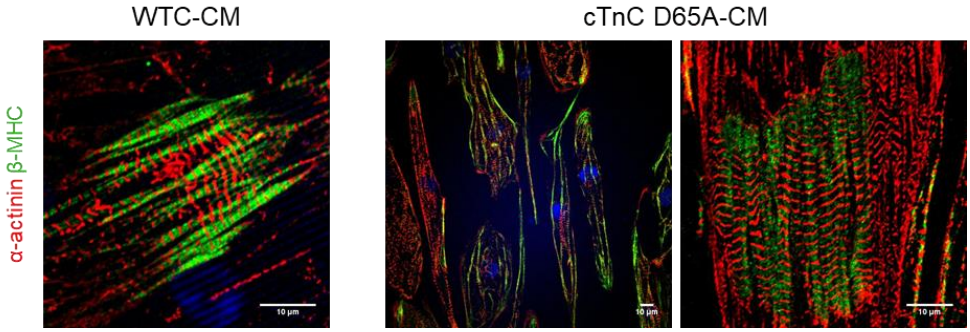

Figure 18 Non-contractile cardiomyocytes have comparable myofibril structures and cell morphology to contractile cardiomyocytes on nanopatterns.

Representative image of WTC-CM and cTnC D65A-CM plated on nanopatterns for 14 days show comparable myofibril structures and bundling between the two cell types. Also, cTnC D65A-CMs elongate to the direction of the pattern. α-actinin (red) and β-MHC (green). Scale bar = 10 µm.

5.5 Discussion

To understand the role of mechanical contraction during cardiac development and myofibrillogenesis, we generated a non-contractile hiPSC-CM line that harbors a point mutation, D65A, in Site II of cTnC to inhibit calcium binding. By inducing mechanical quiescence with a minimal genetic alteration, we did not need to truncate or knock out an entire sarcomere protein, which could have a devastating developmental effect that is apart from mechanical inactivity. We hypothesized that these non-contractile cTnC D65A-CMs would not be able to form myofibrils. However, contrary to our hypothesis, we found well-organized myofibrils in the cTnC D65A-CMs, demonstrating that the absence of mechanical activity in cardiomyocytes does not impact myofibrillogenesis. However, upon closer examination of the myofibrils with structured illumination microscopy, structural differences were found between myofibrils in cTnC D56A-CM and wildtype (WTC-CM). Unlike the highly organized myofibril structures with defined Z-lines in wildtype, myofibrils in cTnC D65A-CMs had slanted Z-lines with less aligned sarcomeres. This finding is interesting as a previous study by Chopra et al. reported complete disassembly of sarcomeres upon blebbistatin treatment and that the transmission of myosin-generated contractility is required to initiate and maintain the process of sarcomere assembly.[138] Our data suggest the sarcomere disassembly after blebbistatin treatment is the effect of preventing mechanical activity and does not infer cardiomyocytes' inability to form sarcomeres in the absence of contraction.

Our work also reports that cardiomyocytes are able to undergo sarcomere protein isoform switch from fetal to adult without mechanical contraction, suggesting cardiac maturation can initiate without the mechanical stimulus. Although cTnC D65A-

CMs underwent myosin heavy chain isoform switch from fetal to adult, the switch happened at a slower rate compared to wildtype, indicating slower cardiac maturation in the absence of mechanical contraction. We further investigated a known cardiac hypertrophic growth signaling pathway, MAPK/ERK, to evaluate the effect of mechanical quiescence in cardiac hypertrophy as we observed lower myofibril density in cTnC D65A-CMs.[154] MEK1-ERK1/2 signaling is responsible for the eccentric and concentric growth of the cardiomyocytes and ERK is activated in response to contraction via membrane bound integrins and mechanotransduction from sarcomeres.[158, 159,155, 160] Inhibition of ERK1/2 in transgenic mice led to lengthening of cardiomyocytes due to the addition of sarcomeres in series, as opposed to activation of ERK1/2 led to hypertrophic response in cardiomyocytes with the addition of sarcomeres in parallel. We found that the activated ERK level was consistently lower in cTnC D65A-CM across three time points compared to wildtype, supporting that without contraction cardiac hypertrophy is limited. Future studies could explore the feasibility of inducing cardiac hypertrophy in the absence of contraction by upregulating ERK in cTnC D65A-CMs. Also, deeper insight into cardiac maturation can be gained if cardiac maturation can be induced from external factors only without the internal contraction. In recent efforts to develop methods to mature hiPSC-CMs, studies have shown passive stretching of engineering heart tissue and physically exercising cardiomyocytes through mechanical or electrical methods improves cardiac maturity.[148, 161, 162] It would be interesting to see if these external stimuli – passive stretching and electrical stimulation – can induce maturation despite the mechanical quiescence in cTnC D65A-CMs. This would answer if internal contraction is required to undergo complete cardiac maturation.

We then investigated how the mechanical quiescence in cardiomyocytes impacts calcium transients. We hypothesized cTnC D65A-CMs would have higher peak amplitude and faster calcium release and reuptake compared to wildtype due to the absence of cardiomyocytes' major cytosolic calcium buffer – site II of cTnC. Contrary to our hypothesis, cTnC D65A-CMs had slower release and reuptake and no difference in peak amplitudes relative to wildtype. One potential explanation for similar calcium transient peak amplitudes could be the Ca^{2+} binding to metal-binding sites III and IV of C lobe in cTnC that have a high Ca^{2+} affinity, while also binding Mg^{2+} with lower affinity.[163] Although the primary Ca^{2+} binding site responsible for initiation of muscle contraction (site II) is nonfunctional in cTnC D65A, sites III and IV are active, allowing Ca^{2+} to bind. In order to understand the fundamental differences in calcium transients such as slower calcium release and reuptake kinetics between wildtype and non-contractile cardiomyocytes, future studies will need to look at the expression levels of calcium handling proteins such as L-type calcium channels, sarco/endoplasmic reticulum $Ca^{2\pm}$ATPase (SERCA), Na^{2+}/Ca^{2+} exchanger (NCX), and ryanodine receptors (RyRs) with RT-qPCR and western blot. Also, measuring calcium transients in various extracellular calcium concentrations (i.e. 0.6mM and 2.5 mM Ca^{2+} Tyrode's buffer) could lend insight into cTnC D65A-CMs' extracellular calcium handling as hiPSC-CMs' calcium transients are largely affected by transmembranal Ca^{2+} influx due to their immaturity.[164]

To confirm the feasibility of initiation and inhibition of contraction in hiPSC-CMs via adenoviral transduction, we transduced wildtype with AV-cTnC D65A and cTnC D65A-CM with AV-cTnC. Three days after transduction, wildtype transduced with cTnC D65A stopped spontaneous contraction. However, it took four to seven days after transduction

for cTnC D65A-CMs to visibly beat, suggesting virally transduced functional cTnC has to outcompete endogenous nonfunctional cTnC to initiate contraction. Upon inhibiting contraction, varying levels of myofibrillar disassembly were observed, most likely due to the heterogeneity of the transduction and expression of the transduced gene. Overall, defective sarcomeres were seen with poorly aligned Z-discs and muscle stress fibers emerged in the periphery of the cell with little to no indication of Z-bodies. On the other hand, when cTnC D65A-CMs were transduced with AV-cTnC, even before spontaneous beating was observed, immunostaining indicated significant myofibrillar assembly was underway. Replacement of nonfunctional cTnC with functional cTnC led to myofibrillar alignment and bundling that improved with longer culture. Also, initiation of contraction resulted in elongated cellular morphology. This demonstrates a new system where we can control contraction in hiPSC-CMs without the use of antagonists and that myofibril assembly is initiated simply with troponin subunit replacement.

To elucidate the potential mechanism for myofibril formation in the absence of mechanical contraction, we cultured cTnC D65A-CMs on nanopatterns to see whether improved cell-matrix adhesion could lead to better myofibril formation. cTnC D65A-CMs were able to follow the topographical cues and elongate in the direction of the pattern and form comparable myofibrils to wildtype. Future studies will look into the expressions of protocostameres by staining for paxillin to compare the expression of cell-matrix adhesion between wildtype and cTnC D65A-CMs on both nanopatterns and flat glass cover slips. Also, since the expression of full-length titin is critical in sarcomere formation, comparing titin expressions in cTnC D65A-CMs and wildtype will be important.[138, 150]

Another exciting area this finding leads us to is the difference in energetics and metabolism without contraction. 95% of ATP used by cardiomyocytes is produced by mitochondria as contraction demands high energetics.[165] Since cTnC D65A-CMs are non-contractile, comparing the differences in mitochondria and the energetics when contraction is removed from the equation using Seahorse assay could lend insight into basal level of mitochondrial function and energetic demands in cardiomyocytes.

For the first time in cardiomyocytes, we have demonstrated myofibrils form without contraction by using a genetically engineered hiPSC-CMs. Also, this study introduces new tools – cTnC D65A cell line and adenoviral vectors for different cTnCs – to study contraction in early stage cardiomyocytes.

Chapter 6. Conclusions and Future Directions

The research presented in this dissertation illustrate the different roles mechanical contraction play in cardiomyocytes for cell-based regenerative therapies and human cardiac development.

In Chapter 3, we investigated the mechanical contributions of transplanted cardiomyocytes in acute MI rodent model by intramyocardially injecting contractile and non-contractile cardiomyocytes. We hypothesized contractile cardiomyocytes would result in greater improvement in cardiac function by contributing to the overall host heart's force generation from electromechanically coupling with the host myocardium. As a model for non-contractile cardiomyocytes, we created hiPSC with both slow skeletal and cardiac troponin I knocked out (TNNI DKO). These hiPSC differentiated into cardiomyocytes and had calcium transients. However, due to their inability to form myofibrils, these cells did not spontaneously beat, confirming their mechanical quiescence. At 3 months post transplantation, echocardiography and cardiac MRI showed improvement in both fractional shortening and left ventricular ejection fraction in contractile and non-contractile cardiomyocyte treatment groups compared to control that received no cell injection. While the control group continued to decline in cardiac function, both contractile and non-contractile cardiomyocytes were able to preserve cardiac function by preventing further decline of systolic function after MI. From these results, we conclude that force generation by grafted cardiomyocytes is not necessary to prevent decline in cardiac function post MI in rodents.

Although these findings demonstrate that cardiac grafts improve cardiac function via passive mechanisms such as reducing the wall stiffness in the fibrotic region or

secreting paracrine factors in rodent MI model, further studies with non-human primates to match the species of the host myocardium and transplanted cardiomyocytes are needed to confirm the transplanted grafts' mechanism of action. Human cardiomyocytes can be paced up to 3 Hz, however, when human cardiomyocytes are subjected to such high frequency for a long period of time, it subsequently causes apoptosis.[166] Therefore, it is possible that the transplanted human cardiac grafts in rat myocardium that normally beats on average at 6Hz could not electromechanically couple, resulting in the absence of the beneficial effect of mechanical force production from the grafts.[167] This hypothesis is strengthened with previous studies that showed transplanted human cardiac grafts in non-human primates post MI led to improved systolic function over the course of 3 months as control group continued to decline in function.[24] Therefore, once these human cardiomyocytes are transplanted into an animal species with more comparable heart rate and mechanical properties to human heart, we could potentially observe the differences in therapeutic efficacies between the contractile and non-contractile cardiomyocyte grafts. If we see similar systolic improvements between the non-human primates that received contractile vs non-contractile cardiomyocytes, we can safely conclude the main therapeutic mechanism of action of transplanted grafts is through paracrine factors, immunomodulation, and decreased wall stiffness. However, if we see maintenance of systolic function in non-human primates with non-contractile graft but improved function in those with contractile grafts, we can conclude passive mechanisms of action (paracrine factors, immunomodulation, decreased wall stiffness, etc) are needed to prevent further decline in cardiac function after MI, however, direct force production from the graft is needed to improve the function over time (**Figure S26**). Understanding how the

transplanted cardiac grafts leads to functional improvement after MI would greatly help the stem cell therapeutic research with optimizing treatment efficacy.

In Chapter 4, we explored the reason for significantly larger grafts sizes resulted by TNNI DKO cardiomyocytes by studying the link between contraction and proliferation in cardiomyocytes. We hypothesized sarcomere assembly decreases proliferation in cardiomyocyte through downregulation of cyclin b1. Using an iPSC-based CRISPR genome-wide screen, we identified p53 as an activator for cardiomyocyte polyploidization that gets activated by sarcomere formation and subsequent contraction. p53 activation leads to activation of p21, a direct p53-target, and downregulates cyclin b1, hindering cardiomyocytes from undergoing mitosis. Both models for sarcomere-deficient cardiomyocytes – cardiac troponin T knock-out and slow skeletal and cardiac troponin I knock-out – showed decreased p21 and increased cyclin b1 levels compared to wildtype. Comparing wildtype and sarcomere-deficient cardiomyocytes, we found cardiomyocytes without sarcomeres have decreased superoxide production and oxygen consumption rates, suggesting oxidative phosphorylation is the link between sarcomere assembly and p53 activation. Upon *in vivo* transplantation, sarcomere-deficient cardiomyocytes resulted in bigger engraftments and higher proliferation rates within the graft, alluding to improved engraftment from increased mitosis and cellular health (i.e. lower p53 level and DNA damage markers). From this we conclude sarcomere assembly, an essential process for mechanical contraction, leads to activation of p53 from increased oxidative phosphorylation, which downregulates cyclin b1 and results in decreased mitosis.

These findings, combined with the findings from Chapter 3, give us an insight into an interesting new therapeutic alternative for MI that harnesses both

remuscularization and proliferation. One of the challenges the stem cell therapy for ischemic cardiomyopathy faces is the low retention and engraftment after cell delivery.[168] We have demonstrated that mechanical quiescence in cardiomyocytes leads to larger engraftment potentially due to higher proliferation after delivery. If we create an inducible cell line that goes from non-contractile to contractile, we can utilize the proliferative benefits of mechanical quiescence by transplanting these initially non-contractile cardiomyocytes to form bigger grafts after MI and then inducing a switch to make the engrafted cardiomyocytes to contract to lead to greater improvement in systolic function. To explore this idea, we can first start by inserting stop codons flanked by loxP sites upstream of both slow skeletal and cardiac troponin I. Then, after the transplantation of these cells and giving them sufficient time to engraft in the host myocardium, we can deliver Cre recombinase to excise the stop codons between the loxP sites, allowing both isoforms of troponin I to be expressed. This will result in spontaneous beating of the engrafted cardiomyocytes and we can evaluate if this combinatorial cell therapy with the inducible switch would result in even greater cardiac function improvement. By combining the proliferative nature of non-contractile cardiomyocytes with mechanical force production from contractile cardiomyocytes, we could overcome the low cell retention and engraftment challenges.

In Chapter 5, we investigated the effect of mechanical contraction in formation of myofibrils in developing cardiomyocytes. We hypothesized contraction was necessary to form myofibrils in early-stage cardiomyocytes. By using non-contractile hiPSC-CMs with a point mutation in calcium binding site II of cardiac troponin C (D65A), we instead found that sarcomeres and myofibrils form in the absence of mechanical contraction. Upon

inhibition of contraction with adenoviral transduction, we saw varying degrees of myofibrillar disarray and emergence of muscle stress fibers in the periphery of the cell. When we exchanged nonfunctional cTnC with functional cTnC, even before the initiation of spontaneous contraction, we observed myofibril assembly and remodeling as myofibrils became highly organized and aligned. However, non-contractile cardiomyocytes showed delayed cardiac maturation as evident by the slower myosin heavy chain isoforms switch. Future studies to compare the global RNA and protein expressions between the wildtype and D65A cardiomyocytes will help us define which molecular mechanisms are responsible for formation of myofibrils and absence of cardiac maturation in the non-contractile cardiomyocytes.

Overall, this dissertation demonstrates the wide variety of effects mechanical contraction play in stem cell therapy for heart regeneration, proliferation in cardiomyocytes, and myofibrillogenesis during early cardiac development. By creating two mechanically quiescent human cardiomyocyte lines that can and cannot form sarcomeres, we now have genetic tools to perform direct comparison studies on the impact of having myofibrils present in the cell when the contraction is removed. Together, these findings provide new insights into cardiac biology and provide new tools to expand our understanding in how mechanical activity impacts complex cellular processes in cardiomyocytes.

References

1. Takahashi, K. & Yamanaka, S. Induction of pluripotent stem cells from mouse embryonic and adult fibroblast cultures by defined factors. *Cell* **126**, 663-676 (2006).
2. Palpant, N.J. et al. Generating high-purity cardiac and endothelial derivatives from patterned mesoderm using human pluripotent stem cells. *Nature protocols* **12**, 15-31 (2017).
3. Lian, X. et al. Directed cardiomyocyte differentiation from human pluripotent stem cells by modulating Wnt/beta-catenin signaling under fully defined conditions. *Nature protocols* **8**, 162-175 (2013).
4. Lian, X. et al. Robust cardiomyocyte differentiation from human pluripotent stem cells via temporal modulation of canonical Wnt signaling. *Proceedings of the National Academy of Sciences* **109**, E1848-E1857 (2012).
5. Lan, F. et al. Abnormal calcium handling properties underlie familial hypertrophic cardiomyopathy pathology in patient-specific induced pluripotent stem cells. *Cell stem cell* **12**, 101-113 (2013).
6. Siu, C.W. et al. Modeling of lamin A/C mutation premature cardiac aging using patient-specific induced pluripotent stem cells. *Aging* **4**, 803-822 (2012).
7. Sun, N. et al. Patient-specific induced pluripotent stem cells as a model for familial dilated cardiomyopathy. *Sci Transl Med* **4**, 130ra147 (2012).
8. Karakikes, I., Termglinchan, V. & Wu, J.C. Human-induced pluripotent stem cell models of inherited cardiomyopathies. *Curr Opin Cardiol* **29**, 214-219 (2014).
9. Yang, X., Pabon, L. & Murry, C.E. Engineering adolescence: maturation of human pluripotent stem cell-derived cardiomyocytes. *Circulation research* **114**, 511-523 (2014).
10. Yang, K.-C. et al. Novel Adult-Onset Systolic Cardiomyopathy Due to MYH7 E848G Mutation in Patient-Derived Induced Pluripotent Stem Cells. *JACC Basic Transl Sci* **3**, 728-740 (2018).
11. Lundy, S.D., Zhu, W.Z., Regnier, M. & Laflamme, M.A. Structural and functional maturation of cardiomyocytes derived from human pluripotent stem cells. *Stem cells and development* **22**, 1991-2002 (2013).
12. Ma, J. et al. High purity human-induced pluripotent stem cell-derived cardiomyocytes: electrophysiological properties of action potentials and ionic currents. *American journal of physiology. Heart and circulatory physiology* **301**, H2006-2017 (2011).
13. Wang, G. et al. Modeling the mitochondrial cardiomyopathy of Barth syndrome with induced pluripotent stem cell and heart-on-chip technologies. *Nature medicine* **20**, 616-623 (2014).
14. Benjamin, E.J. et al. Heart Disease and Stroke Statistics-2019 Update: A Report From the American Heart Association. *Circulation* **139**, e56-e528 (2019).

15. Laflamme, M.A. & Murry, C.E. Heart regeneration. *Nature* **473**, 326 (2011).

16. Kenneth Mallory, G., White, P.D. & Salcedo-Salgar, J. The speed of healing of myocardial infarction: A study of the pathologic anatomy in seventy-two cases. *American Heart Journal* **18**, 647-671 (1939).

17. Laflamme, M.A. et al. Cardiomyocytes derived from human embryonic stem cells in pro-survival factors enhance function of infarcted rat hearts. *Nature biotechnology* **25**, 1015-1024 (2007).

18. Jackman, C.P. et al. Engineered cardiac tissue patch maintains structural and electrical properties after epicardial implantation. *Biomaterials* **159**, 48-58 (2018).

19. Kadota, S. et al. Ribonucleotide reductase-mediated increase in dATP improves cardiac performance via myosin activation in a large animal model of heart failure. *Eur J Heart Fail* **17**, 772-781 (2015).

20. Mohamed, T.M.A. et al. Chemical Enhancement of In Vitro and In Vivo Direct Cardiac Reprogramming. *Circulation* **135**, 978-995 (2017).

21. Vagnozzi, R.J. et al. An acute immune response underlies the benefit of cardiac stem cell therapy. *Nature* **577**, 405-409 (2020).

22. Shiba, Y. et al. Electrical Integration of Human Embryonic Stem Cell-Derived Cardiomyocytes in a Guinea Pig Chronic Infarct Model. *Journal of cardiovascular pharmacology and therapeutics* **19**, 368-381 (2014).

23. Chong, J.J. et al. Human embryonic-stem-cell-derived cardiomyocytes regenerate non-human primate hearts. *Nature* **510**, 273-277 (2014).

24. Liu, Y.-W. et al. Human embryonic stem cell-derived cardiomyocytes restore function in infarcted hearts of non-human primates. *Nature biotechnology* **36**, 597-605 (2018).

25. Weinberger, F. et al. Cardiac repair in guinea pigs with human engineered heart tissue from induced pluripotent stem cells. *Science Translational Medicine* **8**, 363ra148-363ra148 (2016).

26. Abd El Aziz, M.T. et al. Endothelial progenitor cells regenerate infracted myocardium with neovascularisation development. *Journal of advanced research* **6**, 133-144 (2015).

27. Harada, S. et al. Smooth muscle cell sheet transplantation preserve cardiac function and minimize cardiac remodeling in a rat myocardial infarction model. *J Cardiothorac Surg* **11**, 131-131 (2016).

28. Smits, A.M. et al. Human cardiomyocyte progenitor cell transplantation preserves long-term function of the infarcted mouse myocardium. *Cardiovascular research* **83**, 527-535 (2009).

29. Mirotsou, M., Jayawardena, T.M., Schmeckpeper, J., Gnecchi, M. & Dzau, V.J. Paracrine mechanisms of stem cell reparative and regenerative actions in the heart. *Journal of molecular and cellular cardiology* **50**, 280-289 (2011).

30. Hashimoto, H., Olson, E.N. & Bassel-Duby, R. Therapeutic approaches for cardiac regeneration and repair. *Nature reviews. Cardiology* **15**, 585-600 (2018).

31. Sheng, C.C., Zhou, L. & Hao, J. Current stem cell delivery methods for myocardial repair. *BioMed research international* **2013**, 547902 (2013).

32. Gerbin, K.A., Yang, X., Murry, C.E. & Coulombe, K.L.K. Enhanced Electrical Integration of Engineered Human Myocardium via Intramyocardial versus Epicardial Delivery in Infarcted Rat Hearts. *PLOS ONE* **10**, e0131446 (2015).

33. Chen, T.S. et al. Mesenchymal stem cell secretes microparticles enriched in pre-microRNAs. *Nucleic acids research* **38**, 215-224 (2010).

34. Gnecchi, M., Zhang, Z., Ni, A. & Dzau, V.J. Paracrine mechanisms in adult stem cell signaling and therapy. *Circulation research* **103**, 1204-1219 (2008).

35. Simons, M. et al. Pharmacological treatment of coronary artery disease with recombinant fibroblast growth factor-2: double-blind, randomized, controlled clinical trial. *Circulation* **105**, 788-793 (2002).

36. Gyöngyösi, M. et al. NOGA-guided analysis of regional myocardial perfusion abnormalities treated with intramyocardial injections of plasmid encoding vascular endothelial growth factor A-165 in patients with chronic myocardial ischemia: subanalysis of the EUROINJECT-ONE multicenter double-blind randomized study. *Circulation* **112**, I157-165 (2005).

37. Mitchell, A.C., Briquez, P.S., Hubbell, J.A. & Cochran, J.R. Engineering growth factors for regenerative medicine applications. *Acta Biomater* **30**, 1-12 (2016).

38. Simón-Yarza, T. et al. Vascular endothelial growth factor-delivery systems for cardiac repair: an overview. *Theranostics* **2**, 541-552 (2012).

39. Perea-Gil, I., Prat-Vidal, C. & Bayes-Genis, A. In vivo experience with natural scaffolds for myocardial infarction: the times they are a-changin'. *Stem cell research & therapy* **6**, 248 (2015).

40. Mohamed, T.M.A. et al. Regulation of Cell Cycle to Stimulate Adult Cardiomyocyte Proliferation and Cardiac Regeneration. *Cell* **173**, 104-116.e112 (2018).

41. Molkentin, J.D. et al. Fibroblast-Specific Genetic Manipulation of p38 Mitogen-Activated Protein Kinase In Vivo Reveals Its Central Regulatory Role in Fibrosis. *Circulation* **136**, 549-561 (2017).

42. Moon, J. et al. Blockade to pathological remodeling of infarcted heart tissue using a porcupine antagonist. *Proceedings of the National Academy of Sciences of the United States of America* **114**, 1649-1654 (2017).

43. Talman, V. & Ruskoaho, H. Cardiac fibrosis in myocardial infarction-from repair and remodeling to regeneration. *Cell and tissue research* **365**, 563-581 (2016).

44. Alkass, K. et al. No Evidence for Cardiomyocyte Number Expansion in Preadolescent Mice. *Cell* **163**, 1026-1036 (2015).

45. Bergmann, O. et al. Dynamics of Cell Generation and Turnover in the Human Heart. *Cell* **161**, 1566-1575 (2015).

46. Bergmann, O. et al. Evidence for cardiomyocyte renewal in humans. *Science* **324**, 98-102 (2009).

47. Yuan, X. & Braun, T. Multimodal Regulation of Cardiac Myocyte Proliferation. *Circulation research* **121**, 293-309 (2017).

48. Zebrowski, D.C. & Engel, F.B. The cardiomyocyte cell cycle in hypertrophy, tissue homeostasis, and regeneration. *Reviews of physiology, biochemistry and pharmacology* **165**, 67-96 (2013).

49. Derks, W. & Bergmann, O. Polyploidy in Cardiomyocytes: Roadblock to Heart Regeneration? *Circulation research* **126**, 552-565 (2020).

50. Senyo, S.E. et al. Mammalian heart renewal by pre-existing cardiomyocytes. *Nature* **493**, 433-436 (2013).

51. Patterson, M. et al. Frequency of mononuclear diploid cardiomyocytes underlies natural variation in heart regeneration. *Nature genetics* **49**, 1346-1353 (2017).

52. Patterson, M. & Swift, S.K. Residual Diploidy in Polyploid Tissues: A Cellular State with Enhanced Proliferative Capacity for Tissue Regeneration? *Stem cells and development* **28**, 1527-1539 (2019).

53. Bensley, J.G., De Matteo, R., Harding, R. & Black, M.J. Three-dimensional direct measurement of cardiomyocyte volume, nuclearity, and ploidy in thick histological sections. *Scientific reports* **6**, 23756 (2016).

54. Yang, X. et al. Tri-iodo-l-thyronine promotes the maturation of human cardiomyocytes-derived from induced pluripotent stem cells. *Journal of molecular and cellular cardiology* **72**, 296-304 (2014).

55. Nakada, Y. et al. Hypoxia induces heart regeneration in adult mice. *Nature* **541**, 222-227 (2017).

56. Soonpaa, M.H. et al. Cyclin D1 overexpression promotes cardiomyocyte DNA synthesis and multinucleation in transgenic mice. *The Journal of clinical investigation* **99**, 2644-2654 (1997).

57. Liu, Z., Yue, S., Chen, X., Kubin, T. & Braun, T. Regulation of cardiomyocyte polyploidy and multinucleation by CyclinG1. *Circulation research* **106**, 1498-1506 (2010).

58. Heallen, T. et al. Hippo signaling impedes adult heart regeneration. *Development (Cambridge, England)* **140**, 4683-4690 (2013).

59. Lin, Z. et al. Cardiac-specific YAP activation improves cardiac function and survival in an experimental murine MI model. *Circulation research* **115**, 354-363 (2014).

60. Du, A., Sanger, J.M. & Sanger, J.W. Cardiac myofibrillogenesis inside intact embryonic hearts. *Developmental biology* **318**, 236-246 (2008).

61. Rhee, D., Sanger, J.M. & Sanger, J.W. The premyofibril: evidence for its role in myofibrillogenesis. *Cell motility and the cytoskeleton* **28**, 1-24 (1994).

62. Dlugosz, A.A., Antin, P.B., Nachmias, V.T. & Holtzer, H. The relationship between stress fiber-like structures and nascent myofibrils in cultured cardiac myocytes. *The Journal of cell biology* **99**, 2268-2278 (1984).

63. Van der Ven, P.F., Ehler, E., Perriard, J.C. & Furst, D.O. Thick filament assembly occurs after the formation of a cytoskeletal scaffold. *Journal of muscle research and cell motility* **20**, 569-579 (1999).

64. Turnacioglu, K.K., Mittal, B., Dabiri, G.A., Sanger, J.M. & Sanger, J.W. An N-terminal fragment of titin coupled to green fluorescent protein localizes to the Z-bands in living muscle cells: overexpression leads to myofibril disassembly. *Molecular biology of the cell* **8**, 705-717 (1997).

65. Mahdavi, V., Lompre, A.M., Chambers, A.P. & Nadal-Ginard, B. Cardiac myosin heavy chain isozymic transitions during development and under pathological conditions are regulated at the level of mRNA availability. *European heart journal* **5 Suppl F**, 181-191 (1984).

66. Karbassi, E. et al. Cardiomyocyte maturation: advances in knowledge and implications for regenerative medicine. *Nature reviews. Cardiology* (2020).

67. Forouzanfar, M.H. et al. Assessing the global burden of ischemic heart disease, part 2: analytic methods and estimates of the global epidemiology of ischemic heart disease in 2010. *Global heart* **7**, 331-342 (2012).

68. Prabhu, S.D. & Frangogiannis, N.G. The Biological Basis for Cardiac Repair After Myocardial Infarction: From Inflammation to Fibrosis. *Circulation research* **119**, 91-112 (2016).

69. Jain, R., Poleshko, A. & Epstein, J.A. Beating the odds: programming proliferation in the mammalian heart. *Genome medicine* **10**, 36 (2018).

70. Piotrowicz, R. & Wolszakiewicz, J. Cardiac rehabilitation following myocardial infarction. *Cardiology journal* **15**, 481-487 (2008).

71. Cahill, T.J., Choudhury, R.P. & Riley, P.R. Heart regeneration and repair after myocardial infarction: translational opportunities for novel therapeutics. *Nature reviews. Drug discovery* **16**, 699-717 (2017).

72. Caspi, O. et al. Transplantation of human embryonic stem cell-derived cardiomyocytes improves myocardial performance in infarcted rat hearts. *Journal of the American College of Cardiology* **50**, 1884-1893 (2007).

73. Shiba, Y. et al. Human ES-cell-derived cardiomyocytes electrically couple and suppress arrhythmias in injured hearts. *Nature* **489**, 322-325 (2012).

74. Lesman, A. et al. Transplantation of a tissue-engineered human vascularized cardiac muscle. *Tissue engineering. Part A* **16**, 115-125 (2010).

75. Zimmermann, W.H. et al. Engineered heart tissue grafts improve systolic and diastolic function in infarcted rat hearts. *Nature medicine* **12**, 452-458 (2006).

76. Roberts, M.A. et al. Stromal Cells in Dense Collagen Promote Cardiomyocyte and Microvascular Patterning in Engineered Human Heart Tissue. *Tissue engineering. Part A* **22**, 633-644 (2016).

77. Gerbin KA, M.K., Guan X, Martinson AM, Murry CE Delta-1 functionalized hydrogel promotes hESC-cardiomyocyte graft proliferation and maintains heart function post-injury. *Molecular Therapy: Methods & Clinical Development* (2020).

78. Bargehr, J. et al. Epicardial cells derived from human embryonic stem cells augment cardiomyocyte-driven heart regeneration. *Nature biotechnology* **37**, 895-906 (2019).

79. Hatzistergos, K.E. et al. Bone marrow mesenchymal stem cells stimulate cardiac stem cell proliferation and differentiation. *Circulation research* **107**, 913-922 (2010).

80. Mathieu, E. et al. Intramyocardial delivery of mesenchymal stem cell-seeded hydrogel preserves cardiac function and attenuates ventricular remodeling after myocardial infarction. *PLoS One* **7**, e51991 (2012).

81. Zhang, Z. et al. Selective inhibition of inositol hexakisphosphate kinases (IP6Ks) enhances mesenchymal stem cell engraftment and improves therapeutic efficacy for myocardial infarction. *Basic research in cardiology* **109**, 417 (2014).

82. Ye, L. et al. Cardiac repair in a porcine model of acute myocardial infarction with human induced pluripotent stem cell-derived cardiovascular cells. *Cell stem cell* **15**, 750-761 (2014).

83. Ye, L. et al. Cardiac repair in a porcine model of acute myocardial infarction with human induced pluripotent stem cell-derived cardiovascular cells. *Cell stem cell* **15**, 750-761 (2014).

84. Aurora, A.B. & Olson, E.N. Immune modulation of stem cells and regeneration. *Cell stem cell* **15**, 14-25 (2014).

85. Sanganalmath, S.K. & Bolli, R. Cell therapy for heart failure: a comprehensive overview of experimental and clinical studies, current challenges, and future directions. *Circulation research* **113**, 810-834 (2013).

86. Burchfield, J.S. & Dimmeler, S. Role of paracrine factors in stem and progenitor cell mediated cardiac repair and tissue fibrosis. *Fibrogenesis Tissue Repair* **1**, 4-4 (2008).

87. Chen, L., Tredget, E.E., Wu, P.Y. & Wu, Y. Paracrine factors of mesenchymal stem cells recruit macrophages and endothelial lineage cells and enhance wound healing. *PLoS One* **3**, e1886 (2008).

88. Nakagami, H. et al. Novel autologous cell therapy in ischemic limb disease through growth factor secretion by cultured adipose tissue-derived stromal cells. *Arteriosclerosis, thrombosis, and vascular biology* **25**, 2542-2547 (2005).

89. Sadat, S. et al. The cardioprotective effect of mesenchymal stem cells is mediated by IGF-I and VEGF. *Biochemical and biophysical research communications* **363**, 674-679 (2007).

90. Gnecchi, M. et al. Paracrine action accounts for marked protection of ischemic heart by Akt-modified mesenchymal stem cells. *Nature medicine* **11**, 367-368 (2005).

91. Hodgkinson, C.P., Bareja, A., Gomez, J.A. & Dzau, V.J. Emerging Concepts in Paracrine Mechanisms in Regenerative Cardiovascular Medicine and Biology. *Circulation research* **118**, 95-107 (2016).

92. Kreitzer, F.R. et al. A robust method to derive functional neural crest cells from human pluripotent stem cells. *American journal of stem cells* **2**, 119-131 (2013).

93. Burridge, P.W. et al. Chemically defined generation of human cardiomyocytes. *Nature methods* **11**, 855-860 (2014).

94. Smith, A.S.T. et al. NanoMEA: A Tool for High-Throughput, Electrophysiological Phenotyping of Patterned Excitable Cells. *Nano Letters* **20**, 1561-1570 (2020).

95. Halbach, M., Egert, U., Hescheler, J. & Banach, K. Estimation of action potential changes from field potential recordings in multicellular mouse cardiac myocyte cultures. *Cellular physiology and biochemistry : international journal of experimental cellular physiology, biochemistry, and pharmacology* **13**, 271-284 (2003).

96. Lee, P. et al. Simultaneous voltage and calcium mapping of genetically purified human induced pluripotent stem cell-derived cardiac myocyte monolayers. *Circulation research* **110**, 1556-1563 (2012).

97. Vreeker, A. et al. Assembly of the cardiac intercalated disk during pre- and postnatal development of the human heart. *PLoS One* **9**, e94722 (2014).

98. Jiang, Y., Park, P., Hong, S.-M. & Ban, K. Maturation of Cardiomyocytes Derived from Human Pluripotent Stem Cells: Current Strategies and Limitations. *Mol Cells* **41**, 613-621 (2018).

99. Kadota, S., Pabon, L., Reinecke, H. & Murry, C.E. In Vivo Maturation of Human Induced Pluripotent Stem Cell-Derived Cardiomyocytes in Neonatal and Adult Rat Hearts. *Stem Cell Reports* **8**, 278-289 (2017).

100. Fernandes, S. et al. Comparison of Human Embryonic Stem Cell-Derived Cardiomyocytes, Cardiovascular Progenitors, and Bone Marrow Mononuclear Cells for Cardiac Repair. *Stem Cell Reports* **5**, 753-762 (2015).

101. Zimmermann, W.H. et al. Tissue engineering of a differentiated cardiac muscle construct. *Circulation research* **90**, 223-230 (2002).

102. Vunjak-Novakovic, G., Lui, K.O., Tandon, N. & Chien, K.R. Bioengineering heart muscle: a paradigm for regenerative medicine. *Annual review of biomedical engineering* **13**, 245-267 (2011).

103. van Laake, L.W. et al. Extracellular matrix formation after transplantation of human embryonic stem cell-derived cardiomyocytes. *Cellular and molecular life sciences : CMLS* **67**, 277-290 (2010).

104. Pettinato, A.M. et al. Sarcomere function activates a p53-dependent DNA damage response that promotes polyploidization and limits in vivo cell engraftment. *Cell reports* **35**, 109088 (2021).

105. el-Deiry, W.S. et al. WAF1, a potential mediator of p53 tumor suppression. *Cell* **75**, 817-825 (1993).

106. van Berlo, J.H. et al. c-kit+ cells minimally contribute cardiomyocytes to the heart. *Nature* **509**, 337-341 (2014).

107. Gonzalez-Rosa, J.M. et al. Myocardial Polyploidization Creates a Barrier to Heart Regeneration in Zebrafish. *Developmental cell* **44**, 433-446.e437 (2018).

108. Nishii, K. et al. Targeted disruption of the cardiac troponin T gene causes sarcomere disassembly and defects in heartbeat within the early mouse embryo. *Dev Biol* **322**, 65-73 (2008).

109. Huang, X. et al. Cardiac troponin I gene knockout: a mouse model of myocardial troponin I deficiency. *Circ Res* **84**, 1-8 (1999).

110. De Deyne, P.G. Formation of sarcomeres in developing myotubes: role of mechanical stretch and contractile activation. *American journal of physiology. Cell physiology* **279**, C1801-1811 (2000).

111. Lam, C.K. et al. Identifying the Transcriptome Signatures of Calcium Channel Blockers in Human Induced Pluripotent Stem Cell-Derived Cardiomyocytes. *Circ Res* **125**, 212-222 (2019).

112. Bode, A.M. & Dong, Z. Post-translational modification of p53 in tumorigenesis. *Nat Rev Cancer* **4**, 793-805 (2004).

113. Jung, Y.S., Qian, Y. & Chen, X. Examination of the expanding pathways for the regulation of p21 expression and activity. *Cell Signal* **22**, 1003-1012 (2010).

114. Nguyen, T.T. et al. Revealing a human p53 universe. *Nucleic Acids Res* **46**, 8153-8167 (2018).

115. Ayoub, N., Jeyasekharan, A.D., Bernal, J.A. & Venkitaraman, A.R. HP1-beta mobilization promotes chromatin changes that initiate the DNA damage response. *Nature* **453**, 682-686 (2008).

116. Du, Y. et al. Blocking c-Met-mediated PARP1 phosphorylation enhances anti-tumor effects of PARP inhibitors. *Nat Med* **22**, 194-201 (2016).

117. Herzig, S. & Shaw, R.J. AMPK: guardian of metabolism and mitochondrial homeostasis. *Nat Rev Mol Cell Biol* **19**, 121-135 (2018).

118. Laflamme, M.A., Zbinden, S., Epstein, S.E. & Murry, C.E. Cell-based therapy for myocardial ischemia and infarction: pathophysiological mechanisms. *Annual review of pathology* **2**, 307-339 (2007).

119. Zhu, W., Zhao, M., Mattapally, S., Chen, S. & Zhang, J. CCND2 Overexpression Enhances the Regenerative Potency of Human Induced Pluripotent Stem Cell-Derived Cardiomyocytes: Remuscularization of Injured Ventricle. *Circ Res* **122**, 88-96 (2018).

120. Fernandes, S. et al. Human embryonic stem cell-derived cardiomyocytes engraft but do not alter cardiac remodeling after chronic infarction in rats. *Journal of molecular and cellular cardiology* **49**, 941-949 (2010).

121. Weyers, J.J. et al. Sonic Hedgehog upregulation does not enhance the survival and engraftment of stem cell-derived cardiomyocytes in infarcted hearts. *PLoS One* **15**, e0227780 (2020).

122. O'Gara, P.T. et al. 2013 ACCF/AHA guideline for the management of ST-elevation myocardial infarction: a report of the American College of Cardiology Foundation/American Heart Association Task Force on Practice Guidelines. *J Am Coll Cardiol* **61**, e78-e140 (2013).

123. Vivien, C.J., Hudson, J.E. & Porrello, E.R. Evolution, comparative biology and ontogeny of vertebrate heart regeneration. *NPJ Regen Med* **1**, 16012 (2016).

124. Strauss, B. et al. Cyclin B1 is essential for mitosis in mouse embryos, and its nuclear export sets the time for mitosis. *The Journal of cell biology* **217**, 179-193 (2018).

125. Ulmer, B.M. et al. Contractile Work Contributes to Maturation of Energy Metabolism in hiPSC-Derived Cardiomyocytes. *Stem Cell Reports* **10**, 834-847 (2018).

126. Mills, R.J. et al. Functional screening in human cardiac organoids reveals a metabolic mechanism for cardiomyocyte cell cycle arrest. *Proc Natl Acad Sci U S A* **114**, E8372-E8381 (2017).

127. Ahuja, P., Perriard, E., Perriard, J.C. & Ehler, E. Sequential myofibrillar breakdown accompanies mitotic division of mammalian cardiomyocytes. *J Cell Sci* **117**, 3295-3306 (2004).

128. Bicknell, K.A., Coxon, C.H. & Brooks, G. Forced expression of the cyclin B1-CDC2 complex induces proliferation in adult rat cardiomyocytes. *Biochem J* **382**, 411-416 (2004).

129. Engel, F.B., Schebesta, M. & Keating, M.T. Anillin localization defect in cardiomyocyte binucleation. *J Mol Cell Cardiol* **41**, 601-612 (2006).

130. Fischer, M., Quaas, M., Steiner, L. & Engeland, K. The p53-p21-DREAM-CDE/CHR pathway regulates G2/M cell cycle genes. *Nucleic Acids Res* **44**, 164-174 (2016).

131. Nakajima, H., Nakajima, H.O., Tsai, S.C. & Field, L.J. Expression of mutant p193 and p53 permits cardiomyocyte cell cycle reentry after myocardial infarction in transgenic mice. *Circ Res* **94**, 1606-1614 (2004).

132. Pasumarthi, K.B., Tsai, S.C. & Field, L.J. Coexpression of mutant p53 and p193 renders embryonic stem cell-derived cardiomyocytes responsive to the growth-promoting activities of adenoviral E1A. *Circ Res* **88**, 1004-1011 (2001).

133. Kurinna, S. et al. p53 regulates a mitotic transcription program and determines ploidy in normal mouse liver. *Hepatology* **57**, 2004-2013 (2013).

134. Bulatovic, I., Månsson-Broberg, A., Sylvén, C. & Grinnemo, K.H. Human fetal cardiac progenitors: The role of stem cells and progenitors in the fetal and adult heart. *Best practice & research. Clinical obstetrics & gynaecology* **31**, 58-68 (2016).

135. Valenti, O. et al. Fetal cardiac function during the first trimester of pregnancy. *Journal of prenatal medicine* **5**, 59-62 (2011).

136. Racca, A.W. et al. Contractile properties of developing human fetal cardiac muscle. *The Journal of physiology* **594**, 437-452 (2016).

137. Sehnert, A.J. et al. Cardiac troponin T is essential in sarcomere assembly and cardiac contractility. *Nature genetics* **31**, 106-110 (2002).

138. Chopra, A. et al. Force Generation via beta-Cardiac Myosin, Titin, and alpha-Actinin Drives Cardiac Sarcomere Assembly from Cell-Matrix Adhesions. *Developmental cell* **44**, 87-96.e85 (2018).

139. Fenix, A.M. et al. Muscle-specific stress fibers give rise to sarcomeres in cardiomyocytes. *eLife* **7** (2018).

140. Skwarek-Maruszewska, A., Hotulainen, P., Mattila, P.K. & Lappalainen, P. Contractility-dependent actin dynamics in cardiomyocyte sarcomeres. *Journal of Cell Science* **122**, 2119 (2009).

141. Morimoto, S. & Goto, T. Role of troponin I isoform switching in determining the pH sensitivity of Ca(2+) regulation in developing rabbit cardiac muscle. *Biochemical and biophysical research communications* **267**, 912-917 (2000).

142. Siedner, S. et al. Developmental changes in contractility and sarcomeric proteins from the early embryonic to the adult stage in the mouse heart. *The Journal of physiology* **548**, 493-505 (2003).

143. Parmacek, M.S. & Solaro, R.J. Biology of the troponin complex in cardiac myocytes. *Progress in cardiovascular diseases* **47**, 159-176 (2004).

144. Reiser, P.J., Portman, M.A., Ning, X.H. & Schomisch Moravec, C. Human cardiac myosin heavy chain isoforms in fetal and failing adult atria and ventricles. *American journal of physiology. Heart and circulatory physiology* **280**, H1814-1820 (2001).

145. Somi, S. et al. Atrial and ventricular myosin heavy-chain expression in the developing chicken heart: strengths and limitations of non-radioactive in situ hybridization. *The journal of histochemistry and cytochemistry : official journal of the Histochemistry Society* **54**, 649-664 (2006).

146. Wessels, A. et al. Spatial distribution of "tissue-specific" antigens in the developing human heart and skeletal muscle. II. An immunohistochemical analysis of myosin heavy chain isoform expression patterns in the embryonic heart. *The Anatomical record* **229**, 355-368 (1991).

147. Mihic, A. et al. The effect of cyclic stretch on maturation and 3D tissue formation of human embryonic stem cell-derived cardiomyocytes. *Biomaterials* **35**, 2798-2808 (2014).

148. Shimko, V.F. & Claycomb, W.C. Effect of mechanical loading on three-dimensional cultures of embryonic stem cell-derived cardiomyocytes. *Tissue engineering. Part A* **14**, 49-58 (2008).

149. Gillis, T.E., Martyn, D.A., Rivera, A.J. & Regnier, M. Investigation of thin filament near-neighbour regulatory unit interactions during force development in skinned cardiac and skeletal muscle. *The Journal of physiology* **580**, 561-576 (2007).

150. Rebecca J. Zaunbrecher, A.N.A., Kevin Beussman, Andrea Leonard, Marion von Frieling-Salewsky, Paul A. Fields, Lil Pabon, Hans Reinecke, Xiulan Yang, Jesse Macadangdang, Deok-Ho Kim, Wolfgang A. Linke, Nathan J. Sniadecki, Michael Regnier , Charles E. Murry Cronos Titin Is Expressed in Human Cardiomyocytes and Necessary for Normal Sarcomere Function. *Circulation* **140**, 1647-1660 (2019).

151. Macadangdang, J. et al. Capillary force lithography for cardiac tissue engineering. *J Vis Exp* (2014).

152. Gerbin, K.A. et al. Cell states beyond transcriptomics: integrating structural organization and gene expression in hiPSC-derived cardiomyocytes. *bioRxiv*, 2020.2005.2026.081083 (2020).

153. Decker, M.L., Behnke-Barclay, M., Cook, M.G., Lesch, M. & Decker, R.S. Morphometric evaluation of the contractile apparatus in primary cultures of rabbit cardiac myocytes. *Circulation research* **69**, 86-94 (1991).

154. Gallo, S., Vitacolonna, A., Bonzano, A., Comoglio, P. & Crepaldi, T. ERK: A Key Player in the Pathophysiology of Cardiac Hypertrophy. *International journal of molecular sciences* **20** (2019).

155. Kehat, I. et al. Extracellular signal-regulated kinases 1 and 2 regulate the balance between eccentric and concentric cardiac growth. *Circulation research* **108**, 176-183 (2011).

156. Sanger, J.W. et al. How to build a myofibril. *Journal of muscle research and cell motility* **26**, 343-354 (2005).

157. Kassianidou, E. & Kumar, S. A biomechanical perspective on stress fiber structure and function. *Biochimica et biophysica acta* **1853**, 3065-3074 (2015).

158. Tavi, P., Laine, M., Weckström, M. & Ruskoaho, H. Cardiac mechanotransduction: from sensing to disease and treatment. *Trends in pharmacological sciences* **22**, 254-260 (2001).

159. Brancaccio, M. et al. Integrin signalling: the tug-of-war in heart hypertrophy. *Cardiovascular research* **70**, 422-433 (2006).

160. Houser, S.R. & Molkentin, J.D. Does Contractile Ca²⁺ Control Calcineurin-NFAT Signaling and Pathological Hypertrophy in Cardiac Myocytes? *Science Signaling* **1**, pe31 (2008).

161. Abilez, O.J. et al. Passive Stretch Induces Structural and Functional Maturation of Engineered Heart Muscle as Predicted by Computational Modeling. *Stem cells (Dayton, Ohio)* **36**, 265-277 (2018).

162. Chan, Y.C. et al. Electrical stimulation promotes maturation of cardiomyocytes derived from human embryonic stem cells. *Journal of cardiovascular translational research* **6**, 989-999 (2013).

163. Finley, N.L., Howarth, J.W. & Rosevear, P.R. Structure of the Mg2+-Loaded C-Lobe of Cardiac Troponin C Bound to the N-Domain of Cardiac Troponin I: Comparison with the Ca2+-Loaded Structure. *Biochemistry* **43**, 11371-11379 (2004).

164. Itzhaki, I. et al. Calcium handling in human induced pluripotent stem cell derived cardiomyocytes. *PLoS One* **6**, e18037 (2011).

165. Kolwicz, S.C., Jr., Purohit, S. & Tian, R. Cardiac metabolism and its interactions with contraction, growth, and survival of cardiomyocytes. *Circulation research* **113**, 603-616 (2013).

166. Eng, G. et al. Autonomous beating rate adaptation in human stem cell-derived cardiomyocytes. *Nat Commun* **7**, 10312 (2016).

167. Azar, T., Sharp, J. & Lawson, D. Heart rates of male and female Sprague-Dawley and spontaneously hypertensive rats housed singly or in groups. *Journal of the American Association for Laboratory Animal Science : JAALAS* **50**, 175-184 (2011).

168. Terrovitis, J.V., Smith, R.R. & Marbán, E. Assessment and optimization of cell engraftment after transplantation into the heart. *Circulation research* **106**, 479-494 (2010).

Appendix A. Supplemental Figure to Chapter 3

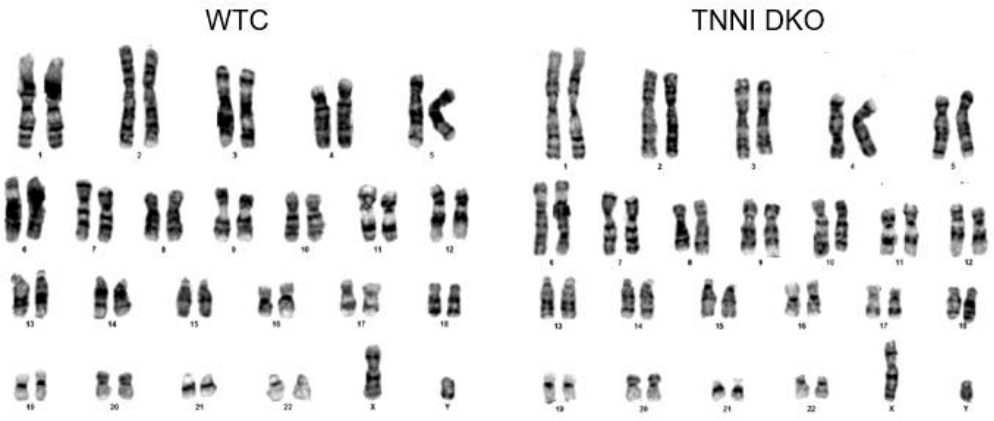

Figure S19 Karyotype results of TNNI DKO and WTC iPSC lines.

The iPSCs generated and used for this work indicate normal chromosome count and morphology.

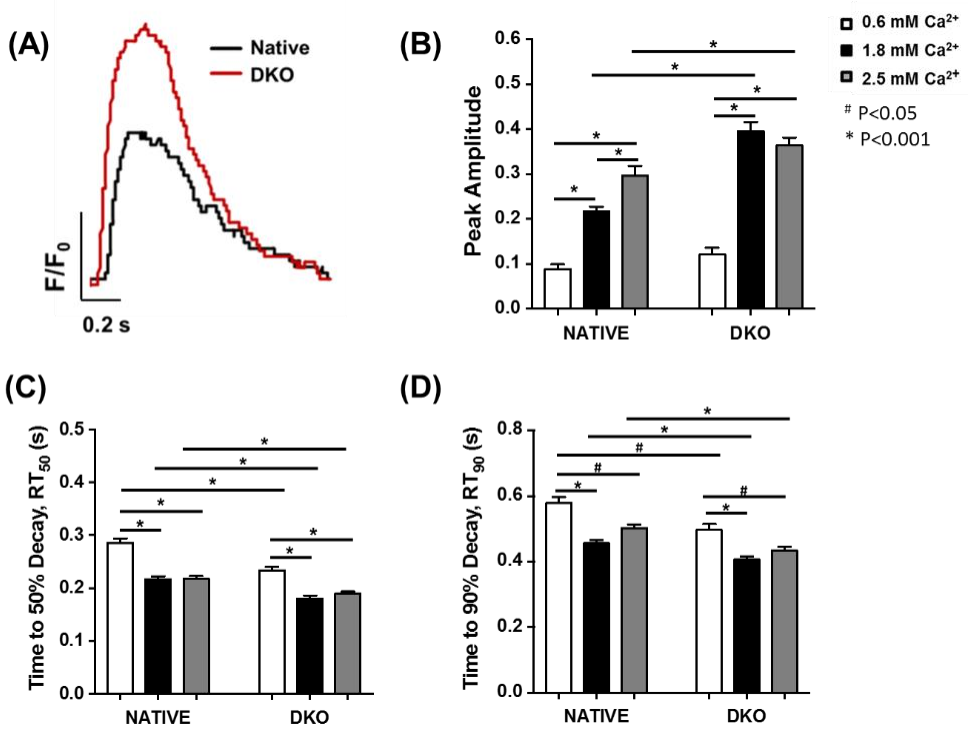

Figure S20 TNNI DKO-CMs have calcium transients.

(A) Representative calcium transient trace from Fura-2 measurements for wildtype (denoted Native) and TNNI DKO-CMs in 1.8 mM Ca^{2+} Tyrode buffer, **(B)** peak amplitude, **(C)** time to 50% decay, and (D) time to 90% decay in three different extracellular Ca^{2+} concentrations (0.6, 1.8, 2.5 mM Ca^{2+}). Data courtesy of Dr. Yuanhua Cheng.

Appendix B. Supplemental Figures to Chapter 4

The following figures are in the Cell Reports publication and have been performed by our collaborators in Dr. Travis Hinson's lab.[104]

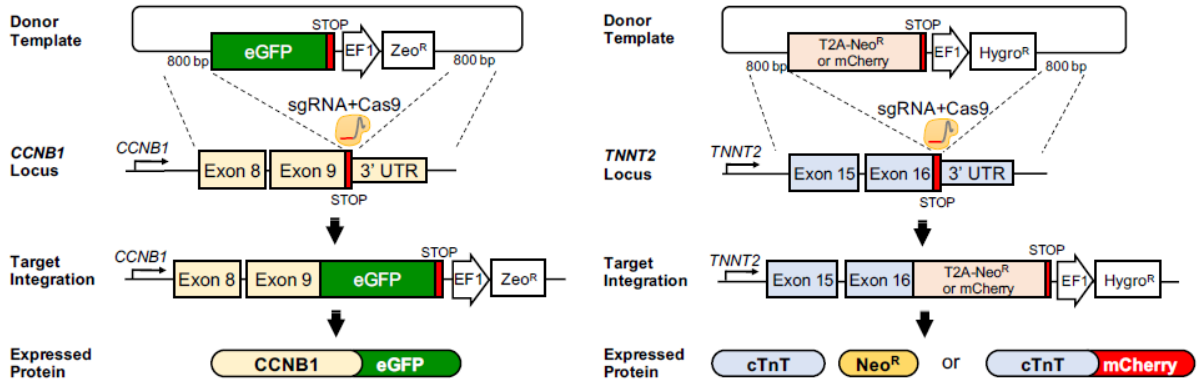

Figure S21 Overview of CRISPR methods to generate CCNB1-eGFP, TNNT2-T2A-NeoR, and TNNT2-mCherry iPSC lines to study polyploidization in differentiated cardiomyocytes.

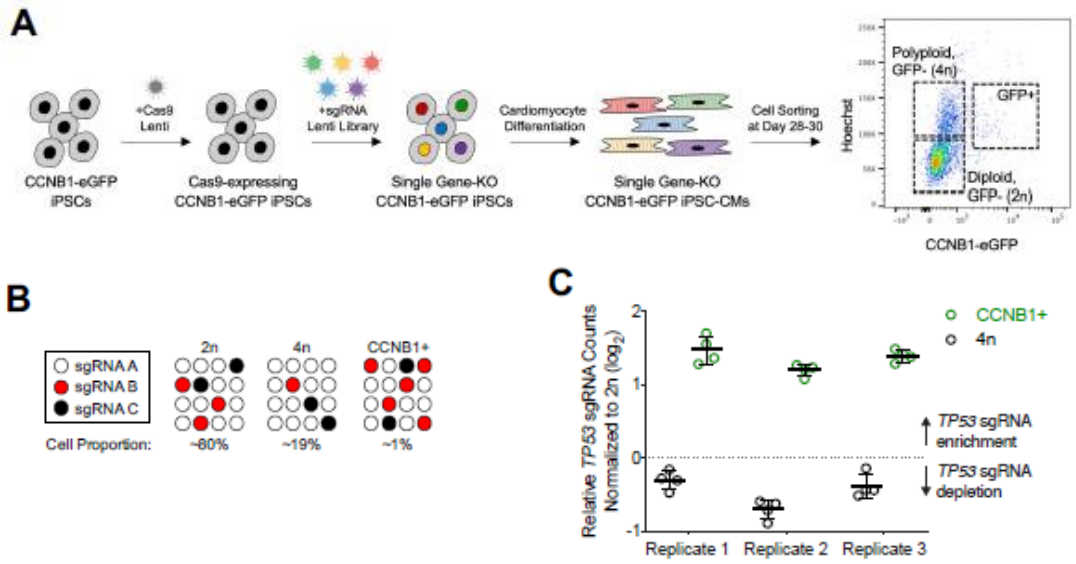

Figure S22 CRISPR screen identifies p53 as an activator or cardiomyocyte polyploidy and inhibitor of CCNB1.

(A) Schematic used to conduct CRISPR screen in CMs differentiated from iPSCs transduced with SpCas9 and sgRNA library, as well as CM collection strategy by FACS. **(B)** Simplified distribution of three theoretical sgRNAs, showing sgRNA B (red) enriched in 4n CCNB1+ CMs and depleted in 4n CCNB1- relative to 2n, as it targets a putative activator of polyploidization and inhibitor of CCNB1 expression. **(C)** All four sgRNAs targeting TP53 are enriched in 4n CCNB1+ CMs and depleted in 4n CCNB1- relative to 2n across three biological CRISPR sub-screen replicates, demonstrating TP53 is an activator of polyploidy and inhibitor of CCNB1 expression.

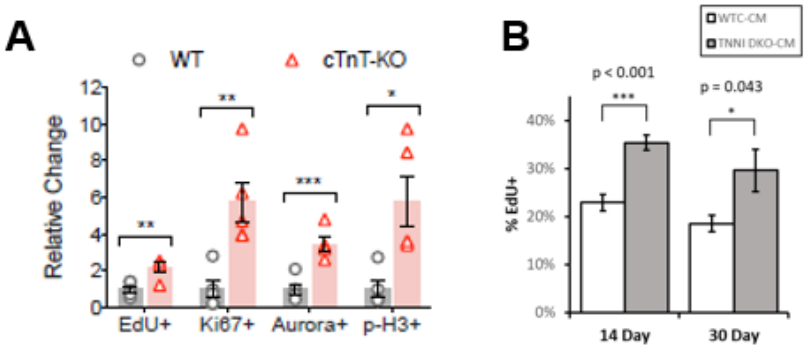

Figure S23 Non-contractile cardiomyocytes are more proliferative *in vitro*.

(A) Flow cytometry of immunostained WT and cTnT-KO CMs demonstrates increased positivity for EdU, Ki67, Aurora A, and p-H3 in cTnT-KO CMs. **(B)** *In vitro* TnI KO-CMs are more proliferative than wildtype

CMs at both 14 and 30 day post differentiation. Data are n≥3 and mean±SEM; significance assessed by Student's t-test and defined by p ≤ 0.05 (*) and p ≤ 0.001 (***).

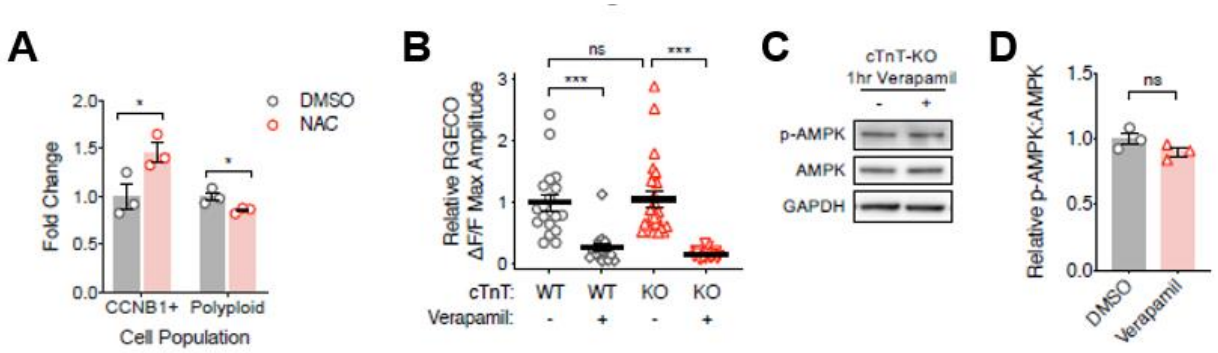

Figure S24 Genetic and pharmacological methods for reduction of cardiomyocyte polyploidization.

(A) Treatment of WT CMs with the antioxidant N-acetylcysteine (NAC) from Day 9 of differentiation reduces polyploidization and increases the proportion of CCNB1+ CMs as quantified by FACS analysis at Day 20. Despite sarcomere assembly, targeting oxidative stress is sufficient to reduce polyploidization in parallel with CCNB1 upregulation. **(B)** Quantification of ΔF/F maximal amplitude for the genetically-encoded calcium indicator RGECO produced by WT and cTnT-KO CMs ± verapamil treatment. Data are expressed relative to WT + DMSO control and demonstrate similar calcium transients between WT and cTnT-KO CMs at baseline, as well as similar responses to verapamil (n=18-26 CMs). **(C)** Representative immunoblots with **(D)** quantification of protein lysates from cTnT-KO CMs treated with verapamil for 1 hr and probed for p-AMPK, AMPK, and GAPDH. Data are n≥3 and mean±SEM; significance assessed by t-test (A, C-D) or ANOVA with Holm-Sidak correction (B) and defined by P > 0.05 (ns), P ≤ 0.05 (*), P ≤ 0.01 (**), and P ≤ 0.001 (***).

Appendix C. Supplemental Figures to Chapter 5

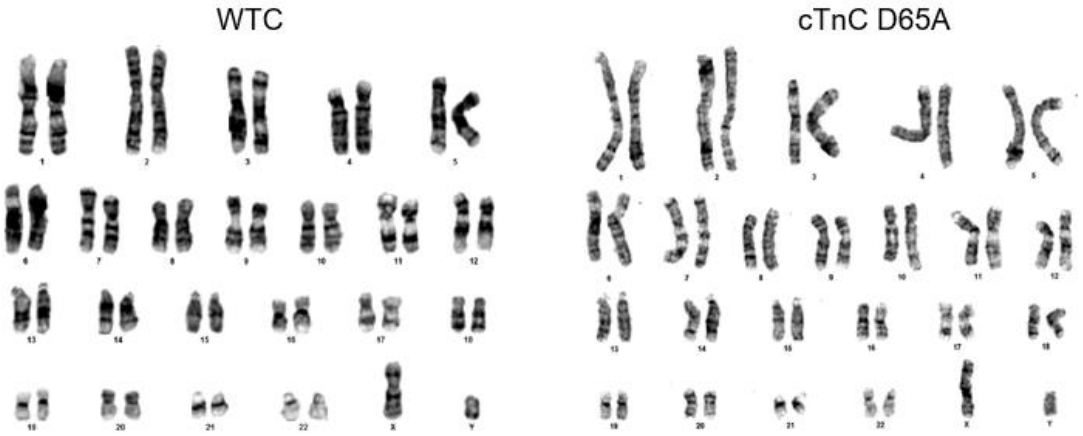

Figure S25 Karyotype results of cTnC D65A and WTC iPSC lines.

The iPSCs generated and used for this work indicate normal chromosome count and morphology.

Appendix D. Supplemental Figures to Chapter 6

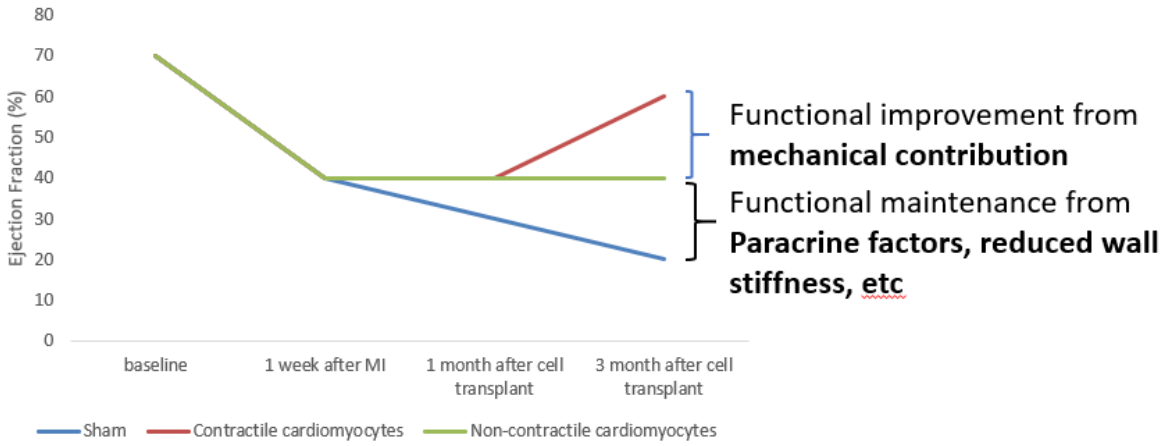

Figure S26 Hypothetical result from a non-human primate experiment to understand graft's mechanism of action.

VITA

Dasom (Christine) Yoo was born in Seoul, South Korea in 1994. She immigrated to the United States of America in 2006 with her parents and brother. She received her Bachelor of Science in Bioengineering from the University of Washington in 2016 with departmental honors. During her undergraduate studies, she worked on synthesizing neuroprotective polymeric nanoparticles that reduce oxidative stress after traumatic brain injury under the guidance of Drs. Patrick Stayton and Anthony Convertine. She earned her Ph.D. in Bioengineering from the University of Washington in 2021.